



**Calhoun: The NPS Institutional Archive**  
**DSpace Repository**

---

Theses and Dissertations

1. Thesis and Dissertation Collection, all items

---

2008-06

Indian Ocean surface circulations and their  
connection to Indian Ocean dipole, identified  
from Ocean Surface Currents Analysis Real  
Time (OSCAR) data

Rana, Haris Sarwar

Monterey, California. Naval Postgraduate School

---

<http://hdl.handle.net/10945/4038>

---

*Downloaded from NPS Archive: Calhoun*



Calhoun is the Naval Postgraduate School's public access digital repository for research materials and institutional publications created by the NPS community. Calhoun is named for Professor of Mathematics Guy K. Calhoun, NPS's first appointed -- and published -- scholarly author.

**Dudley Knox Library / Naval Postgraduate School**  
**411 Dyer Road / 1 University Circle**  
**Monterey, California USA 93943**

<http://www.nps.edu/library>



# **NAVAL POSTGRADUATE SCHOOL**

**MONTEREY, CALIFORNIA**

## **THESIS**

**INDIAN OCEAN SURFACE CIRCULATIONS AND THEIR  
CONNECTION TO INDIAN OCEAN DIPOLE, IDENTIFIED  
FROM OCEAN SURFACE CURRENTS ANALYSIS  
REAL TIME (OSCAR) DATA**

by

Haris Sarwar Rana

June 2008

Thesis Advisor:  
Second Reader:

Peter C. Chu  
Charles Sun

**Approved for public release; distribution is unlimited**

THIS PAGE INTENTIONALLY LEFT BLANK

<b>REPORT DOCUMENTATION PAGE</b>			<i>Form Approved OMB No. 0704-0188</i>	
Public reporting burden for this collection of information is estimated to average 1 hour per response, including the time for reviewing instruction, searching existing data sources, gathering and maintaining the data needed, and completing and reviewing the collection of information. Send comments regarding this burden estimate or any other aspect of this collection of information, including suggestions for reducing this burden, to Washington headquarters Services, Directorate for Information Operations and Reports, 1215 Jefferson Davis Highway, Suite 1204, Arlington, VA 22202-4302, and to the Office of Management and Budget, Paperwork Reduction Project (0704-0188) Washington DC 20503.				
<b>1. AGENCY USE ONLY (Leave blank)</b>		<b>2. REPORT DATE</b> June 2008		<b>3. REPORT TYPE AND DATES COVERED</b> Master's Thesis
<b>4. TITLE AND SUBTITLE</b> Indian Ocean Surface Circulations and their Connection to Indian Ocean Dipole, Identified from Ocean Surface Currents Analysis Real Time (OSCAR) Data			<b>5. FUNDING NUMBERS</b>	
<b>6. AUTHOR(S)</b> Haris Sarwar Rana				
<b>7. PERFORMING ORGANIZATION NAME(S) AND ADDRESS(ES)</b> Naval Postgraduate School Monterey, CA 93943-5000			<b>8. PERFORMING ORGANIZATION REPORT NUMBER</b>	
<b>9. SPONSORING /MONITORING AGENCY NAME(S) AND ADDRESS(ES)</b> N/A			<b>10. SPONSORING/MONITORING AGENCY REPORT NUMBER</b>	
<b>11. SUPPLEMENTARY NOTES</b> The views expressed in this thesis are those of the author and do not reflect the official policy or position of the Department of Defense or the U.S. Government.				
<b>12a. DISTRIBUTION / AVAILABILITY STATEMENT</b> Approved for public release: distribution is unlimited.			<b>12b. DISTRIBUTION CODE</b>	
<b>13. ABSTRACT (maximum 200 words)</b> <p>Ocean surface circulation is an essential component of the world climate system. In this study the Ocean Surface Currents Analysis – Real Time (OSCAR) data, derived from satellite altimeter and scatterometer is used to investigate the connection between the Indian Ocean Dipole and eastward equatorial jet. The raw OSCAR data set was refined using the Optimal Spectral Decomposition method (OSD). Data was analyzed to show the seasonal variability of the surface currents in the Indian Ocean with emphasize on Somali current, North Arabian Sea, and Bay of Bengal.</p> <p>To investigate the link between the Eastward Equatorial jets (Wyrтки jets) and the Indian Ocean Dipole (IOD) Mode events, complex EOF analysis was applied to the currents in the Equatorial region. This analysis revealed that the spatial anomaly of the currents along the equator can directly relate to the occurrence of a Dipole Mode event. Further zonal currents anomalies and vector plots, for the years with Dipole Mode events, also depicted the anomalous behavior of the equatorial jets during a Dipole Mode event. This study demonstrates that satellite based altimetry data can be used to refine the climatological knowledge of a certain region in the world.</p>				
<b>14. SUBJECT TERMS</b> Oceanography, Indian Ocean, Ocean Currents Analysis Real-time (OSCAR), Currents, Indian Ocean Dipole (IOD), Monsoon Cycle, Optimal Spectral Decomposition (OSD), Complex EOF, Somali Current, North Arabian Sea, Bay of Bengal, Wyrтки Jets, Dipole Mode Index, Mine Warfare, Chemical Spill, Search and Rescue, Currents and Energy, Large Scale Climate Diagnostics			<b>15. NUMBER OF PAGES</b> 91	
			<b>16. PRICE CODE</b>	
<b>17. SECURITY CLASSIFICATION OF REPORT</b> Unclassified		<b>18. SECURITY CLASSIFICATION OF THIS PAGE</b> Unclassified		<b>19. SECURITY CLASSIFICATION OF ABSTRACT</b> Unclassified
<b>20. LIMITATION OF ABSTRACT</b> UU				



THIS PAGE INTENTIONALLY LEFT BLANK

**Approved for public release; distribution is unlimited**

**INDIAN OCEAN SURFACE CIRCULATIONS AND THEIR CONNECTION TO  
INDIAN OCEAN DIPOLE, IDENTIFIED FROM OCEAN SURFACE  
CURRENTS ANALYSIS REAL TIME (OSCAR) DATA**

Haris Sarwar Rana  
Lieutenant, Pakistan Navy  
B.S., Pakistan Naval Academy, 2001

Submitted in partial fulfillment of the  
requirements for the degree of

**MASTER OF SCIENCE IN PHYSICAL OCEANOGRAPHY**

from the

**NAVAL POSTGRADUATE SCHOOL  
June 2008**

Author: Haris Sarwar Rana

Approved by: Peter C. Chu  
Thesis Advisor

Charles Sun  
Second Reader

Mary L. Batteen  
Chairman, Department of Oceanography

THIS PAGE INTENTIONALLY LEFT BLANK

## **ABSTRACT**

Ocean surface circulation is an essential component of the world climate system. In this study, the Ocean Surface Currents Analysis – Real Time (OSCAR) data, derived from satellite altimeter and scatterometer, is used to investigate the connection between the Indian Ocean Dipole and eastward equatorial jet. The raw OSCAR data set was refined using the Optimal Spectral Decomposition method (OSD). Data was analyzed to show the seasonal variability of the surface currents in the Indian Ocean with emphasis on the Somali current, North Arabian Sea, and Bay of Bengal.

To investigate the link between the Eastward Equatorial jets (Wyrтки jets) and the Indian Ocean Dipole (IOD) Mode events, complex EOF analysis was applied to the currents in the Equatorial region. This analysis revealed that the spatial anomaly of the currents along the equator can directly relate to the occurrence of a Dipole Mode event. Further zonal currents anomalies and vector plots, for the years with Dipole Mode events, also depicted the anomalous behavior of the equatorial jets during a Dipole Mode event. This study demonstrates that satellite-based altimetry data can be used to refine the climatological knowledge of a certain region in the world.

THIS PAGE INTENTIONALLY LEFT BLANK

## TABLE OF CONTENTS

<b>I.</b>	<b>INTRODUCTION.....</b>	<b>1</b>
<b>A.</b>	<b>GENERAL INFORMATION.....</b>	<b>1</b>
<b>B.</b>	<b>THE INDIAN OCEAN.....</b>	<b>2</b>
<b>C.</b>	<b>POLITICAL AND ECONOMIC IMPORTANCE OF INDIAN OCEAN.....</b>	<b>3</b>
<b>D.</b>	<b>CLIMATOLOGY OF INDIAN OCEAN FROM PREVIOUS STUDIES.....</b>	<b>5</b>
<b>II.</b>	<b>OCEAN SURFACE CURRENTS ANALYSIS – REAL TIME (OSCAR) DATA BASE.....</b>	<b>9</b>
<b>A.</b>	<b>INTRODUCTION.....</b>	<b>9</b>
<b>B.</b>	<b>DATA PROCESSING.....</b>	<b>10</b>
<b>C.</b>	<b>THE INTERACTIVE WEB-BASED ACCESS.....</b>	<b>11</b>
<b>D.</b>	<b>DATA DOWNLOAD AND DISPLAY.....</b>	<b>13</b>
<b>III.</b>	<b>OPTIMAL SPECTRAL DECOMPOSITION (OSD) METHOD.....</b>	<b>19</b>
<b>A.</b>	<b>INTRODUCTION.....</b>	<b>19</b>
<b>B.</b>	<b>SPECTRAL DECOMPOSITION.....</b>	<b>20</b>
<b>C.</b>	<b>OPTIMAL MODE TRUNCATION.....</b>	<b>21</b>
<b>IV.</b>	<b>SEASONAL VARIABILITY.....</b>	<b>23</b>
<b>A.</b>	<b>DATA PROCESSING.....</b>	<b>23</b>
<b>B.</b>	<b>SURFACE CIRCULATIONS.....</b>	<b>23</b>
<b>C.</b>	<b>WHOLE INDIAN OCEAN.....</b>	<b>23</b>
1.	Southern Hemisphere.....	23
2.	Summer Monsoon.....	24
3.	Winter Monsoon.....	26
4.	Equatorial Regime.....	29
<b>D.</b>	<b>SOMALI CURRENT.....</b>	<b>31</b>
1.	Seasonal Development.....	32
2.	Winter Monsoon.....	35
3.	Comparison with Earlier Studies.....	37
<b>E.</b>	<b>NORTH ARABIAN SEA.....</b>	<b>37</b>
<b>F.</b>	<b>BAY OF BENGAL.....</b>	<b>40</b>
<b>G.</b>	<b>MONSOON CURRENTS.....</b>	<b>43</b>
1.	Southwest Monsoon Current (SMC).....	44
2.	Northeast Monsoon Current (NMC).....	45
<b>V.</b>	<b>INDIAN OCEAN DIPOLE AND EASTWARD EQUATORIAL JET.....</b>	<b>47</b>
<b>A.</b>	<b>THE INDIAN OCEAN DIPOLE (IOD).....</b>	<b>47</b>
<b>B.</b>	<b>DIPOLE MODE INDEX.....</b>	<b>49</b>
<b>C.</b>	<b>THE EASTWARD EQUATORIAL JET (OR WYRTKI JET).....</b>	<b>50</b>
<b>D.</b>	<b>COMPLEX EFO ANALYSIS OF THE CURRENT DATA ALONG THE EQUATOR AND COMPARISON WITH DMI.....</b>	<b>50</b>

E.	EQUATORIAL JET DURING POSITIVE DIPOLE MODE EVENTS..	54
F.	EQUATORIAL JETS DURING NEGATIVE DIPOLE MODE EVENTS.....	56
VI.	PRACTICAL APPLICATIONS.....	59
A.	OPERATIONAL USES.....	59
1.	Ocean Currents and Mine Warfare .....	59
2.	Search and Rescue at Sea .....	59
3.	Planning for an Economical Passage.....	60
4.	Monitoring Chemical Pollutants and Oil Spills .....	60
B.	SCIENTIFIC USES .....	60
1.	Ocean Currents as a Source of Energy .....	60
2.	Large-Scale Climate and Synoptic Diagnostics.....	61
VII.	SUMMARY .....	63
	LIST OF REFERENCES .....	67
	INITIAL DISTRIBUTION LIST .....	73

## LIST OF FIGURES

Figure 1-1.	Indian Ocean as seen on the Globe (From: <a href="http://www.nga.mil">www.nga.mil</a> ).....	3
Figure 1-2.	A summary of the monsoon system in the Indian Ocean. The top part indicates the wind cycle; the lower part shows the major currents that develop in response to the wind (From: Tomczak & J. S Godfrey, 1994). .....	6
Figure 2-1.	The OSCAR website (From: <a href="http://www.oscar.noaa.gov">www.oscar.noaa.gov</a> ).....	9
Figure 2-2.	OSCAR data processing flow diagram (From: <a href="http://www.oscar.noaa.gov">www.oscar.noaa.gov</a> ).....	10
Figure 2-3.	Lat-Time section plot options page (From: <a href="http://www.oscar.noaa.gov">www.oscar.noaa.gov</a> ). .....	11
Figure 2-4.	Latitude-Longitude map plot options page (From: <a href="http://www.oscar.noaa.gov">www.oscar.noaa.gov</a> ).....	12
Figure 2-5.	Time-Series plot options page (From: <a href="http://www.oscar.noaa.gov">www.oscar.noaa.gov</a> ). .....	12
Figure 2-6.	Time-Longitude section plot options page (From: <a href="http://www.oscar.noaa.gov">www.oscar.noaa.gov</a> ). ....	13
Figure 2-7.	Data Download options page (From: <a href="http://www.oscar.noaa.gov">www.oscar.noaa.gov</a> ).....	14
Figure 2-8.	(Top) Vector overlay of surface currents; (Bottom) Vector overlay of surface currents anomaly. Large eastward anomalies can be seen in eastern equatorial pacific (From: <a href="http://www.oscar.noaa.gov">www.oscar.noaa.gov</a> ).....	15
Figure 2-9.	Latitude-Longitude map of Meridional and Zonal Current Mean centered on May 2, 2008 (From: <a href="http://www.oscar.noaa.gov">www.oscar.noaa.gov</a> ). .....	16
Figure 2-10.	Latitude-Longitude map of Meridional and Zonal current anomaly centered on May 2, 2008 (From: <a href="http://www.oscar.noaa.gov">www.oscar.noaa.gov</a> ).....	16
Figure 2-11.	Time-Series plot (From: <a href="http://www.oscar.noaa.gov">www.oscar.noaa.gov</a> ).....	17
Figure 2-12.	Latitude-Time section of Zonal and Meridional currents (From: <a href="http://www.oscar.noaa.gov">www.oscar.noaa.gov</a> ).....	17
Figure 2-13.	Time-Longitude section of Zonal and Meridional currents (From: <a href="http://www.oscar.noaa.gov">www.oscar.noaa.gov</a> ).....	18
Figure 3-1.	Global surface velocity vectors on January 2-6, 2007 (From: OSCAR data).....	19
Figure 3-2.	Reconstructed global surface velocity vectors on January 2-6, 2007 (From OSCAR data using the OSD method).....	22
Figure 4-1.	Monsoon wind stress from the NCEP climatology for a) January; b) April; c) July; d) October (From: Schott & McCreary, 2001). .....	24
Figure 4-2.	Mean Surface Circulation pattern of Indian Ocean during July, derived from satellite-based altimeter data. ....	25
Figure 4-3.	A schematic representation of identified current branches during the southwest monsoon, including some chokepoint transport numbers ( $Sv=10^6 m^3 s^{-1}$ ). Current branches indicated (see also Figure 9) are the South Equatorial Current (SEC), South Equatorial Countercurrent (SECC), Northeast and Southeast Madagascar Current (NEMC and SEMC), East African Coast Current (EACC), Somali Current (SC), Southern Gyre (SG), and Great Whirl (GW); and associated upwelling wedges: Socotra Eddy (SE), Ras al Hadd Jet (RHJ), and upwelling wedges off Oman, West Indian Coast Current (WICC), Laccadive High and Low (LH and LL), East Indian Coast Current (EICC), Southwest and Northeast Monsoon Current (SMC and NMC), South Java Current (JC), and	



	Leeuwin Current (LC). See text for details. (From: Schott & McCreary, 2001). ....	26
Figure 4-4.	Mean Surface Circulation pattern of Indian Ocean during December, derived from satellite-based altimeter data. ....	27
Figure 4-5.	As in Figure 4-3, but for Northeast Monsoon (From: Schott & McCreary, 2001) .....	28
Figure 4-6.	Mean Surface Circulation pattern of Indian Ocean during January, derived from satellite-based altimeter data after OSD.....	29
Figure 4-7.	Mean Surface Circulation pattern of Indian Ocean during a) April, b) October; derived from satellite altimeter data. ....	30
Figure 4-8.	Climatological temperature at a-b) The surface during January and July, c-f) 100 m depth during January, May, July, and November, areas of relatively high temperature are shaded (From: Rao and Sivakumar, 2000). ...	31
Figure 4-9.	Reversal of Somali Current derived from mean altimeter data. ....	32
Figure 4-10.	Mean surface Somali currents for a) April, b) July, derived from satellite-based altimeter data.....	33
Figure 4-11.	Mean Somali current circulation pattern during a) August, b) October, derived from satellite altimeter data. ....	34
Figure 4-12.	Mean Somali current circulation pattern during winter monsoon, derived from satellite-based altimeter data. ....	35
Figure 4-13.	Schematic diagram of Somali current upper layer flow pattern over the course of the year (From: Schott & McCreary, 2001). ....	36
Figure 4-14.	Schematic Diagram of Somali current upper layer pattern over the course of the year derived from satellite-based altimeter data. ....	36
Figure 4-15.	Mean surface circulation pattern of the North Arabian Sea all through the year, derived from satellite-based altimeter data, showing a) January, b) April, c) July, d) October. ....	38
Figure 4-16.	Surface current vectors from drifter climatology; a) July - September, and b) December - February (From: Schott and McCreary, 2001). ....	39
Figure 4-17.	Mean surface circulation pattern of the Bay of Bengal all through the year, derived from satellite-based altimeter data showing a) January, b) April, c) July, d) October.....	42
Figure 4-18.	Surface currents in Bay of Bengal from the ship drift data; a) July, b) November (From: Eigenheer & Quadfasel, 2000).....	43
Figure 4-19.	Monsoon current transport south of India - Sri Lanka; a) Decomposition into depth bins using two different extrapolation schemes from top instrument level towards the surface: extrapolation of moored current meter shear from upper most levels (solid) or using ship drifts as surface values (dashed). The heavy curve on the left hand side shows annual mean, b) transport time-series, based on shear extrapolation; dots mark shipboard ADCP sections for comparison (From: Schott et al., 1994). ....	44
Figure 5-1.	Schematic diagram of SST anomalies (red shading, warming; blue, cooling) during a positive IOD event. White patches indicate increased convective activity. Arrows indicate wind direction. (From: A.Suryachandra Rao. Frontier Research Center for Global Change).....	47

Figure 5-2.	Schematic diagram of SST anomalies (red shading, warming; blue, cooling) during a negative IOD event. White patches indicate increased convective activity. Arrows indicate wind direction. (From: A.Suryachandra Rao., Frontier Research Center for Global Change).....	48
Figure 5-3.	Dipole Mode Index for the period 1992 – 2006. ....	49
Figure 5-4.	Amplitude of EOF Mode-1.....	51
Figure 5-5.	Amplitude of EOF a) Mode-2, b) Mode-3.....	52
Figure 5-6.	Amplitude of EOF Mode-4.....	53
Figure 5-7.	(a) Climatology of zonal currents ( $\text{cm s}^{-1}$ ) along the equator derived for satellite based observational data; (b) Anomaly of zonal currents during a positive Dipole Mode event year 1994, (c) Year 1997, and (d) Year 2006.....	54
Figure 5-8.	(a) 13-year mean climatology of surface currents along the equator during November, (b) Surface currents anomaly during November 1997.....	55
Figure 5-9.	(a) Climatology of zonal currents ( $\text{cm s}^{-1}$ ) along the equator derived for satellite based observational data; (b) Anomaly of zonal currents during Negative Dipole mode event year 1996, (c) year 1998, and (d) year 2001.....	57
Figure 5-10.	(a) 13-year mean climatology of surface currents along the equator during October, (b) Surface currents anomaly during October 1996.....	58

THIS PAGE INTENTIONALLY LEFT BLANK

## LIST OF TABLES

Table 5-1.	Percentage of Variance of first four EOF Modes. ....	51
------------	--	----

THIS PAGE INTENTIONALLY LEFT BLANK

## **ACKNOWLEDGMENTS**

First of all, I wish to thank my parents, who have been a source of inspiration and guidance to me throughout my life, and my utmost gratitude to my beautiful wife whose patient, loving nature and unflagging support made this project possible. I would also like to credit my young son whose innocent smiles at the end of the day renewed my vigor. I love you.

I also wish to thank Dr. Peter Chu for offering me a research opportunity involving the Indian Ocean region. His continuous guidance, encouragement, extreme good nature and timely suggestions made the hard work very interesting and pleasant. My special thanks to Dr. Charles Sun at NOAA for providing invaluable comments and guidelines in the completion of this thesis. Many thanks to Mr. Chenwu Fan and Mr. Mike Cook for providing the necessary assistance in computer programming.

Finally, I wish to thank the Pakistan Navy and the Naval Postgraduate School for providing me this precious learning experience. Funding for this thesis was provided by NOAA/NODC.

THIS PAGE INTENTIONALLY LEFT BLANK

# **I. INTRODUCTION**

## **A. GENERAL INFORMATION**

Much work has been done in the past to understand the surface circulation in the Indian Ocean. One of the most interesting features about the Indian Ocean climatology is its seasonal reversal or, in other words, the monsoon cycle. Its surface circulation is highly analogous to the seasonal pattern of the winds in the region. This study uses satellite-based altimetry data to analyze the surface circulation patterns in the Indian Ocean region. To accomplish this task, the observational satellite-based altimeter data from <http://www.oscar.noaa.gov/index.html> was utilized. The website contains near real-time ocean surface currents derived from satellite altimeter (JASON -1, GFO and ENVISAT) and scatterometer data with  $1^\circ \times 1^\circ$  resolution for the world oceans from  $59.5^\circ$  S to  $59.5^\circ$  N. This data is posted online as OSCAR (Ocean Surface Current Analysis – Real-time) data. This is an invaluable resource as it can be used for large-scale climate diagnostics and prediction, fisheries management, monitoring; debris drift, larvae drift, oil spills, fronts and eddies. This data can also be utilized for planning search and rescue, naval and maritime operations such as mine warfare. The methodology of OSCAR combines geostrophic, Ekman and Stommel shear dynamics, and a complimentary term from the surface buoyancy gradient. The second chapter gives a brief synopsis of the OSCAR database. The application and uses of surface current analysis are discussed in the last chapter.

Along with all the good in the OSCAR data, there are weaknesses. One of its main weaknesses is the inability to reveal ocean boundary currents, such as the Gulf Stream and Kuroshio. They are not adequately distinguishable in the plots produced by the raw OSCAR data. To refine the OSCAR data, this study used the OSD (Optimal Spectral Decomposition) method. After reconstructing the OSCAR data through OSD, the resultant data produced adequately realistic surface circulation of the lateral boundary currents. Details about the OSD method to process the noisy OSCAR data are given in the third chapter.



One of the most dynamic research avenues, in context to Indian Ocean climatology, is the phenomenon of the Indian Ocean Dipole (IOD). Although occurrence of this climate mode can be traced to ancient history, it was not identified until 1999. This is a climate mode whose occurrence is dominant in the tropical regions of the Indian Ocean. A Dipole event brings heavy rainfall over the east African region and droughts/forest fires in the Indonesian region or vice versa. The fifth chapter will analyze certain surface circulation patterns to see how we can identify the occurrence of a dipole event while seeing the anomaly in surface circulation patterns along the equator.

## **B. THE INDIAN OCEAN**

The Indian Ocean (Figure 1-1) is the world's third largest ocean. It is bounded by Asia to the north (including the Indian subcontinent, after which it is named); by Africa to the west; by Indochina, Malaysia, Indonesia, and Australia to the east; and by Antarctica to the south. The Indian Ocean has a north-south extent of about 9600 km from Antarctica to the inner Bay of Bengal. It spans up to 7800 km in the east-west direction between Southern Africa and Western Australia. Excluding its southern part, it has an area of about  $48 \times 10^6 \text{ km}^2$  and, with the Southern part, the area increases up to  $74.1 \times 10^6 \text{ km}^2$  (Tomczak & Godfrey, 1994). It separates from the Atlantic Ocean at  $20^\circ$  east meridian and from the Pacific at  $147^\circ$  east meridian. In the North, the Indian Ocean extends up to approximately  $30^\circ$  north latitude in the Persian Gulf.<sup>1</sup> There are several small islands throughout the ocean which includes Madagascar, Comoros, Seychelles, Maldives, Mauritius, and Sri Lanka.

The Indian Ocean region is the home to the world's first known urban civilization: the evidence of trade through water in this region can be traced to ancient times. This region has remained very important in terms of its export to other parts of the world. In the olden times, due to its rich agriculture, its prominent product was agricultural goods. Although it has been the region of political interest to all the world's strongest nations, no nation dominated this Ocean until the mid-1800s when the United Kingdom took control of most of its surrounding parts. Because it houses the world's

---

<sup>1</sup> Tomczak and Godfrey, (1994).

most crude oil reserves, it now again has gained a lot of attention politically and economically. In the present time, mostly India and Australia dominate the Ocean. However, after the fall of the Twin Towers in U.S., the new global war against terrorism has resulted in US-led coalition forces that are making a difference in overall dominance in the region.



Figure 1-1. Indian Ocean as seen on the Globe (From: [www.nga.mil](http://www.nga.mil))

### C. POLITICAL AND ECONOMIC IMPORTANCE OF INDIAN OCEAN

In the recent past, the Indian Ocean region has become a place of strategic importance to the world's greatest powers. The reason may be that the Indian Ocean region has played a vital role in overall facilitation to global maritime trade. The major reasons which make Indian Ocean very important in context to global maritime trade are

crude oil reserves, population, location, historical influences, and growing economies.<sup>2</sup> To see how the Indian Ocean has gained tremendous political and economic importance in the past few decades, there will be a brief discussion of a few major factors in the following subsections.

Today the Indian Ocean houses some of the busiest waterways in the world. These waterways include the Suez Canal in Egypt, Bab-el-Mandeb (along Djibouti and Yemen border), Straits of Hormuz (along Iran and Oman border), and Straits of Malacca (along Indonesia and Malaysia border). All these narrow channels, or “chokepoints,” are critical to world crude oil trade as huge amounts of oil pass through them.<sup>3</sup> An estimated 40% of the world’s offshore oil production comes from the Indian Ocean.<sup>4</sup> In political context, the Persian Gulf remains a crucial passageway. This is because all the world’s dynamic economies, which are highly dependant on foreign oil, require safe trading routes in and out of these passages. The dependence of the world’s biggest economies on foreign oil imported from the Indian Ocean rim can be judged from this fact: in present time, it has been estimated that European, Japanese and U.S. economies respectively import 70%, 76%, and 25% of their crude oil requirements from the Gulf region (Nazrey Khalid, 2005). China, as one of the fast- emerging and growing economies in the world, also has vital trading and energy interests in the Indian Ocean’s waters. The rapid economic progress in developing nations, such as India and South Africa, also adds up their interest in the safe passageways in the Indian Ocean region.<sup>5</sup> In short, it can be said that these paths not only serve as the strategic and economic lifeblood of many countries along them, but also play important roles as the main waterways for global trade especially in the energy sector. Thus, the importance of the Indian Ocean as a facilitator to the world’s trade cannot be undermined.

---

<sup>2</sup> Nazery Khalid (2005).

<sup>3</sup> World Oil Transit Chokepoints, Report by Energy Information Administration. Washington, DC. March 2004.

<sup>4</sup> World Fact Book (CIA).

<sup>5</sup> Nazery Khalid (2005).

Besides the huge oil trade in the Indian Ocean region, the vast consumer market makes the Indian Ocean region economically dynamic. The population of the Indian Ocean rim is close to two billion. This provides an enormous market for trade and consumerism.<sup>6</sup> Recently there has been a significantly increasing trend: countries in this region moved from inward-looking economies to now opening up their economies at many different avenues. This development has also given rise to new opportunities for international trade most of which is through water. Hence, with all that has been discussed above about the Indian Ocean, it is evident that it will continue to play a crucial role in the overall facilitation to global maritime trade.

For centuries, the Indian Ocean region has remained politically important. After the end of the first Gulf War in the early 1990s, its importance has increased exponentially in terms of providing safe passages to the maritime trade. The Indian Ocean rim consists of the world's fast growing economies of India, Far East, and the Gulf region. All these economies, along with other big world economies, want peace and stability in this region to acquire safer trade. The vitality of safety of these passages can be judged from the consistent patrolling of U.S.-led coalition naval forces in the northern Indian Ocean. In short, it can be said that as the world's bigger economies' appetite for oil is growing and developing nations are coming on the road to massive industrialization, the Indian Ocean region will gain more and more importance proportionally.

#### **D. CLIMATOLOGY OF INDIAN OCEAN FROM PREVIOUS STUDIES**

Before we proceed to analyze the Satellite based altimeter data to investigate the Indian Ocean region it is necessary that we should have an idea about the general dynamics and climatology of this region. Amongst the general climatology it is the wind flow which affects the ocean surface currents the most. Therefore in the following subsections we will see how the conventional wind flow in the Indian Ocean region looks like. Most of the work presented here is taken from Regional Oceanography by Tomczak and Godfrey (1994).

---

<sup>6</sup> Sheth (2002).

One of the interesting features of the Indian Ocean wind flow pattern is its seasonal reversal. This is generally known as the monsoon cycle. This reversal in turn produces reversed climatological conditions especially in the northern Indian Ocean. The effects of this climatological cycle can be felt even up to southern subtropics. Figure 1-2 summarizes the monsoon cycle of the Indian Ocean. How this seasonal reversal is developed, and what are its effects on the surrounding regions, is briefly discussed in this subsection.

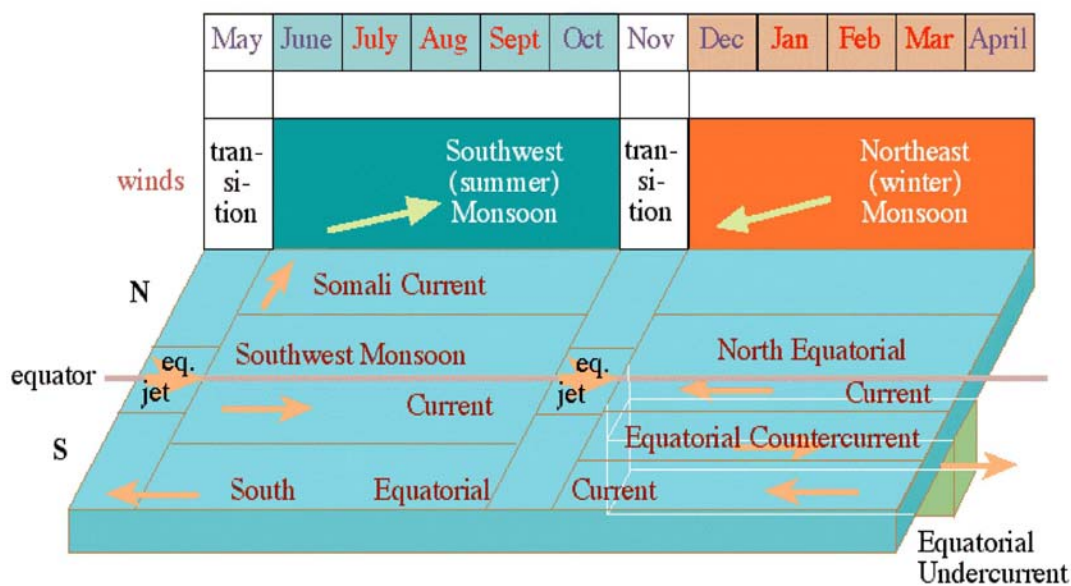


Figure 1-2. A summary of the monsoon system in the Indian Ocean. The top part indicates the wind cycle; the lower part shows the major currents that develop in response to the wind (From: Tomczak & J. S Godfrey, 1994).

In northern hemisphere winter (from December to March), the northeast monsoon determines the climatology of the northern part of the Indian Ocean. During this time, high pressure develops over the Indian land mass. The reason is two-fold: in winter the land mass cools up quickly as compared to the ocean surface and relatively hot air over the ocean tends to rise. This creates a zone of low pressure over the ocean. Because of this pressure, gradient northeasterly winds flow over the tropical region. These winds over the northern Indian Ocean are the Trades. However, due to their seasonal cycle they

are known as the northeast monsoon (the word 'monsoon' is an Arabic word meaning seasonally reversing winds). During this time, the Inter-tropical Convergence Zone (ITCZ) and the Doldrums are located south of the equator at about 5°S (Tomczak and Godfrey, 1994). Most of the air pressure gradient during this time is retained behind the Tibetan Plateau, whereas the air pressure gradient over the ocean is small. This results in a wind of moderate force over the ocean. This wind is also dry; therefore, the winter season is dry over most of southern Asia.

During this time, in the southern hemisphere, the climatology is determined by the low pressure in the tropical region and by the high pressure in the sub tropical belts. As a result of this pressure, gradient Southeast Trades' flow is relatively stronger and uniform than in the Pacific Ocean. Similar to the other oceans along the eastern coast, the wind flow is southerly. Alternatively, Australia's Northwest Shelf winds become southwesterly. This avoids the low heat over the Australian continent. This climatological pattern during the southern hemisphere's summer brings rain to northern Australia. This season also brings rain throughout the doldrums, with the Indonesian region getting maximum rainfall.

In the northern hemisphere's summer, it is the southwest monsoon that determines the climatology of the Indian Ocean. During this time of the year, the land mass heats up quickly due to the intense hot climate over the land compared to the ocean's relative coolness. Due to this pressure dynamics, a deep low pressure develops over northern Arabia and Pakistan. Australia in the southern hemisphere winter now has a center of high pressure. The atmospheric high north of Kerguelen Islands is also shifted westward towards southern Africa. The pressure gradient between Arabia and Madagascar is about 22 hPa. This never exceeds 6 hPa during the winter season (Tomczak and Godfrey, 1994). As a result of this climatological change, the winds over the northern Indian Ocean completely reverse their direction and a wind jet blows in a northerly direction. This southwest monsoon in the northern hemisphere is the continuation of southern hemisphere Trades which, during this time of the year, between 10° and 20°S are stronger than anywhere else in the world (Tomczak and Godfrey, 1994). Over the ocean there is a very little change in the ITCZ but during the southwest monsoon the frequent

disturbances breakaway and it settles down south of the Himalayas. The southwest monsoon passes over the low in the Indian sub-continent to bring the well-known monsoon rains and floods to the region, which is very critical to the agriculture of this region.

## II. OCEAN SURFACE CURRENTS ANALYSIS – REAL TIME (OSCAR) DATA BASE

### A. INTRODUCTION

The web site dedicated to access Ocean Surface Currents Analyses – Real-time (OSCAR) data at <http://www.oscar.noaa.gov/index.html> is an invaluable resource that provides near real-time world oceans surface current fields. Subsequently, these fields can be used for different operational purposes. These surface current fields are automatically computed with the combination of gridded data derived from satellite-based altimeters and scatterometer (Bonjean et al., 2004). The automatic mechanism to compute this data has been developed at Earth and Space Research (ESR), whereas, the web-based access system is developed at Pacific Marine Environmental Laboratory (PMEL). Figure 2-1 shows a snap shot of the home page of the web server.

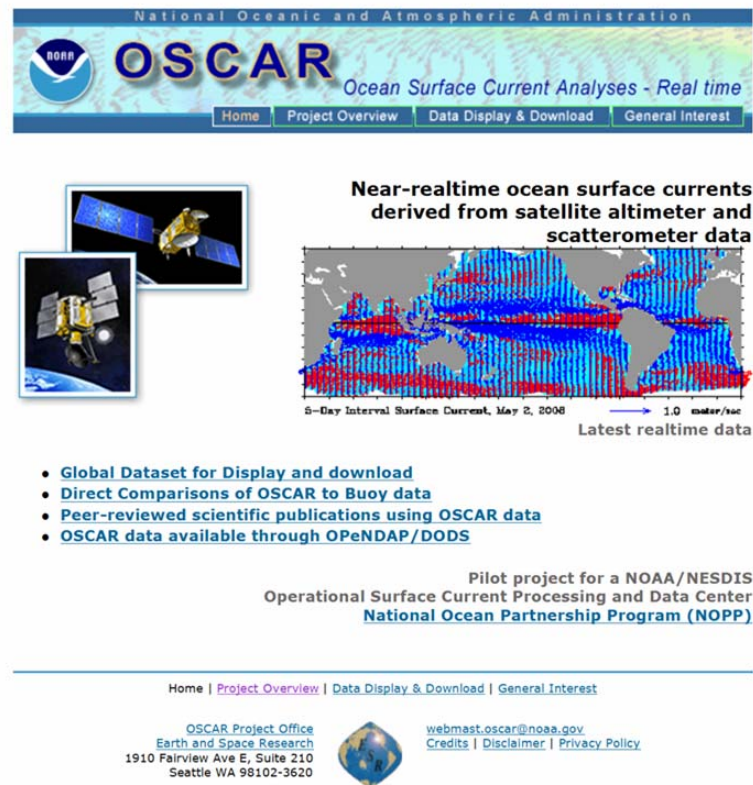


Figure 2-1. The OSCAR website (From: [www.oscar.noaa.gov](http://www.oscar.noaa.gov)).



## B. DATA PROCESSING

The OSCAR near real-time surface current fields are available to the users every five days starting from October 1992 for the world oceans from 60 N to 60 S. Figure 2-2, taken from the OSCAR website, shows the flow diagram of how data is being processed and what organizations are participating to make it useful for the end user. The automated system developed at ESR collects up-to-date sea surface height (SSH), wind and sea surface temperature (SST) data. These are used to calculate ocean surface current fields that can then be accessed and downloaded from the web server.

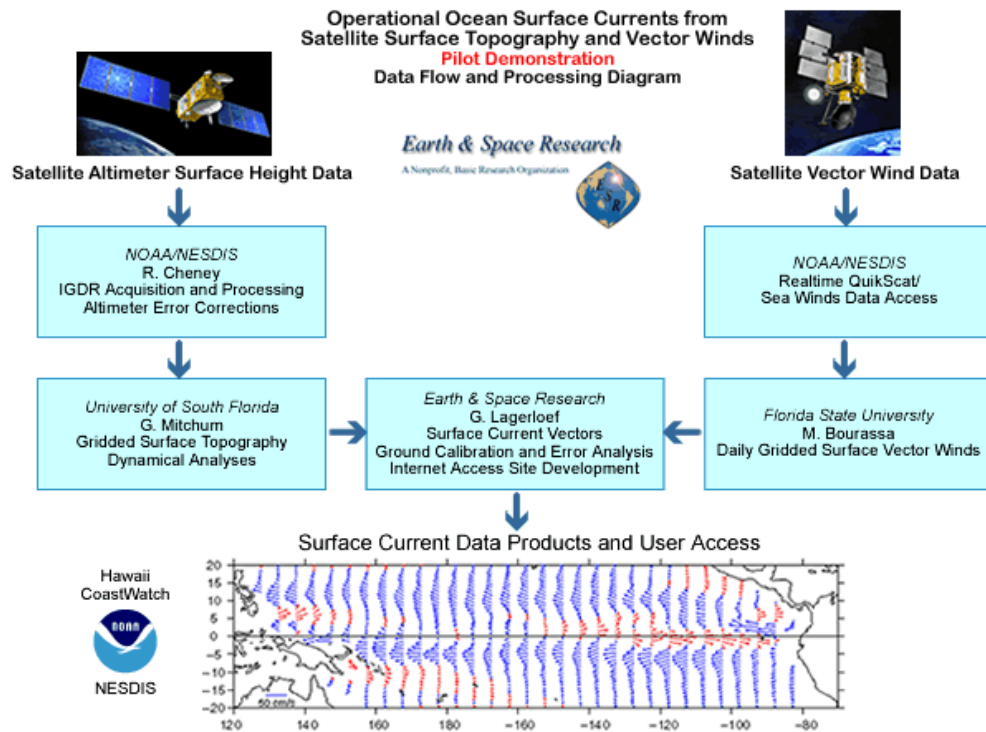


Figure 2-2. OSCAR data processing flow diagram (From: [www.oscar.noaa.gov](http://www.oscar.noaa.gov)).

The system gets the ocean surface topography, or the sea surface height data, from satellite-based altimeters JASON-1 (10-day cycle), GFO, and ENVISAT. The geostrophic winds' data is derived from QUIKSCAT satellite. Initially, from 1992 to 2006, the ocean surface current fields were derived from satellite-based altimeters TOPEX/POSEIDON and ERS1-2 and radiometer SSM/I. Downloadable data files from

the website can be used for many subsequent scientific and operational purposes. This may include search and rescue planning, mine warfare climate diagnostics, and monitoring drifts of different suspended particles. In many studies, this data has been used to monitor large-scale eddies.

### C. THE INTERACTIVE WEB-BASED ACCESS

The interactive web-based access to OSCAR data uses JavaScript-based applications. The user can either select the desired region and time frame to get an online plot to analyze the climatological dynamics in that particular area or the data files can be downloaded for further analysis. The JavaScript-based user interface provides users great flexibility in extraction or display of the data, as their needs demand. Users can select latitude-longitude maps, latitude-time sections, time-longitude sections, and time-series plots of desired geographical region and time period. Figures 2-3 to 2-6 show different user interfaces that are provided on the website.

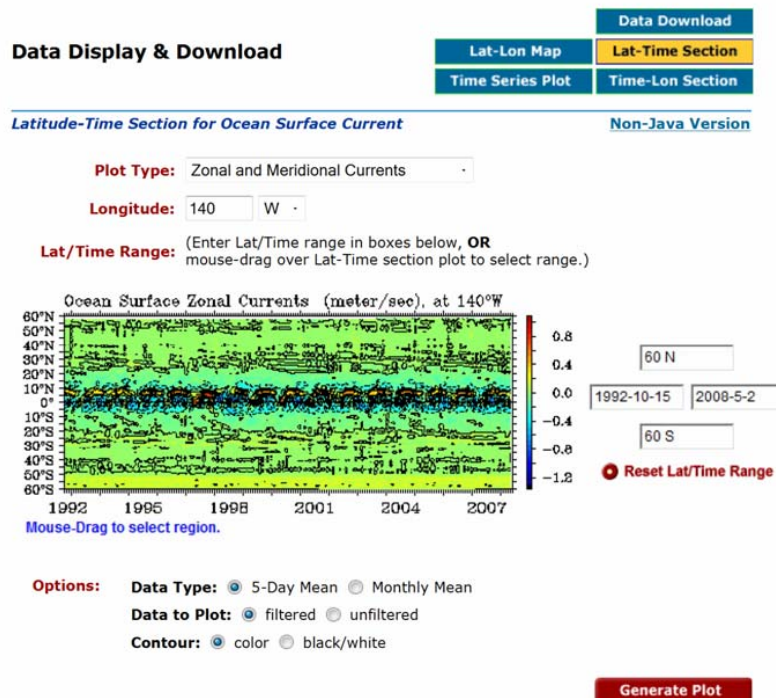


Figure 2-3. Lat-Time section plot options page (From: [www.oscar.noaa.gov](http://www.oscar.noaa.gov)).

### Data Display & Download

**Latitude-Longitude Map for Ocean Surface Current**

[Non-Java Version](#)

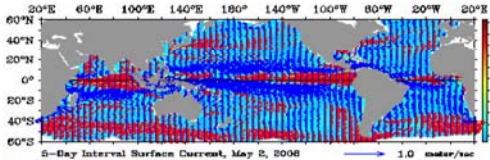
<b>Data Download</b>
<b>Lat-Lon Map</b>
<b>Lat-Time Section</b>
<b>Time Series Plot</b>
<b>Time-Lon Section</b>

---

**Data Type:** ☒ 5-day Interval ☐ Monthly Mean  
☐ Mean over user selected time range  
☐ Long Term Mean (1993-2006)  
☐ Seasonal Mean (user select date range)

**Plot Type:** Vector overlay Speed  
(plot type marked with \* are not available for long term mean and seasonal mean data.)

**Location:** (Enter Longitude and Latitude Range in boxes below,  
**OR** mouse-drag over map to select region.)



5-Day Interval Surface Current, May 2, 2008      1.0 m/s  
 Mouse-Drag to select region.

**Date:** for 5-day or monthly mean: 2008 · May · 1  
(start from Oct 15, 1992)  
**OR,**  
 for mean over user selected time range or seasonal mean:  
**Month/Day Range:** Jan · / all · to Mar · / all ·  
**Year Range:** 1993 · to 2007 ·

**Options:** Data to Plot: ☒ filtered ☐ unfiltered data  
 Contour: ☒ color ☐ none

Figure 2-4. Latitude-Longitude map plot options page (From: [www.oscar.noaa.gov](http://www.oscar.noaa.gov)).

### Data Display & Download

**Time Series for Ocean Surface Current**

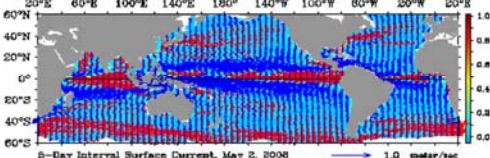
[Non-Java Version](#)

<b>Data Download</b>
<b>Lat-Lon Map</b>
<b>Lat-Time Section</b>
<b>Time Series Plot</b>
<b>Time-Lon Section</b>

---

**Select a geographical range for averaged Time Series:**

**Location:** (Enter Longitude and Latitude Range in boxes below,  
**OR** mouse-drag over map to select region.)



5-Day Interval Surface Current, May 2, 2008      1.0 m/s  
 Mouse-Drag to select region.

**Date Range:** 1993 · Jan · 1 · to 2008 · May · 1 ·

**Options:** Data to Plot: ☒ filtered ☐ unfiltered

**Variables to Plot:** ☒ u ☒ v ☒ u-anomaly ☒ v-anomaly

Figure 2-5. Time-Series plot options page (From: [www.oscar.noaa.gov](http://www.oscar.noaa.gov)).

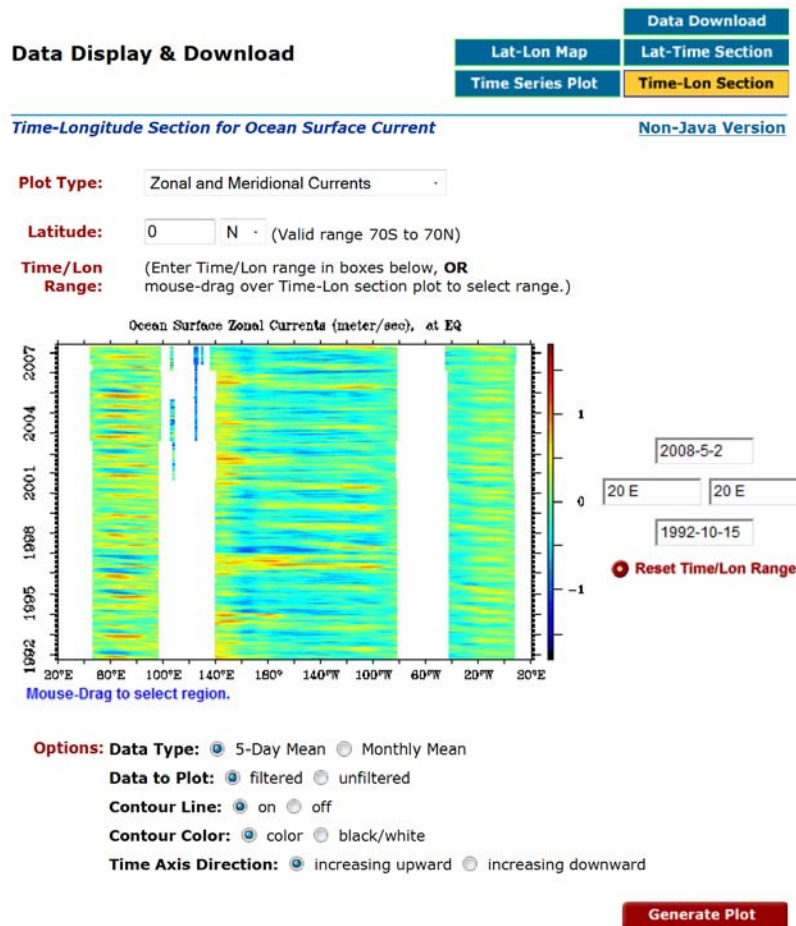


Figure 2-6. Time-Longitude section plot options page (From: [www.oscar.noaa.gov](http://www.oscar.noaa.gov)).

#### D. DATA DOWNLOAD AND DISPLAY

Data can be downloaded from the website. Geographical limits and other parameters can be applied through the Data Download interface (Figure 2-7). The download interface gives the user a variety of options to download data per one's unique needs. For download only, unfiltered data is available and the user can select 5-day mean, monthly mean or long-term mean data sets. In terms of variables, either (U, V) mean or anomaly data can be downloaded. All data sets can also be downloaded from the dapper server (Sirott et al., 2004) at <http://dapper.pmel.noaa.gov/dapper/oscar>. All the downloadable files are in the netCDF format and can be further processed with Matlab.

## Data Display & Download

Data Download	
Lat-Lon Map	Lat-Time Section
Time Series Plot	Time-Lon Section

---

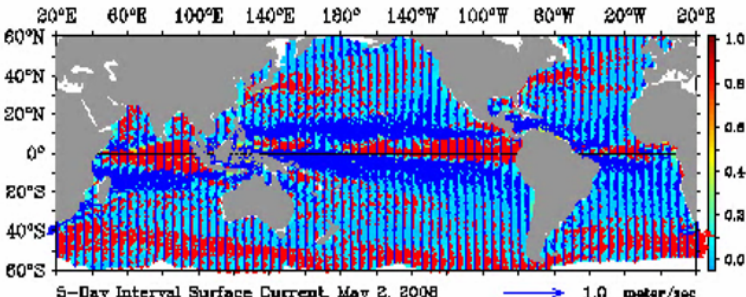
Data Download for Ocean Surface Current
Non-Java Version

**Data Type:**   ☒ 5-day Mean   ☐ Monthly Mean   ☐ Long Term Mean (1993-2006)

**Filter Type:**   ☒ unfiltered

**Variable Type:**   ☒ U & V mean   ☐ U & V anomaly

**Location:**   (Enter Longitude and Latitude Range in boxes below,  
**OR** mouse-drag over map to select region.)



Mouse-Drag to select region.

● Reset Location Range

**Date Range:**   1992 · Oct · 15 · to 2008 · May · 5 ·

Figure 2-7. Data Download options page (From: [www.oscar.noaa.gov](http://www.oscar.noaa.gov)).

One of the handiest features of OSCAR website is that a user can directly get plots for the region of interest. Online surface currents' plots can be generated in the shape of a Lat-Lon Map, Lat-Time Section, Time-Lon Section, and Time-Series Plot. For online plots, a variety of options are available to generate the desired surface currents' plot. Selectable options are "Data Type" in which one can select 5-day interval data, monthly mean, mean over selected range and long- term or seasonal mean (Figure 2-4). "Plot Type" describes the shape of the final plot that can be a vector mean or a vector anomaly plot. Plots can also be generated solely for the meridional or zonal current components (Figures 2-9 and 2-10). Users can also set the time and geographical limits of



the final plot. For online display, both filtered and unfiltered data are available. For vector overlay anomaly red color has already been set in the system for eastward anomaly (Figure 2-8) and blue for westward anomaly. Scaling can also be applied to the plots.

Time-Series plot (Figure 2-11) can be generated for any desired range of time starting from 1992 either with filtered or unfiltered data. Also Lat-Time plot (Figure 2-12) and Time-Lon plot (Figure 2-13) can be generated online for the desired selection of Latitude and Time or Time and Longitude.

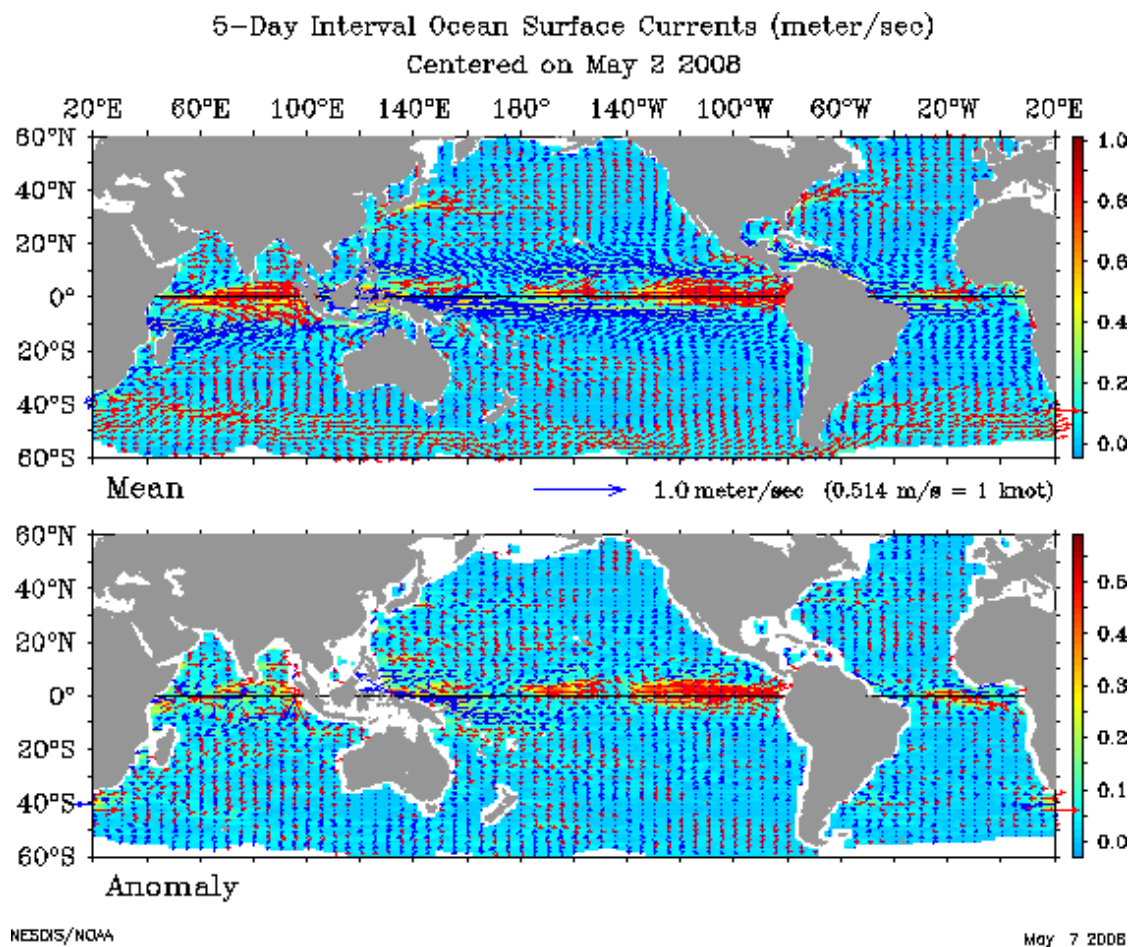


Figure 2-8. (Top) Vector overlay of surface currents; (Bottom) Vector overlay of surface currents anomaly. Large eastward anomalies can be seen in eastern equatorial pacific (From: [www.oscar.noaa.gov](http://www.oscar.noaa.gov)).

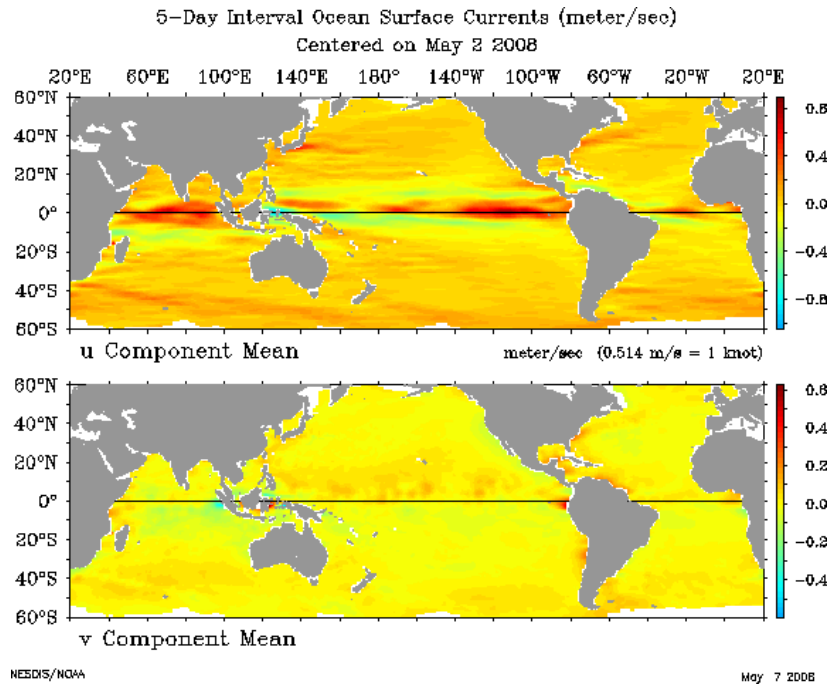


Figure 2-9. Latitude-Longitude map of Meridional and Zonal Current Mean centered on May 2, 2008 (From: [www.oscar.noaa.gov](http://www.oscar.noaa.gov)).

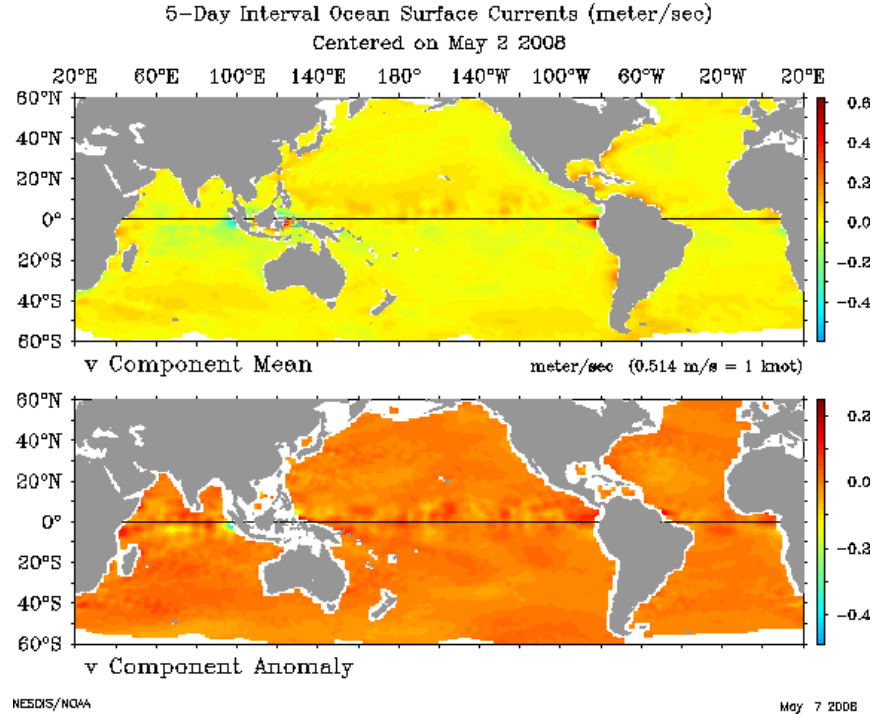


Figure 2-10. Latitude-Longitude map of Meridional and Zonal current anomaly centered on May 2, 2008 (From: [www.oscar.noaa.gov](http://www.oscar.noaa.gov)).

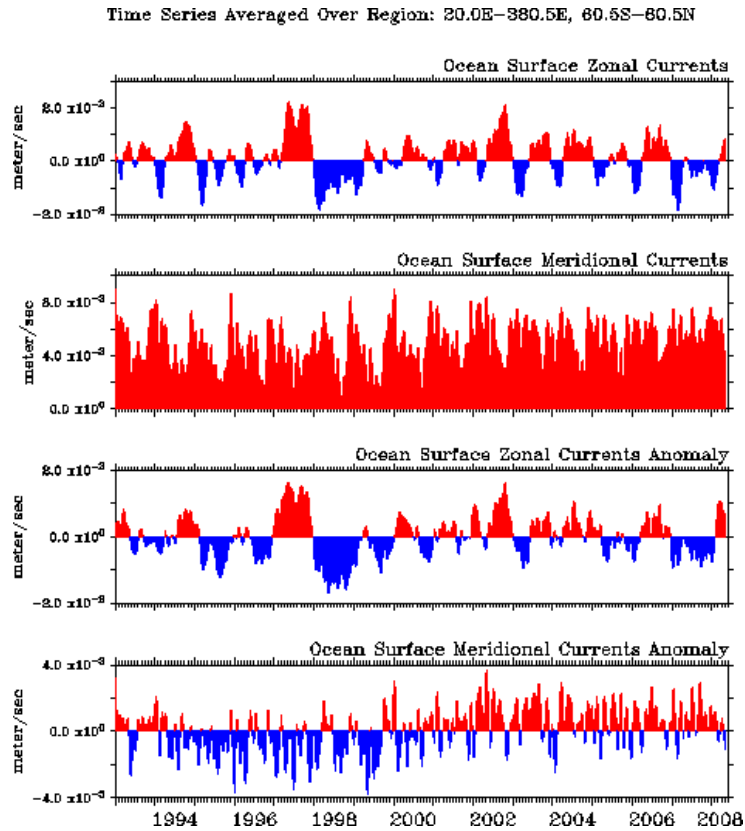


Figure 2-11. Time-Series plot (From: [www.oscar.noaa.gov](http://www.oscar.noaa.gov)).

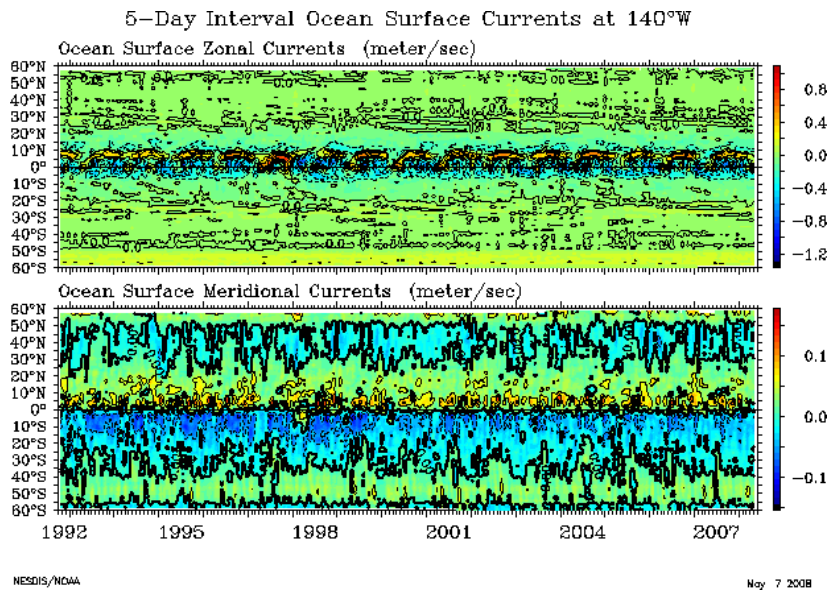


Figure 2-12. Latitude-Time section of Zonal and Meridional currents (From: [www.oscar.noaa.gov](http://www.oscar.noaa.gov)).



### 5-Day Interval Ocean Surface Currents at EQ

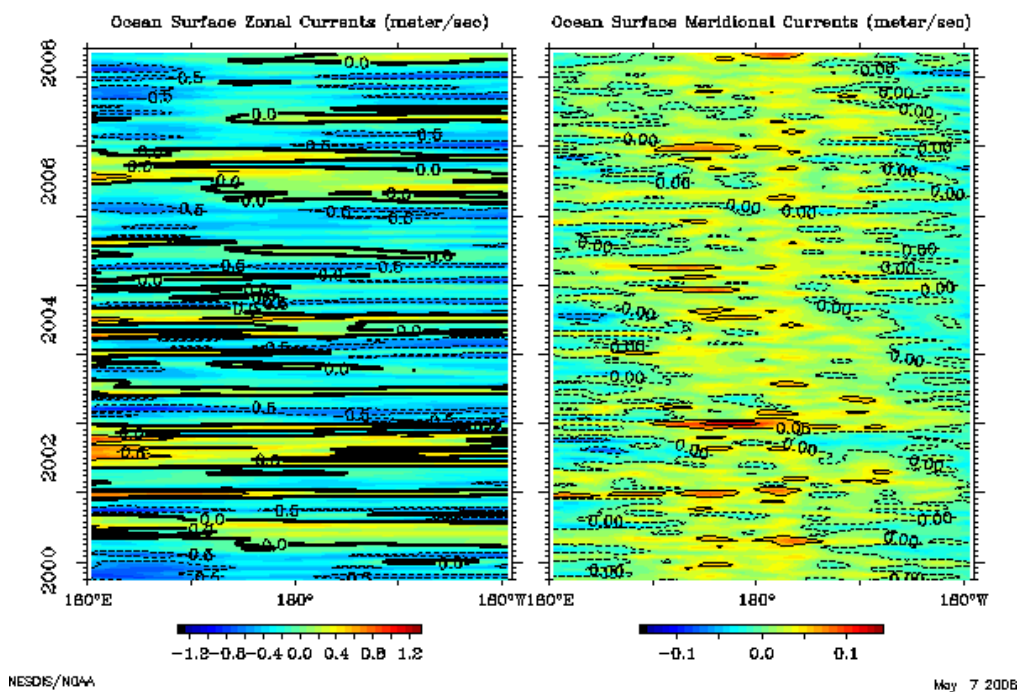


Figure 2-13. Time-Longitude section of Zonal and Meridional currents (From: [www.oscar.noaa.gov](http://www.oscar.noaa.gov)).

### III. OPTIMAL SPECTRAL DECOMPOSITION (OSD) METHOD

#### A. INTRODUCTION

A major weakness of the OSCAR dataset is its inability to reveal the coastal boundary currents, such as the Gulf Stream and the Kuroshio. Besides, the data is quite noisy (Figure 3-1).

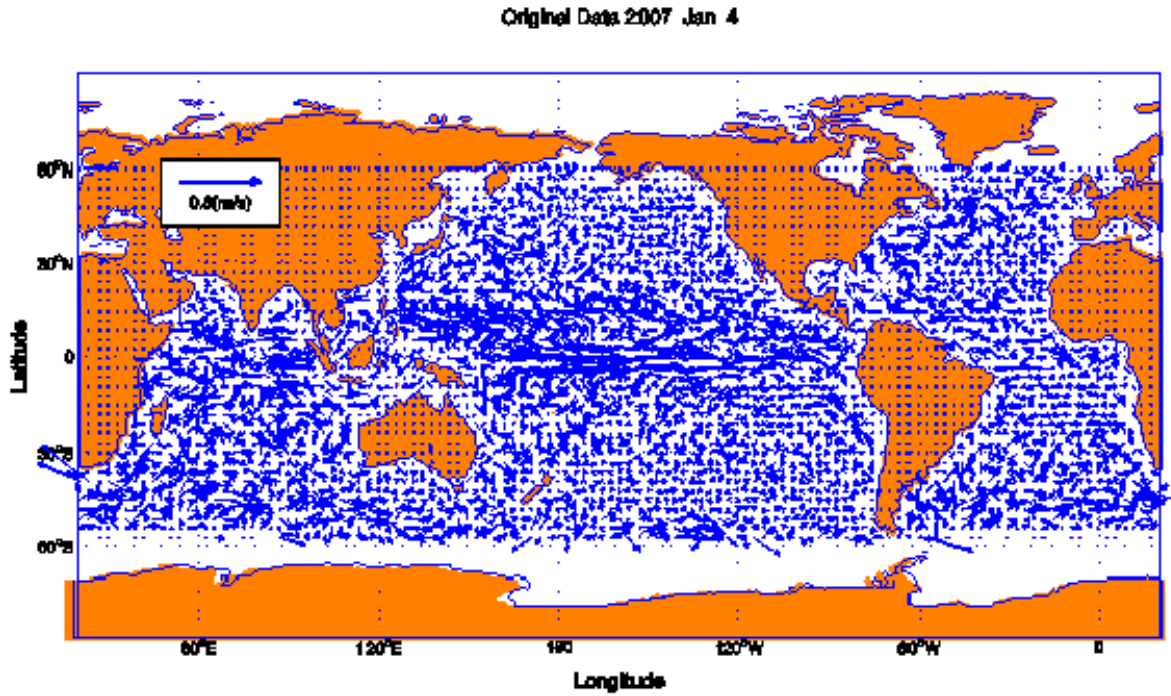


Figure 3-1. Global surface velocity vectors on January 2-6, 2007 (From: OSCAR data)

To improve the deficiencies of the OSCAR data system, this study uses the Optimal Spectral Decomposition (OSD) method. Any field (temperature, salinity, or velocity) can be decomposed into generalized Fourier series using the OSD method. The three-dimensional field is then represented by linear combination of the products of basis functions (or the so-called modes) and corresponding Fourier coefficients. If a rectangular closed ocean basin is considered, the basis functions are sinusoidal functions. If a realistic ocean basin is considered, the basis functions are the eigen-values of the

three-dimensional Laplace operator with real topography. The Fourier coefficients are determined from observational data through solving a set of linear algebraic equations. One major benefit of using the OSD method is that the boundary conditions for the ocean variables (temperature, salinity, and velocity) are always satisfied (Chu et al., 2003a, b; 2004, 2007).

## B. SPECTRAL DECOMPOSITION

Following Chu et al., 2003a, and Chu et al., 2005, a velocity field  $\mathbf{U}(\mathbf{x}_o, t)$  at any point of the area of interest  $\Omega$  can be written in the form of parameter-weighted sums of the harmonic  $Z_i(\mathbf{x}_o)$  and basis  $\Psi_k(\mathbf{x}_0)$  functions by

$$\mathbf{U}(\mathbf{x}_o, t) = \sum_{s=1}^S b_s(t) [\mathbf{k} \times \nabla Z_s(\mathbf{x}_o)] + \sum_{k=1}^K a_k(t) [\mathbf{k} \times \nabla \Psi_k(\mathbf{x}_o)] \quad (3-1)$$

The coefficients  $b_s(t)$  and  $a_k(t)$  in Eq. (3-1) are functions of time;  $\mathbf{k}$  is the unit vector orthogonal to the surface  $z=\text{const}$  and pointing upward; and  $\nabla = (\nabla_\varphi, \nabla_\lambda)$  is the horizontal gradient operator. A set of harmonic functions,  $Z_s$ , is introduced to account for the multi-connection feature of  $S$  (i.e., existence of islands) and/or disconnected rigid boundaries (if applicable).

The harmonic and basis functions used in (3-1) satisfy the following equations

$$\Delta Z_s = 0, \quad \Delta \Psi_k = -\nu_k \Psi_k \quad (3-2)$$

where  $\Delta$  is the horizontal Laplacian operator and  $\nu_k$  are eigen-values of corresponding spectral problem. Boundary conditions (to be specified in the next Section), in general, assume imposing of no-flux through a rigid boundary and normal derivatives along an open boundary.

For the given harmonic,  $Z_i(\mathbf{x}_o)$ , and basis,  $\Psi_k(\mathbf{x}_0)$ , functions, and a series of original OSCAR velocities,  $\mathbf{U}_{obs}$ , Eq. (3-1) is used to construct an appropriate variation problem and estimate unknown spectral coefficients  $\mathbf{a} = [a_1, \dots, a_K]^t$ ,  $\mathbf{b} = [b_1, \dots, b_S]^t$ , and the optimal truncation number  $K$ . Here,  $\dots^t$  is the transpose operator. When the spectral

coefficients,  $\mathbf{a} = [a_1, \dots, a_K]^t$ ,  $\mathbf{b} = [b_1, \dots, b_S]^t$ ,  $\mathbf{c} = [c_1, \dots, c_M]^t$ , and the optimal truncation numbers,  $K$  and  $M$ , have been estimated, Eq. (3-1) is used again to project the velocity on the OSCAR grid.

### C. OPTIMAL MODE TRUNCATION

The optimal mode truncation number ( $M_{opt}$ ) is defined as the critical mode number with the set of spectral coefficients  $\{a_k\}$  least sensitive to observational data sampling and noise. For sample size of  $P$  and mode truncation of  $M$ , the spectral coefficients  $\{a_k\}$  are estimated by the least square difference between observed and calculated values,

$$J_{emp} = J(\tilde{a}_1, \dots, \tilde{a}_K, P, M) = \frac{1}{P} \sum_{j=1}^P \left( c^{(j)} - \sum_{m=1}^K \tilde{a}_m(z, t) \Psi_m^{(j)}(\mathbf{x}, z) \right)^2 \rightarrow \min \quad (3-3)$$

where the symbol “ $\sim$ ” represents the estimated value at  $(\mathbf{x}, t)$ . For homogeneously sampled data, with low noise and without systematic error, the empirical cost function  $J_{emp}$  should tend to 0 monotonically as  $M$  increases to infinity. The set of the spectral coefficients  $\{a_k\}$  depends on the mode truncation  $M$ . Optimal estimation of  $\{a_k\}$  is equivalent to the determination of  $M_{opt}$  [Ivanov et al., 2001a and Chu et al., 2003 a, b].

$$\text{A modified cost function} \quad J \leq \frac{J_{emp}}{1 - \sqrt{\frac{M \left( \ln \frac{P}{M} + 1 \right) - \ln(1 - \tau)}{P}}}, \quad (3-4)$$

is used to determine the optimal mode truncation  $M_{opt}$ . Here,  $\tau$  is the probability of  $|J - J_{emp}| \rightarrow 0$  as  $M$  increases.

For the global oceans,  $M_{opt}$  is 30–50 for the basin-scale ( $\sim 300$  km) variability and 150 for the mesoscale ( $\sim 20$  km) variability [Chu et al., 2005a]. For sparse and noisy data, it is difficult to get reliable and stable estimates of all the necessary spectral coefficients, but the first few spectral coefficients are reliable and stable. Figure 3-2 shows the global velocity vectors on January 2-6, 2007 after using the OSD method on the OSCAR data. It

shows that the global circulations are much more reasonable with evident boundary currents, such as the Gulf Stream and the Kuroshio.

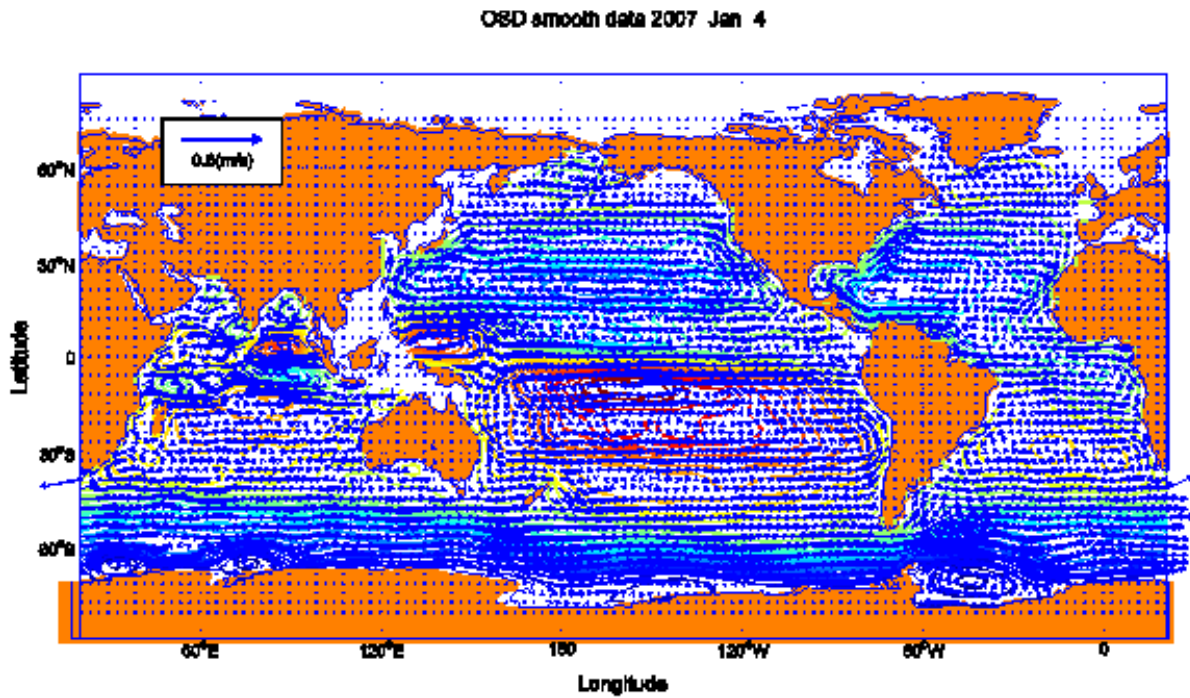


Figure 3-2. Reconstructed global surface velocity vectors on January 2-6, 2007 (From OSCAR data using the OSD method).

## **IV. SEASONAL VARIABILITY**

### **A. DATA PROCESSING**

The monthly mean surface currents were reconstructed from the OSD-reprocessed OSCAR data. This data was derived from 1993 - 2006 satellite altimetry. This study will first look at the whole Indian Ocean during the two monsoon regimes; then it will discuss, in detail, the circulation patterns of the three most dynamic regions of the Indian Ocean (Somali Current, North Arabian Sea, and Bay of Bengal).

### **B. SURFACE CIRCULATIONS**

In Chapter I, the study showed visuals of the conventional seasonal wind flow in the Indian Ocean region, which is the main contributing factor in driving the ocean surface circulations. In this chapter, this study will analyze the seasonal variability in surface circulation patterns for the Indian Ocean using the OSD-reprocessed satellite altimeter data. For the whole Indian Ocean, this study analyzes the two typical monsoon regimes and performs side-by-side comparisons with results from the most recent studies.

### **C. WHOLE INDIAN OCEAN**

#### **1. Southern Hemisphere**

Figures 4-2 and 4-4 show a broad zonal eastward flow of the South Equatorial Current (SEC). The southeasterly Trades drive this (Figure 4-1). This broad zonal flow supplies the western boundary currents along the eastern coast of Madagascar (Figure 4-2). The same flow pattern has also been observed by Schott and McCreary, (2001). In about the center of Madagascar, the SEC splits into northward and southward flowing branches. The northern branch, which is known as the Northeast Madagascar Current (NEMC), supplies the East African Coast Current (EACC). The southward branch flow as the Southeast Madagascar Current (SEMC). From the results produced by the altimetry data, it was observed that ocean currents south of about 15° S do not show much seasonal variability. Therefore, results from altimeter data, Figures 4-2 and 4-4

show almost the same branches in SEC regimes in both seasons. The same has been observed by others e.g., Swallow et al. (1988), and represented in an earlier study by Schott and McCreary (2001) in Figures 4-3 and 4-5.

## 2. Summer Monsoon

Figure 4-2 shows the mean surface circulation of the Indian Ocean during July derived from the satellite-based altimeter data. During the summer monsoon as described in the previous studies, the SEC and EACC supply the northward flowing Somali current. Figure 4-2 clearly shows that part of Somali current is recirculating to form the “Southern Gyre” near the south of the equator. The other part is moving in the northward direction. A gyre, known as the “Great Whirl,” is formed just north after crossing the equator. The same has also been observed by Schott and McCreary (2001). Figure 4-3 also shows the presence of a small eddy, the “Socotra Eddy,” which is not evident in the current field produced with the satellite altimeter data (Figure 4.2).

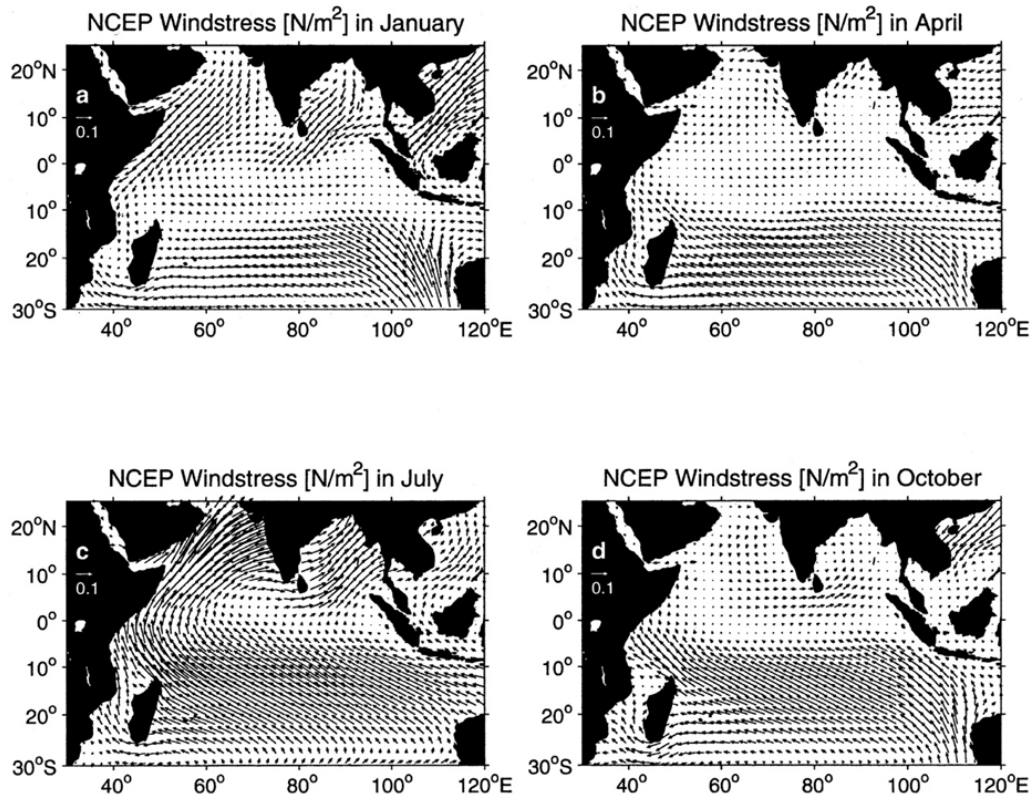


Figure 4-1. Monsoon wind stress from the NCEP climatology for a) January; b) April; c) July; d) October (From: Schott & McCreary, 2001).

During summer, the Southwest Monsoon Current (SMC) flows eastward (Figure. 4-2). This flow is also confirmed by Schott and McCreary (2001) (Figure 4-3). Figure 4-2 shows that SMC is supplied by the outflow of Somali current and that some of its supply seems to be coming from the southward-flowing West Indian Coastal Current (WICC). Along the eastern coast of India, we can see a weak flow of the East Indian Coastal Current (EICC) which flows northeastward all along the coast (Figures 4-2 and 4-3). The EICC gets most of its supply from the Southwest Monsoon Current (SMC) to the east of Sri Lanka. Along the eastern coast of Madagascar, South Equatorial current (SEC) splits up into two branches: one moves northward as the Northeast Madagascar Current (NEMC); the other moves southward as the Southeast Madagascar Current (SEMC). Presence of an eddy can also be seen towards the northwestern edge of Madagascar. This has also confirmed by the previous studies. In case of the Leeuwin Current, the general southward flowing direction cannot be seen in the results of this study. This is a weakness of the satellite altimetry data.

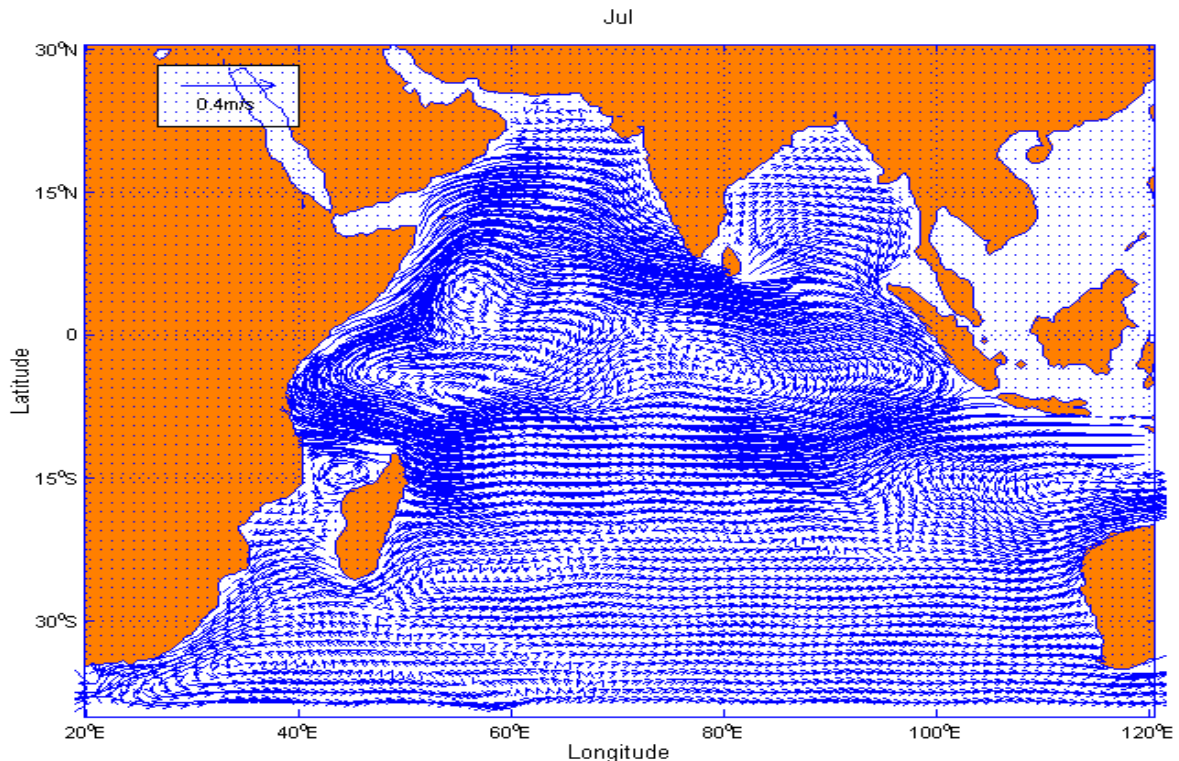


Figure 4-2. Mean Surface Circulation pattern of Indian Ocean during July, derived from satellite-based altimeter data.



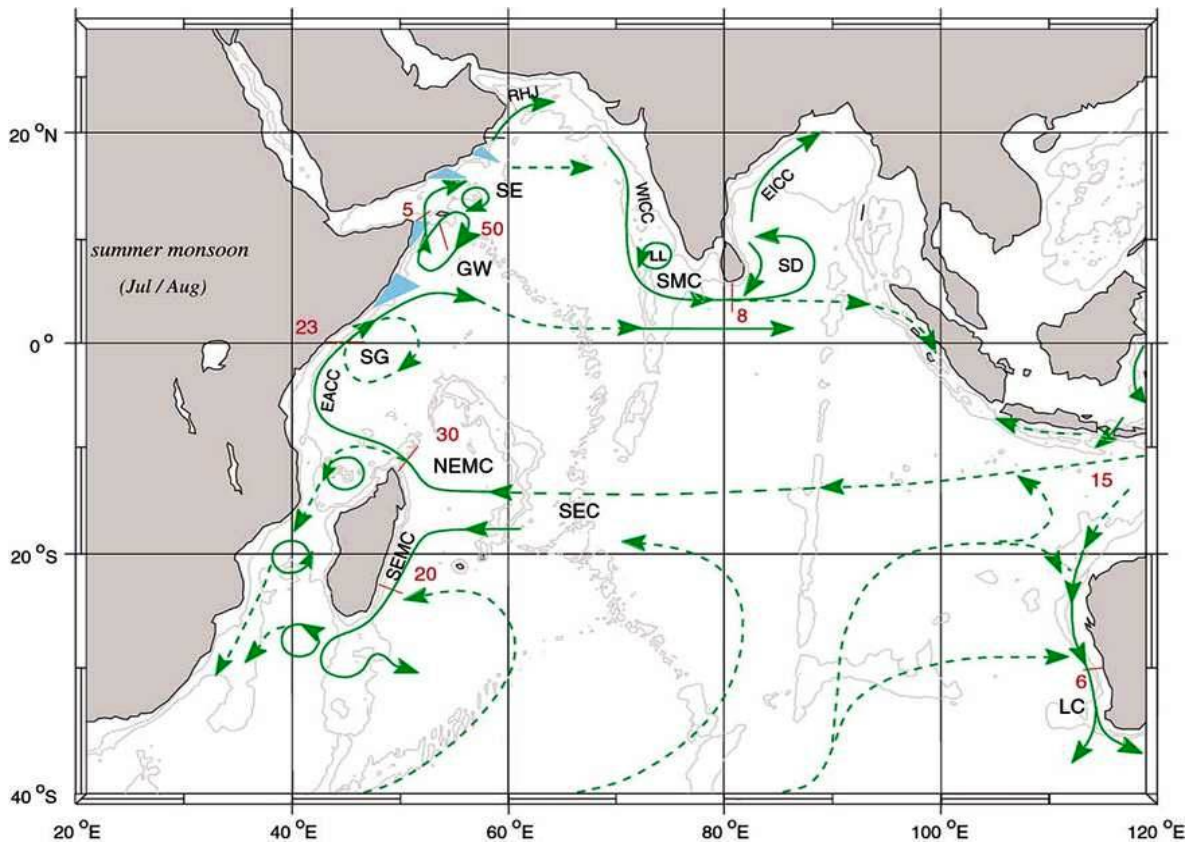


Figure 4-3. A schematic representation of identified current branches during the southwest monsoon, including some chokepoint transport numbers ( $Sv=10^6 m^3 s^{-1}$ ). Current branches indicated (see also Figure 9) are the South Equatorial Current (SEC), South Equatorial Countercurrent (SECC), Northeast and Southeast Madagascar Current (NEMC and SEMC), East African Coast Current (EACC), Somali Current (SC), Southern Gyre (SG), and Great Whirl (GW); and associated upwelling wedges: Socotra Eddy (SE), Ras al Hadd Jet (RHJ), and upwelling wedges off Oman, West Indian Coast Current (WICC), Laccadive High and Low (LH and LL), East Indian Coast Current (EICC), Southwest and Northeast Monsoon Current (SMC and NMC), South Java Current (JC), and Leeuwin Current (LC). See text for details. (From: Schott & McCreary, 2001).

### 3. Winter Monsoon

Figure 4.4 shows the mean surface circulation of the Indian Ocean during December, derived from the satellite based altimeter data. It can be seen that the northward flowing East African Coastal Current (EACC) and the southward flowing

Somali Current meet in a confluence zone at about 1-4° S. Then both supply the eastward flowing South Equatorial Countercurrent (SECC) (Figure 4-4). This pattern is the same in Schott and McCreary (2001) (Figure 4-5). On the eastern end of the SECC, the South Java Current (Figure 4-4) flows southeastward. The same circulation pattern of SECC can also be seen in Figure 4-5.

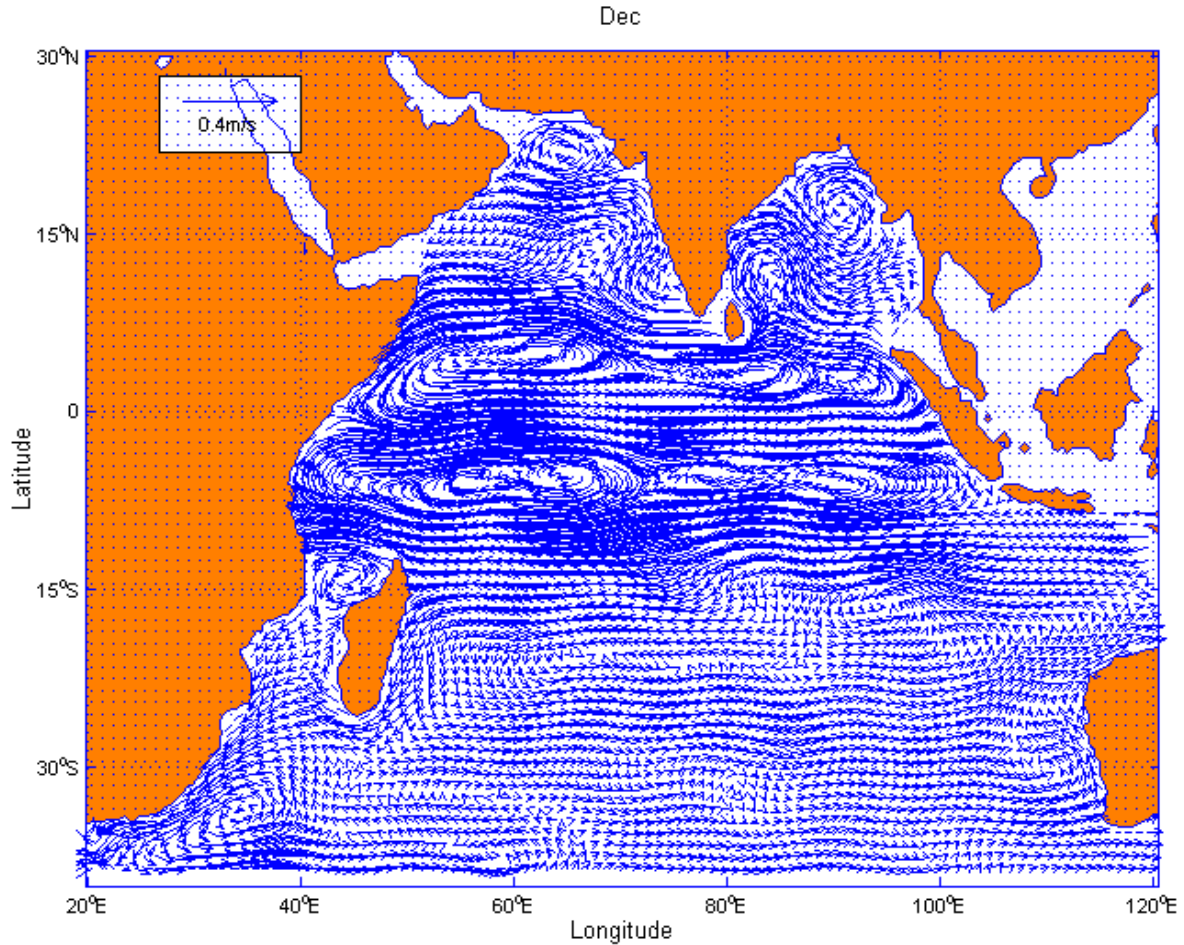


Figure 4-4. Mean Surface Circulation pattern of Indian Ocean during December, derived from satellite-based altimeter data.

During this time of the year, the southerly flowing Somali current is supplied from the westward flow in the Arabian Sea. This inflow into the Somali current seems to be coming in several branches. A lower latitude supply is originating from the westward flowing Northeast Monsoon Current (NMC) south of Sri Lanka. This also supplies the WICC after circulating around the Laccadive High. This circulation feature is not

prominent in the results generated for December, but it can be seen as further in winter (Figure 4-6). This feature was also explained by Bruce et al. (1994). The second branch that seems to be inputting the Somali current comes from the westward flow south of Socotra. This flow maybe getting input from WICC as well (Figure 4-4).

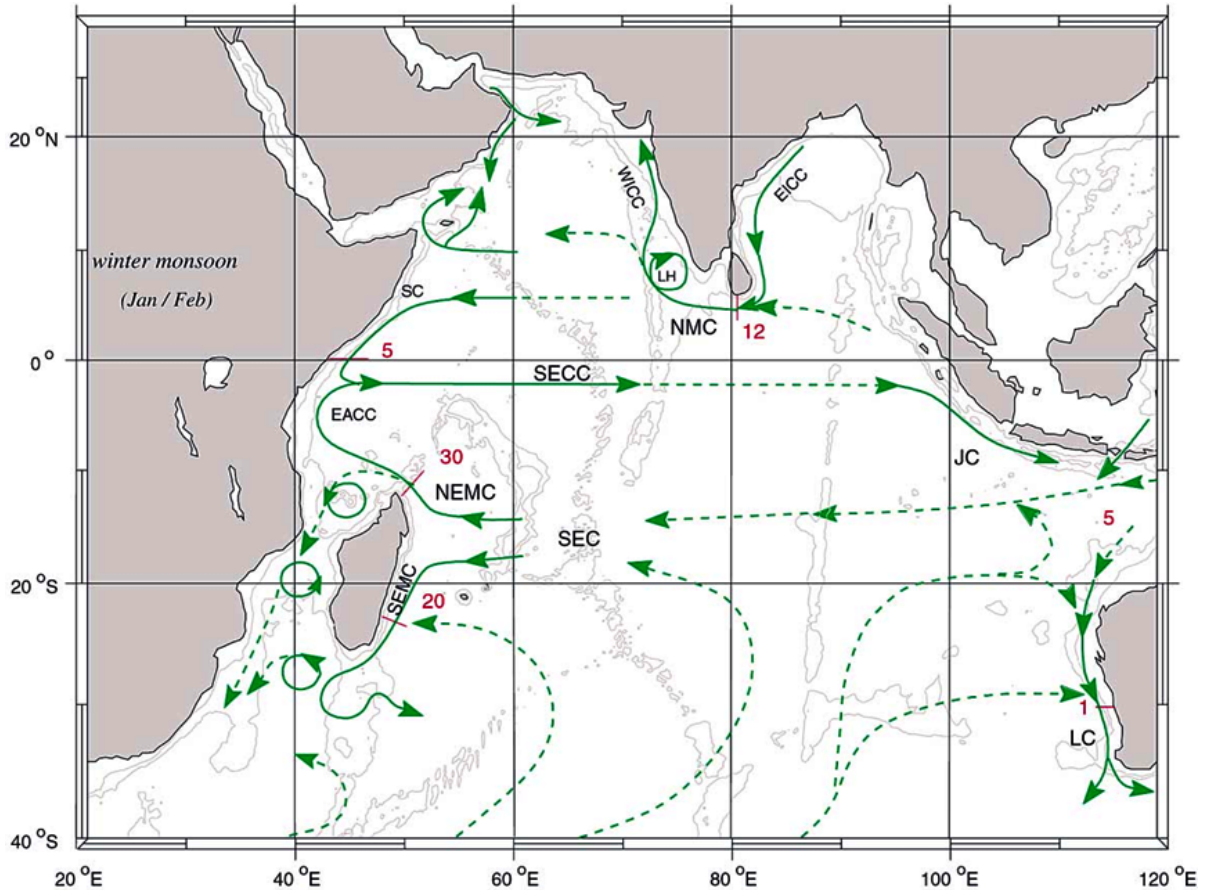


Figure 4-5. As in Figure 4-3, but for Northeast Monsoon (From: Schott & McCreary, 2001)

After analyzing the circulation pattern in the Bay of Bengal, this study observed that the EICC reverses direction twice a year: (Figures 4-2 and 4-7a) when it is moving northeastward and, after that, (Figure 4-7b) when it is moving in southwestward. In the interior of the Bay, a basin-wide clockwise gyre (Figure 4-7a) was observed from February to May. This gyre disappears during the summer monsoon, when the boundary

current splits at the 10°N confluence as observed by Schott and McCreary (2001). During the winter season, there seems to be a clockwise circulating gyre in the interior of the Bay. The EICC attached to it seems to have a southward flow.

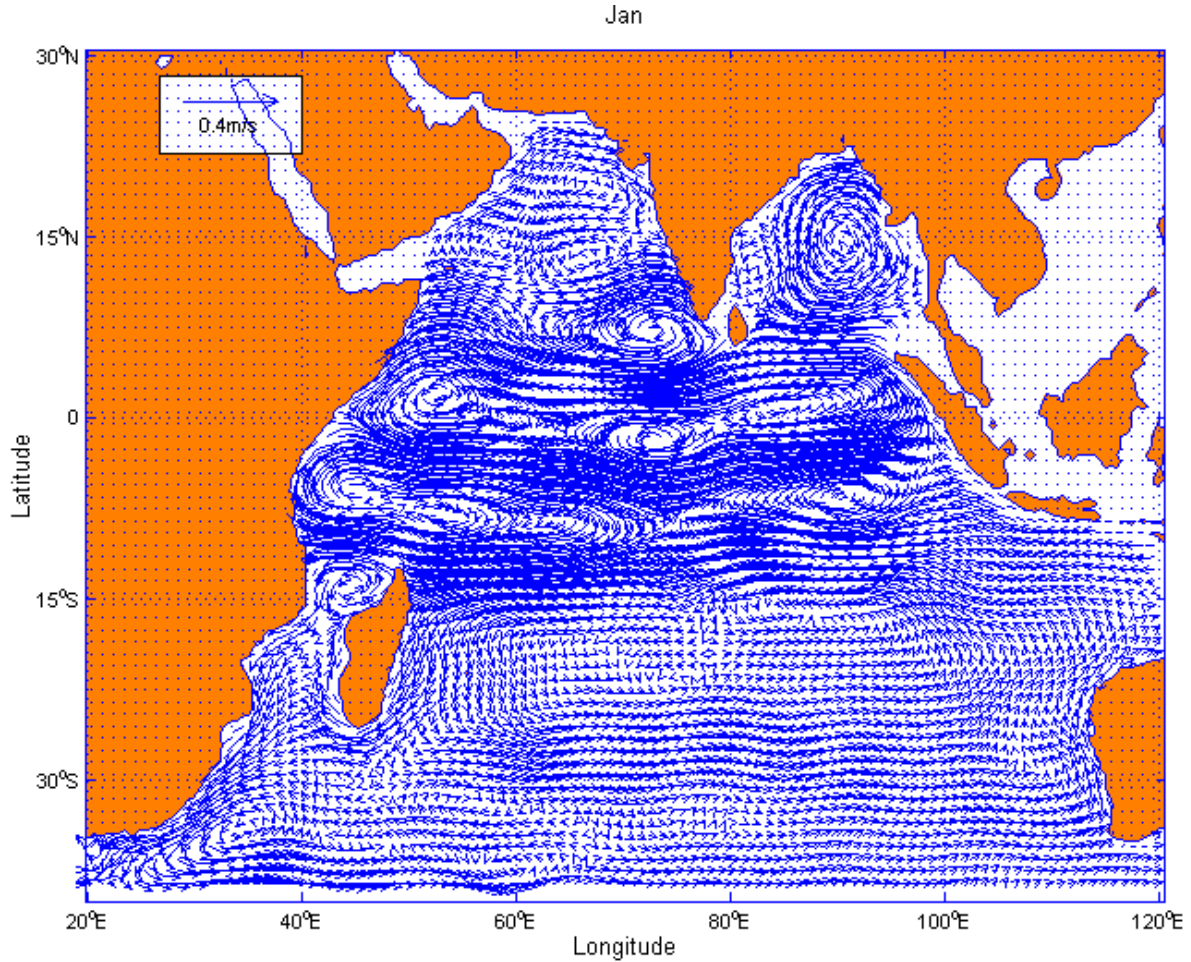


Figure 4-6. Mean Surface Circulation pattern of Indian Ocean during January, derived from satellite-based altimeter data after OSD.

#### 4. Equatorial Regime

A phenomenon, which is unique to the Indian Ocean due to the semiannual eastward winds along the equator (Figure 4-1b,d), is the flow of strong eastward surface jets (Wyrtki, 1973). These jets appear during the transition seasons between the monsoons, i.e., April to June and October to December. These jets carry warm upper-layer waters eastward. They lower sea levels and decrease mixed-layer thickness in the west, but increase them in the east (e.g., Rao et al., 1989; Figure 4-8b,d), thereby causing



an eastern temperature maximum in the 100-m map (Figure 4-8d,f). The strong eastward flow of these jets can be seen in Figures 4-7a and b along the equator. These eastward-flowing, upper-layer, current anomalies propagate pole-ward along the eastern boundary of the basin (Schott and McCreary, 2001).

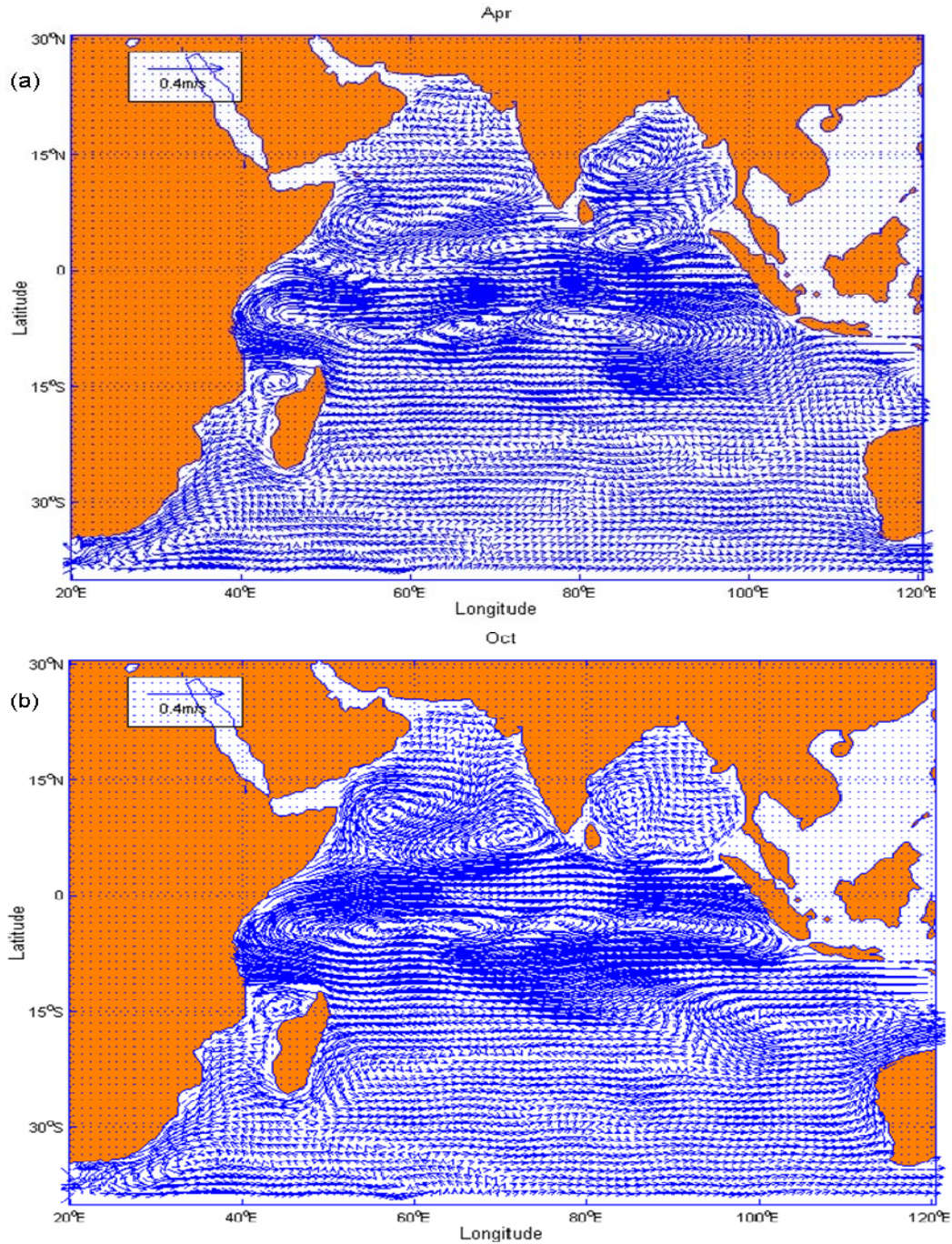


Figure 4-7. Mean Surface Circulation pattern of Indian Ocean during a) April, b) October; derived from satellite altimeter data.

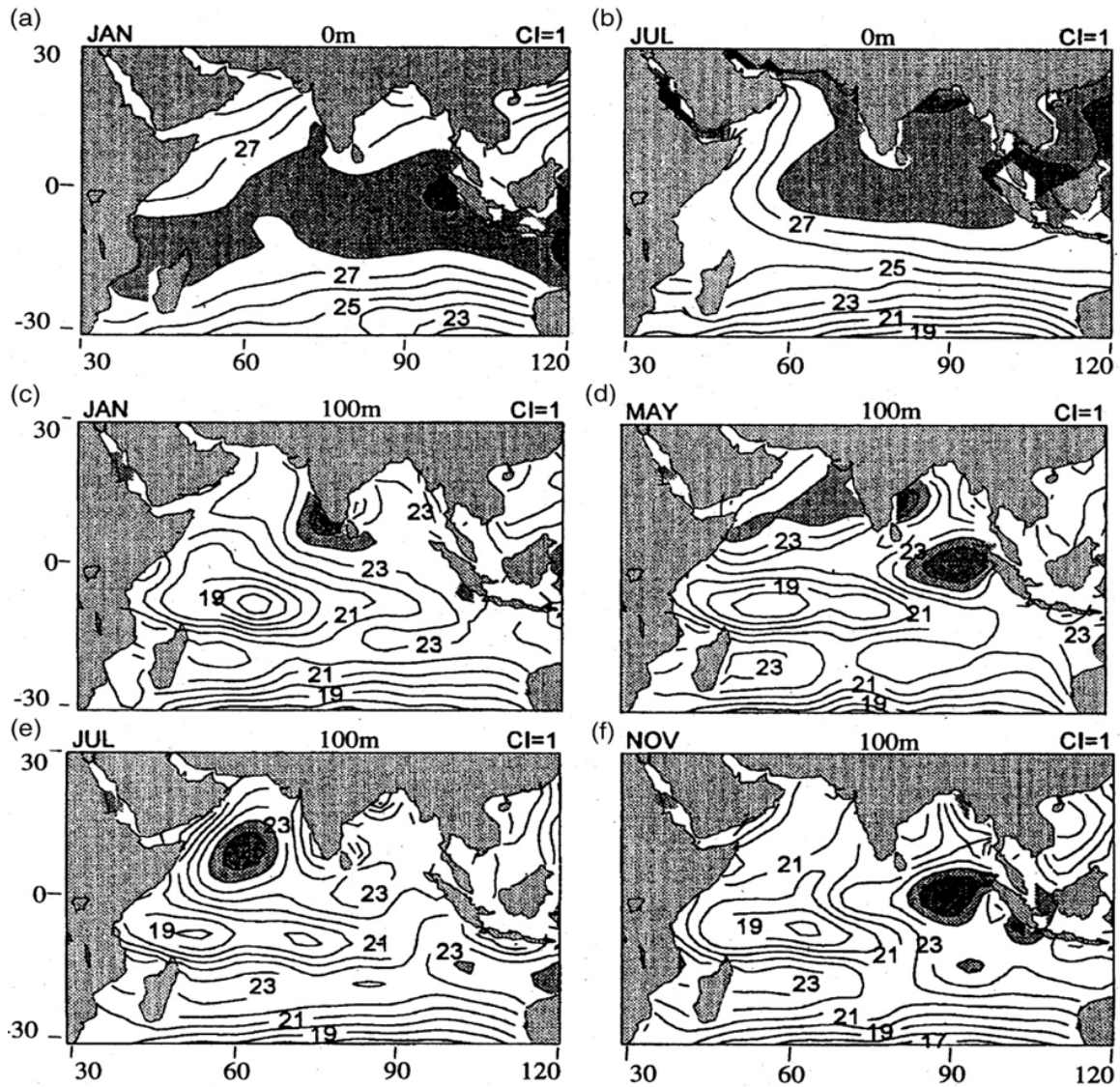


Figure 4-8. Climatological temperature at a-b) The surface during January and July, c-f) 100 m depth during January, May, July, and November, areas of relatively high temperature are shaded (From: Rao and Sivakumar, 2000).

#### D. SOMALI CURRENT

Traditionally, analyzing the annual cycle of the Somali Current system with its reversal of an entire current system (Figure 4-9) has remained an area of strong interest to the Indian Ocean oceanographic community. This section briefly analyzes the seasonal variability of the Somali Current and also compares this study's results with previous studies on this topic.



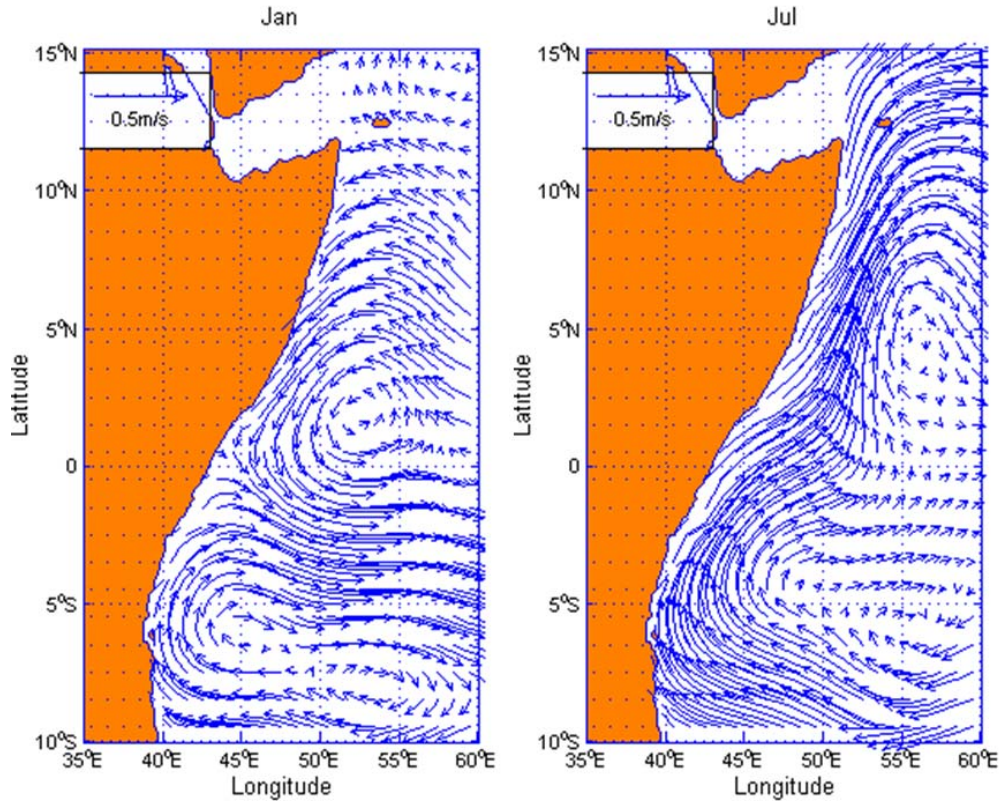


Figure 4-9. Reversal of Somali Current derived from mean altimeter data.

### 1. Seasonal Development

To see the seasonal development of the Somali Current, data for the specific area was extracted and vector plots were made for each month. The following paragraphs will show how the Somali current develops seasonally and compare this study's findings side-by-side with published studies. Figure 4-13 shows the seasonal development of the Somali Current system originally described by Schott et al., (1990) and was updated by the same author in 2001.

**March–May:** From satellite altimeter-derived data, this study observed that, before the onset of the monsoon, the southern Somali Current is an extension of the East African Coast Current (EACC) that flows northward. Just about south of the equator it turns offshore. The data also shows evidence of a gyre, which is most likely the Great

Whirl. Previous studies do not show the presence of such a gyre during this time of the season. At this time the season width scale of the Somali current is of the order of 50–100 km (Schott and McCreary, 2001).

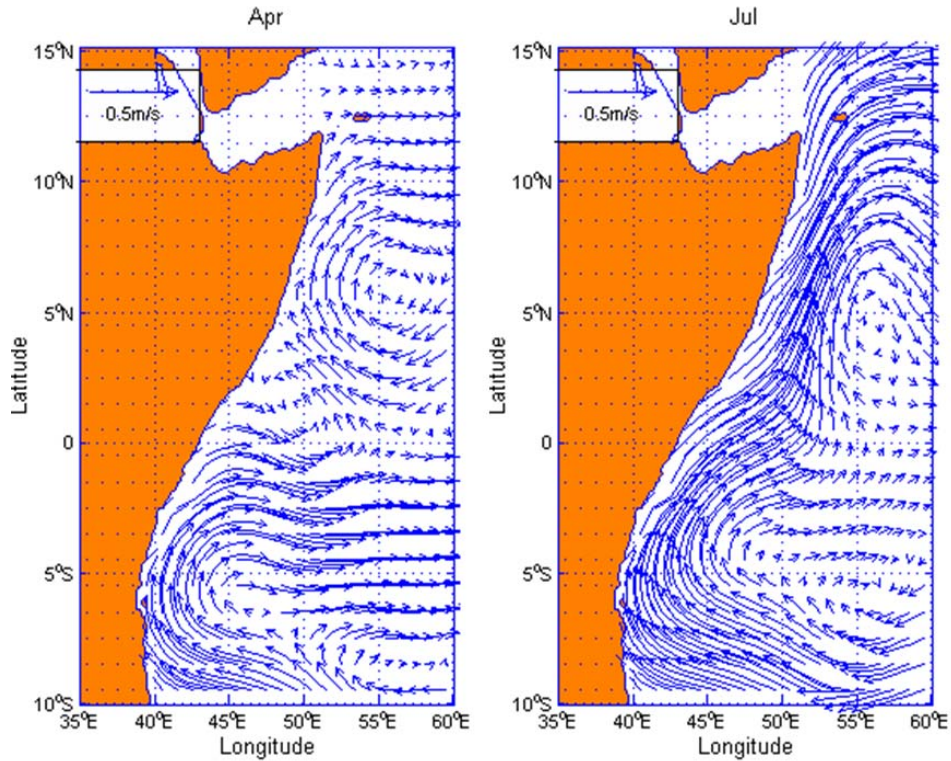


Figure 4-10. Mean surface Somali currents for a) April, b) July, derived from satellite-based altimeter data.

**June–July:** As the monsoon season starts in June, the “Great Whirl” is seen on lower latitude than in April (Figure 4-10b). Schott and Quadfasel (1982) made observations from moorings in the northern Somali Current regime. During their observational year, there was an unexpected start of the monsoon and, after this start, they reported distinct westward-propagating signals. They understood them as the first-mode of Rossby waves. Their conclusion was that the start of the Great Whirl was a response to the strong anticyclonic wind-stress curl offshore of the Somali coast by these long Rossby waves. They reflected into short Rossby waves at the boundary and accumulated energy there. At this time of the year, the Somali Current is strongest and



tends to flow northward along the coast. The observation made by Schott et al., (1990) also explains the creation of a gyre at about 4°N, where part turns eastward and part flows back across the equator in a circulation pattern which is termed as the ‘Southern Gyre.’ This also shows up in this thesis study’s results, but at lower latitude at about 4°S (Figure 4-10b). Why it shows up at a lower latitude needs more study which has not been covered in this study.

**August–September:** In the after part of the summer monsoon, the Great Whirl seems to be maintaining its position (Figure 4-11a). Transports in this late summer monsoon phase can exceed 70 Sv (Fischer et al., 1996; Schott et al., 1997). During this time, the Somali current flows generally northward all along the coast.

**October–November:** At the end of the southwest monsoon season, the Somali Current turns offshore at 2-3°S, while the Great Whirl has now shifted to a higher latitude (Figure 4-11b). During this time of the year, the flow is generally northward but its strength has reduced definitely. The evidence of Great Whirl even present till the end of the year is also explained by Bruce et al. (1981).

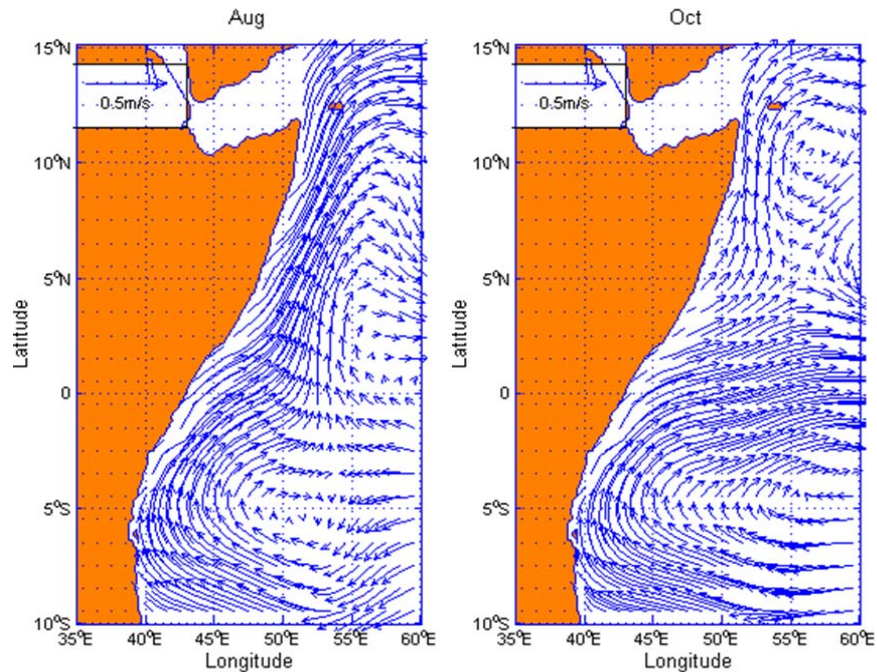


Figure 4-11. Mean Somali current circulation pattern during a) August, b) October, derived from satellite altimeter data.

## 2. Winter Monsoon

In the winter northeast monsoon, the winds blow southward away from the Indian subcontinent (Figure 4-1a). Due to this reversal of the wind pattern, the Somali Current also reverses its flow towards the south. During winter, the southward flowing cross-equatorial Somali current meets the northward flowing EACC in a confluence at about 2–4°S. Then, both flows input the eastward flowing South Equatorial Countercurrent (Figure 4.12). This flow pattern is also confirmed by Du'eing & Schott (1978) and Swallow et al. (1991). At the equator, the southward Somali Current is quite shallow, carrying 5 Sv in the upper 150 m. This is because there is a northward undercurrent at this time (Schott and McCreary, 2001).

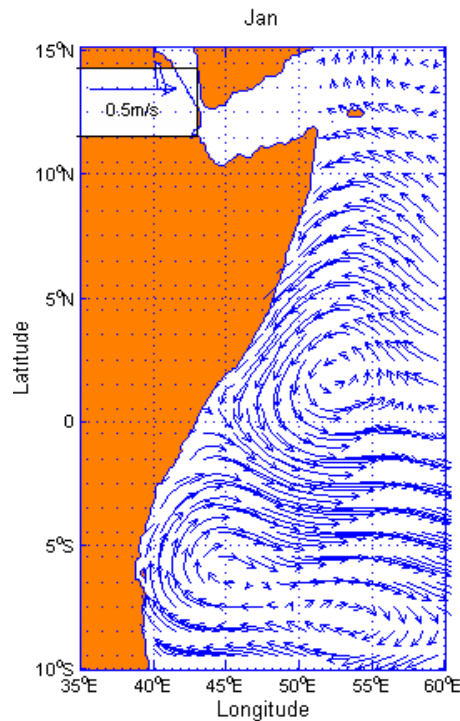


Figure 4-12. Mean Somali current circulation pattern during winter monsoon, derived from satellite-based altimeter data.

Even at this time of the year, the Great Whirl is seen between 0–5°N. Numerous observations had been made in the northern Somali Current for the winter monsoon.

Bruce et al. (1981) reported that the Great Whirl can actually sustain summer monsoon conditions below the developing winter monsoon surface circulation for some time into the winter monsoon.

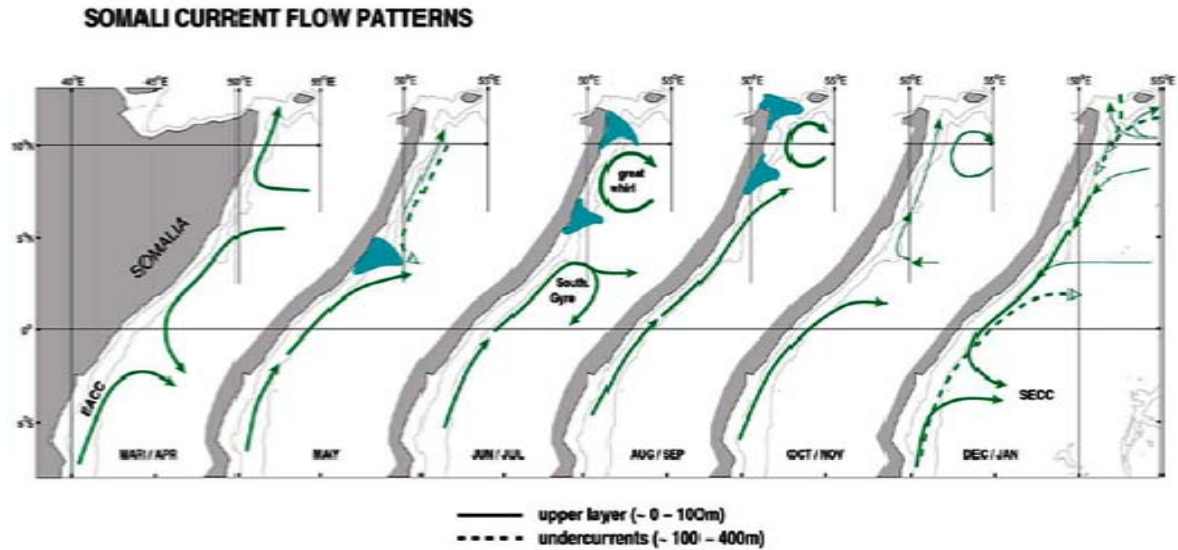


Figure 4-13. Schematic diagram of Somali current upper layer flow pattern over the course of the year (From: Schott & McCreary, 2001).

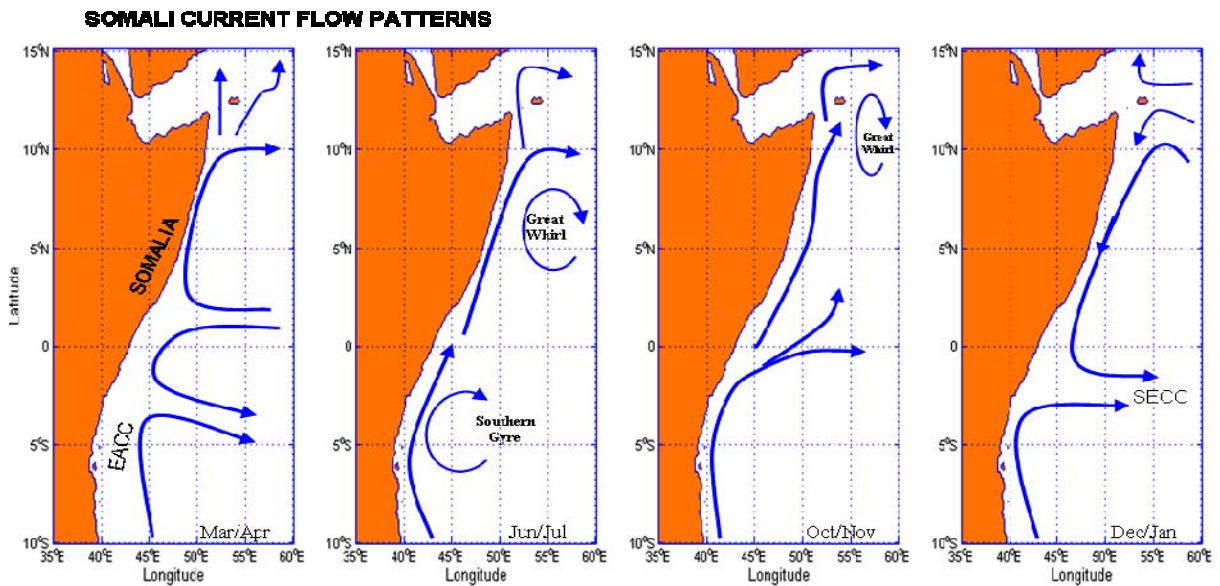


Figure 4-14. Schematic Diagram of Somali current upper layer pattern over the course of the year derived from satellite-based altimeter data.

### **3. Comparison with Earlier Studies**

Comparing this study's results (Figure 4-14) from satellite altimeter data with Schott and McCreary (2001)'s schematic diagram (Figure 4-13) from ship drift data, it can be observed that the general circulation pattern of the Somali Current is almost the same. Few features are exceptions, such as the position of the southern gyre and the true depiction of the currents near the land boundaries. Thus, with the altimeter's data, this study clearly observed the mesoscale features of a certain part of the ocean. However, it is difficult to distinguish between the small-scale features and the features along the coast.

#### **E. NORTH ARABIAN SEA**

In the North Arabian Sea, broad eastward flow during the summer monsoon across the whole latitude range of the Arabian Sea can be seen (Figure 4-15c). The exact condition is also observed from the ship drift currents (Figure 4-16a). In this study's results, we cannot see the presence of the Laccadive Low off the southwest tip of India (Figure 4-15c) during the summer Monsoon season. Schott and McCreary (2001) observed this in previous studies. As we move further towards the end of summer monsoon in October (Figure 4-15d), one can clearly observe the circulation of the Laccadive Low along the southwestern tip of India moving in an anti-clockwise direction. At this time of the year, the SECC has started flowing eastward almost along the equator. The southwest monsoon current flows eastward along the southern tip of India.

As part of the Joint Global Ocean Flux Study (JGOFS), for the years 1994–1996, the northern Arabian Sea has been comprehensively studied. In the JGOFS study during the summer monsoon, it was observed that a northeastward coastal jet developed along the south coast of Oman in early May which persisted throughout the summer. This jet has been called Ras Al Hadd Jet by Bo'hm et al. (1999). This jet flows past Ras al Hadd at the southeast corner of Oman (Figure 4-3) and meanders into the Gulf of Oman. As explained by Flagg and Kim (1998) and Bo'hm et al. (1999) this jet is linked to an anticyclonic gyre just south of its offshore turning point and a cyclonic gyre to its north.



These small-scale gyres cannot be seen in this study, but the flow pattern of the jet can be seen along the eastern tip of the Arabian Peninsula (Figure 4-15c).

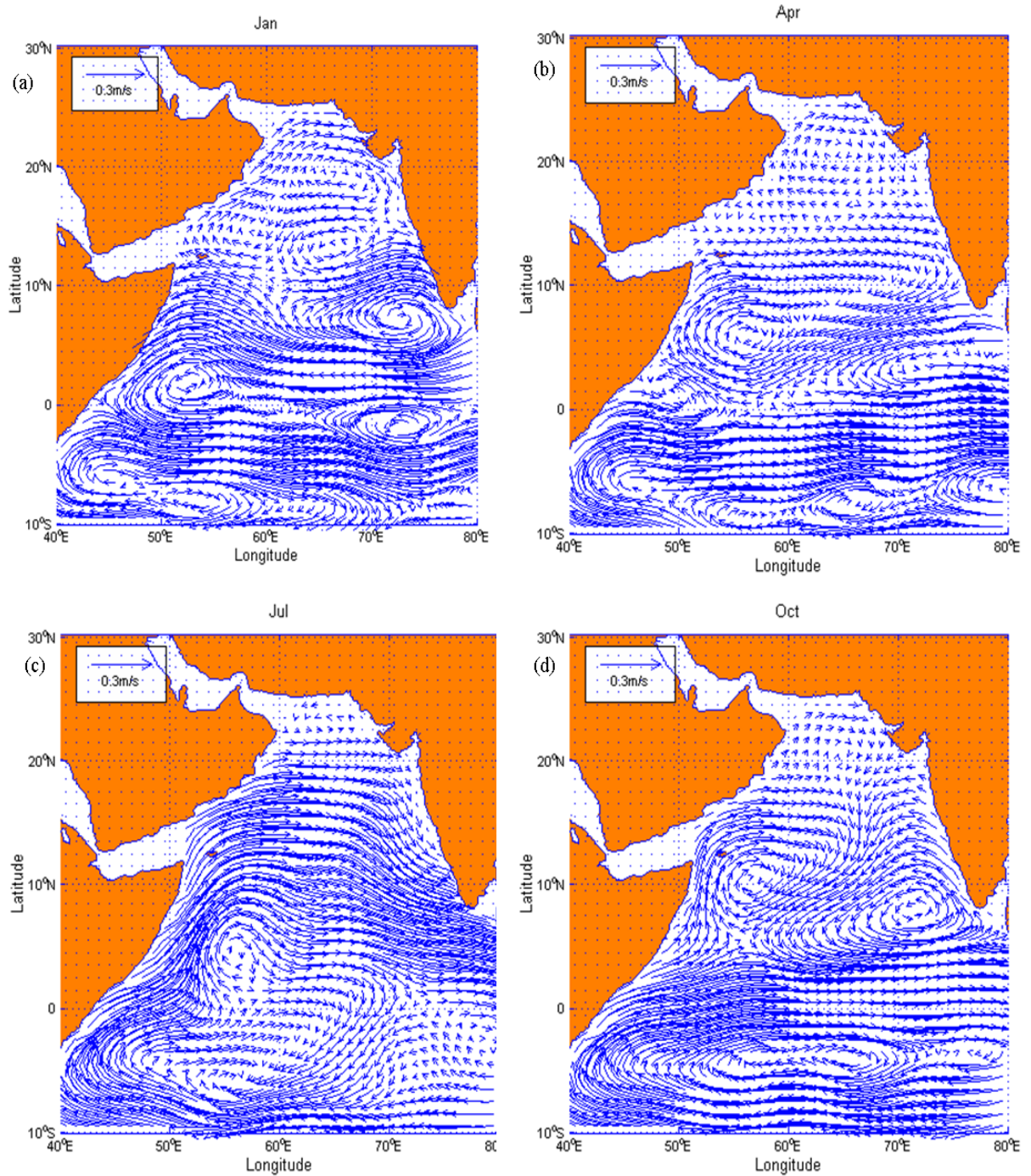


Figure 4-15. Mean surface circulation pattern of the North Arabian Sea all through the year, derived from satellite-based altimeter data, showing a) January, b) April, c) July, d) October.

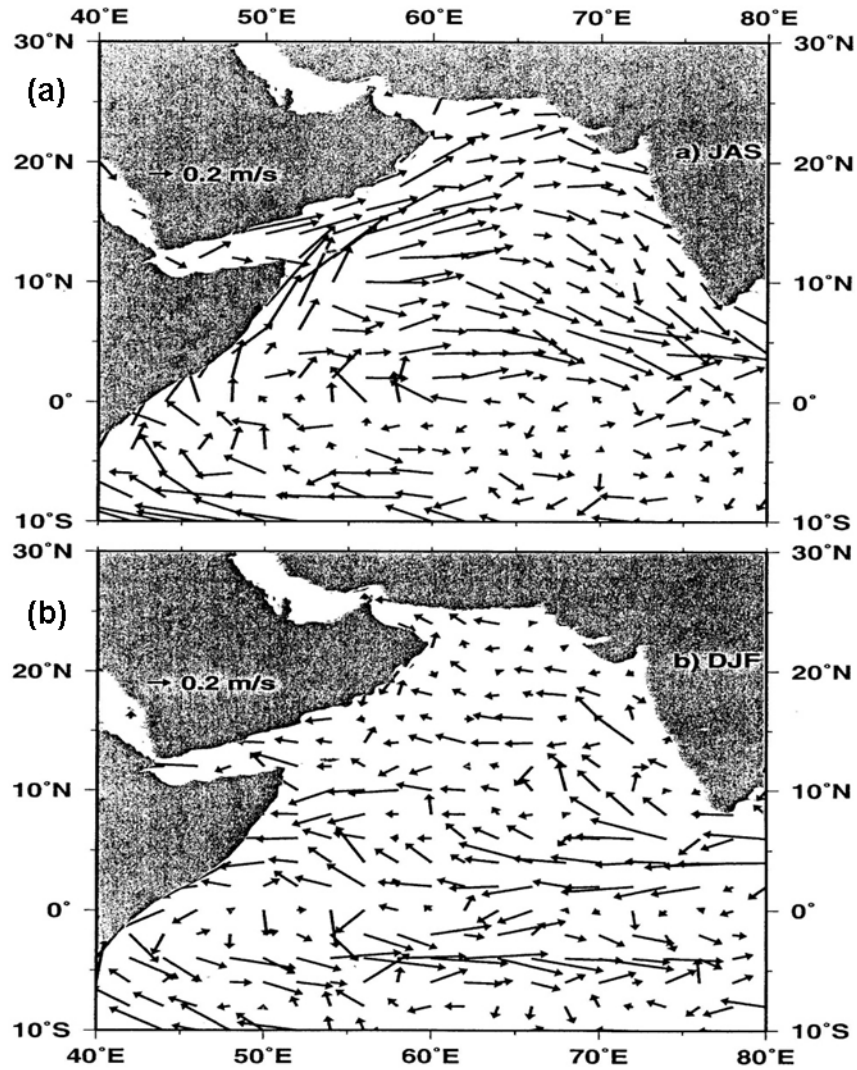


Figure 4-16. Surface current vectors from drifter climatology; a) July - September, and b) December - February (From: Schott and McCreary, 2001).

When observing the winter circulation pattern in the North Arabian Sea (Figure 4-15a), a basin wide clockwise gyre and, along the northern coast, weak easterly currents were seen. As we move down towards the south, westerly currents appeared that can also be seen in the ship drifts in the northern Arabian Sea (Figure 4-16b). In January and April, the western-boundary current of the Gulf of Oman north of Ras al Hadd is comparatively weak which is also observed by Flagg & Kim (1998). As explained by Schott and McCreary (2001) (Figure 4.3), the presence of the Laccadive High (LH) can be seen along the southwestern tip of India moving in the clockwise direction. The SECC

is flowing eastward and the northeast monsoon current is flowing in the westerly direction. This has also been observed by Schott & McCreary, 2001 (Figure 4-5). In general during the winter monsoon, the mean flow is westward. Shi et al., (2000) also explains this with the addition that this westward flow is accompanied by down-welling along the coast and an offshore-directed pressure gradient. Moving further offshore, a mesoscale eddy along the equator at about  $71^{\circ}$  E (Figure 4.15a) moving in anti-clockwise direction is seen. This mesoscale feature needs more study because studies carried out during 2001 also do not explain anything about it.

As the winter northeast monsoon dies down in April (Figure 4-15b), the general circulation pattern is still the same in the northern Arabian Sea with some weak westward flow. Along the coast of Pakistan we can see weak eastward current. During this time of the year the Somali Current has started moving in northeasterly direction along the coast. At about equator it comes in confluence with the East African Coast Current (EACC) which is supplying the South Equatorial Counter Current (SECC). The Great Whirl can also be clearly seen during this time of year.

## **F. BAY OF BENGAL**

The surface circulations in the western part of the Bay of Bengal are strongly influenced by the seasonal reversal of the wind stress forcing. The climatological situation in the western part of the bay is similar to that in the western Arabian Sea. For EICC, the local winds have weaker effects because remote forcing is relatively more important for the EICC than they are for the Somali Current. As explained by Schott and McCreary (2001), the crossing of remotely forced coastally trapped-waves, and Rossby waves in the interior of the bay, are major contributors to the EICC variability. One of the other major factors, which prevents the accurate determination of only geostrophic currents in the bay, is the large fresh-water flux from both rainfall and river discharges (Schott & McCreary, 2001).

The seasonal cycle of the surface circulation in the Bay of Bengal from satellite altimetry is presented in Figure 4-17. We observe that as for the Arabian Sea, circulation patterns in the interior of the Bay of Bengal contain many mesoscale features, but there is

no evidence of any seasonally reoccurring coastal gyres like the Southern Gyre and the Great Whirl. As the summer monsoon begins, the northward surface currents in the EICC off India do not strengthen. However, there are weak northward currents along the eastern coast of India (Figure 4-17c). In the summer, there are hardly any mesoscale features inside the Bay of Bengal. Rather, the general flow inside the bay is eastward at this time of year. The same pattern can also be seen by results from ship drift data shown in Figure 4-18a. This eastward flow is weaker along the coast and strengthens as it flows further south inside the bay. Its maximum strength is located just south of the bay. That is the southwest monsoon current. In October (Figure 4-17d) when the summer monsoon has almost diminished, an entirely reversed circulation pattern inside the bay is present. Now EICC seems to be moving southward along the east coast of India and has more strength as compared to it in summer. A mesoscale feature can also be seen inside the Bay as a large-scale eddy appears in the southwestern boundary of the Bay along EICC. In the eastern part of the Bay, the weak currents are flowing in a northerly direction. Inside the bay, the currents are moving mostly counterclockwise.

During winter monsoon in January (Figure 4-17a), circulation inside the Bay is completely transformed into a mesoscale eddy moving in a clockwise direction. The strength of the currents inside the Bay has also increased as compared to summer. In the southern part of EICC, confluence occurs at about  $17^{\circ}$  N. Here another smaller eddy is moving in an opposite direction. Moving further south the general flow is towards the west. In an analysis of sections observed during December 1991, between the northern end of the Bay and  $10^{\circ}$ N, Shetye et al. (1996) found the geostrophic transport relative to 1000 dbar increased southward from 2 Sv to about 8 Sv.

The winter monsoon dies down in April. The clockwise circulation pattern inside the bay still persists while the center of circulation now has shifted towards western side of the bay (Figure 4-17b). During this time of year, EICC seems to be flowing towards north along the east coast of India. In the southern part of the bay, the general circulation is towards the west. This circulation pattern is also confirmed by Shetye et al., (1993) who also estimated a transport of about 10 Sv for the northward EICC at this time and



concluded that it was the western-boundary current associated with a wind-driven anticyclonic gyre in the interior of the bay.

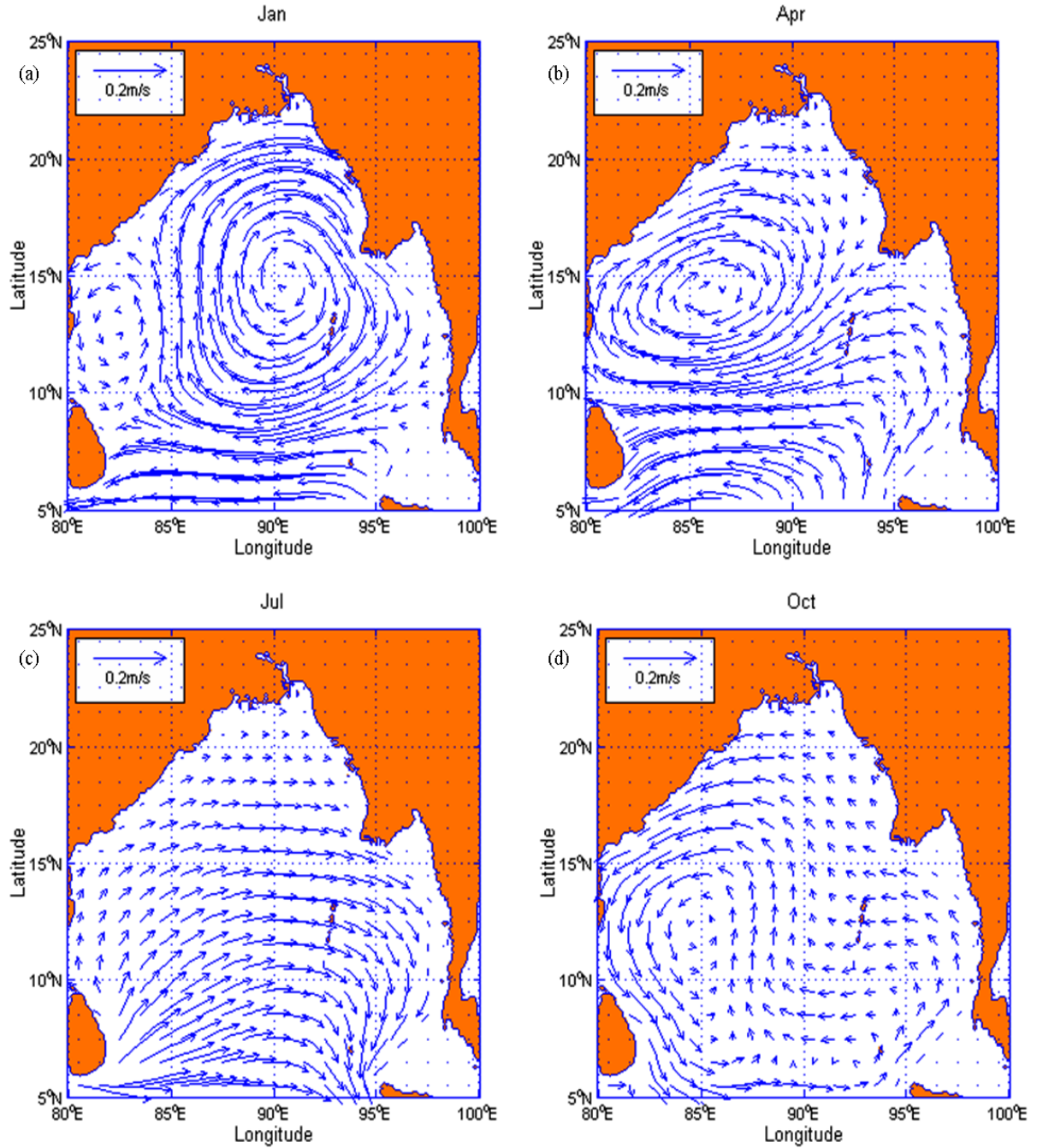


Figure 4-17. Mean surface circulation pattern of the Bay of Bengal all through the year, derived from satellite-based altimeter data showing a) January, b) April, c) July, d) October.

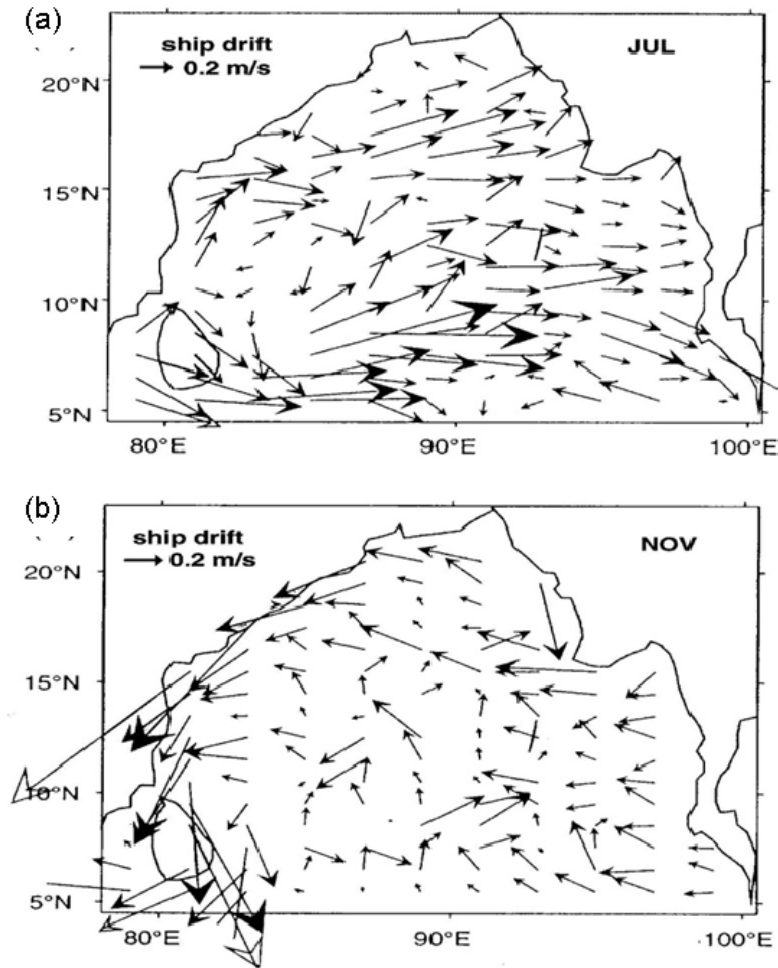


Figure 4-18. Surface currents in Bay of Bengal from the ship drift data; a) July, b) November (From: Eigenheer & Quadfasel, 2000).

## G. MONSOON CURRENTS

In this subsection, the focus is on the variability solely in the monsoon currents in the northern Arabian Sea. The region between Sri Lanka and the equator is a bottleneck for the zonal currents in the northern Indian Ocean. They provide the major pathway for the exchange of water between the Arabian Sea and Bay of Bengal. As known from ship drift observations (Cutler and Swallow, 1984), this current reverses with the monsoons. It flows eastward as SMC from June to September (Figures 4-15c and 4-16a) and westward, as NMC, from November to February (Figures 4-15a and 4-16b).

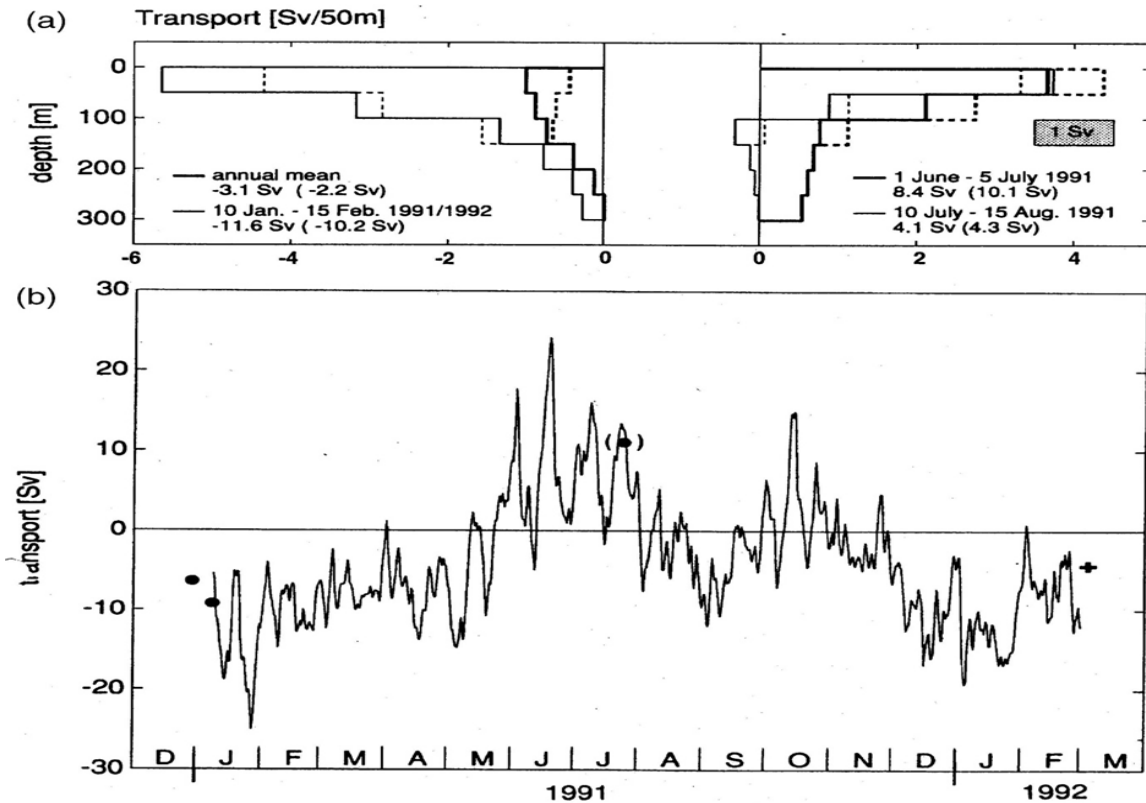


Figure 4-19. Monsoon current transport south of India - Sri Lanka; a) Decomposition into depth bins using two different extrapolation schemes from top instrument level towards the surface: extrapolation of moored current meter shear from upper most levels (solid) or using ship drifts as surface values (dashed). The heavy curve on the left hand side shows annual mean, b) transport time-series, based on shear extrapolation; dots mark shipboard ADCP sections for comparison (From: Schott et al., 1994).

### 1. Southwest Monsoon Current (SMC)

Figure 4-2 shows the flow pattern of the southwest monsoon current at the southern tip of India. During the summer, this current moves eastward with greater strength than other current regimes near it (Figures 4-2 and 4-3). The same flow pattern of SMC was also observed by Schott et al. (1994). The SMC decayed so quickly with depth that its transport had to be determined either by extrapolating ADCP and current meter observations to the surface or by using seasonal mean ship drift currents as surface values (Figure 4-19a). Based on shear extrapolation, the eastward SMC transport between 4–6°N was estimated to be 8.4 Sv, with 70% in the top 100 m. From the current and

transport time-series, they also saw the strong intraseasonal variability (Figure 4-19b). The source of water for the SMC eventually must be in the western Arabian Sea. After passing Sri Lanka, much of the SMC turns northward into the Bay of Bengal; whereas some of it turns southward (Figure 4-2). Finally, this current inputs to the current systems along the western coast of Malaysian islands.

## **2. Northeast Monsoon Current (NMC)**

The NMC flows westward south of India (Figures 4-4 and 4-5). During 1991, its transport was observed to be 11 Sv (Schott et al., 1994). This transport is larger than the estimated SMC transport and results in a net annual-mean transport of 2.5 Sv to the west for 1991 (Figure 4-20a). In this study's results, the NMC flow persists through March. Hacker et al. (1998) saw the same. The NMC partly carries fresher water from the Bay of Bengal the properties of which are detectable in the WICC (Stramma et al., 1996). It seems that most of the source of NMC is from the recirculating water brought eastward north of the equator. This finding is the same as concluded by Hacker et al. (1998).

THIS PAGE INTENTIONALLY LEFT BLANK

## V. INDIAN OCEAN DIPOLE AND EASTWARD EQUATORIAL JET

### A. THE INDIAN OCEAN DIPOLE (IOD)

In 1999, the Indian Ocean Dipole (IOD) was discovered by Professor Yamagata, Dr Saji, and associates of the Climate Variations Program of Frontier Research System for Global Change (Vinayachandran et al., 1999). They described it as an inter-annually occurring climate mode in the tropical parts of the Indian Ocean. The occurrence of Dipole Mode events can be traced back through the coral record to the mid-Holocene period which dates about 11,000 years before present to present. As typical to other climate oscillations, the IOD climate mode has a 'positive' phase and a 'negative' phase (Figures 5-1 and 5-2).

#### Positive Dipole Mode

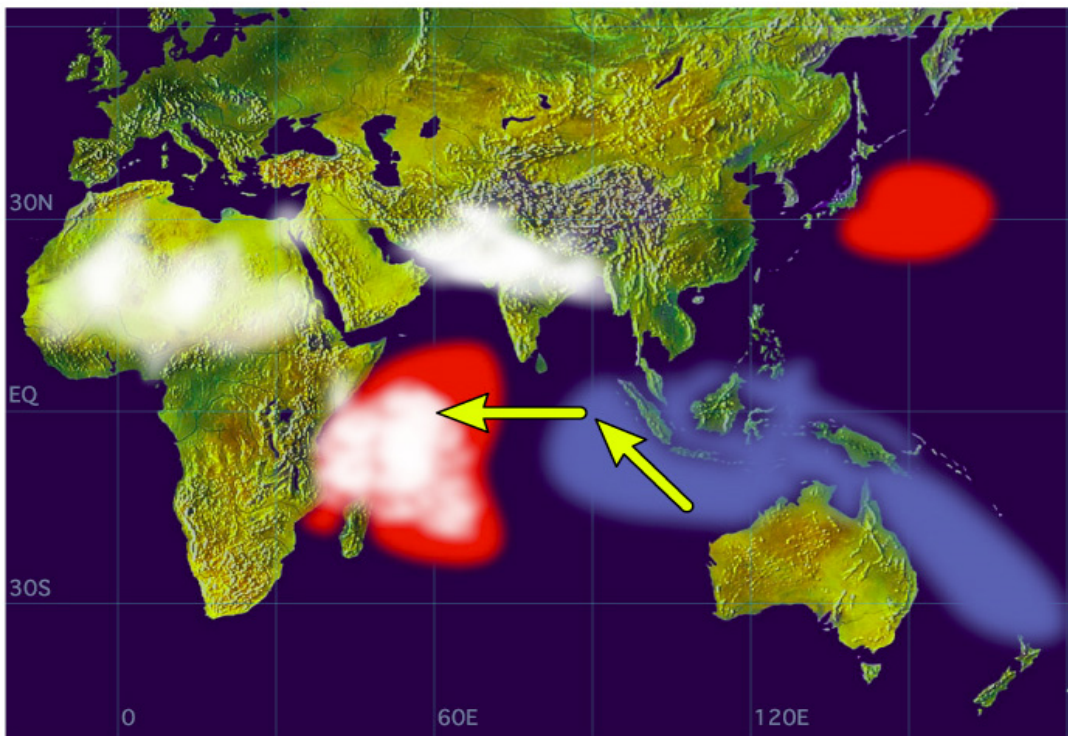


Figure 5-1. Schematic diagram of SST anomalies (red shading, warming; blue, cooling) during a positive IOD event. White patches indicate increased convective activity. Arrows indicate wind direction. (From: A.Suryachandra Rao. Frontier Research Center for Global Change).

During a positive IOD event (Figure 5-1), the sea surface temperature (SST) rises in the western equatorial Indian Ocean, which is along the eastern coast of Africa, and from the northern half of Madagascar to the northern edge of Somalia. The SST drops in the southeastern part of the Indian Ocean, which is along the northern coast of Australia, the eastern coast of Japan, and throughout Indonesia. In Figures 5-1 and 5-2, the red color denotes rise in SST and the blue color corresponds to fall in SST. Associated with these changes, the normal convection situated over the eastern Indian Ocean warm pool shifts to the west and brings heavy rainfall over eastern Africa and severe droughts/forest fires over the Indonesian region.

### Negative Dipole Mode

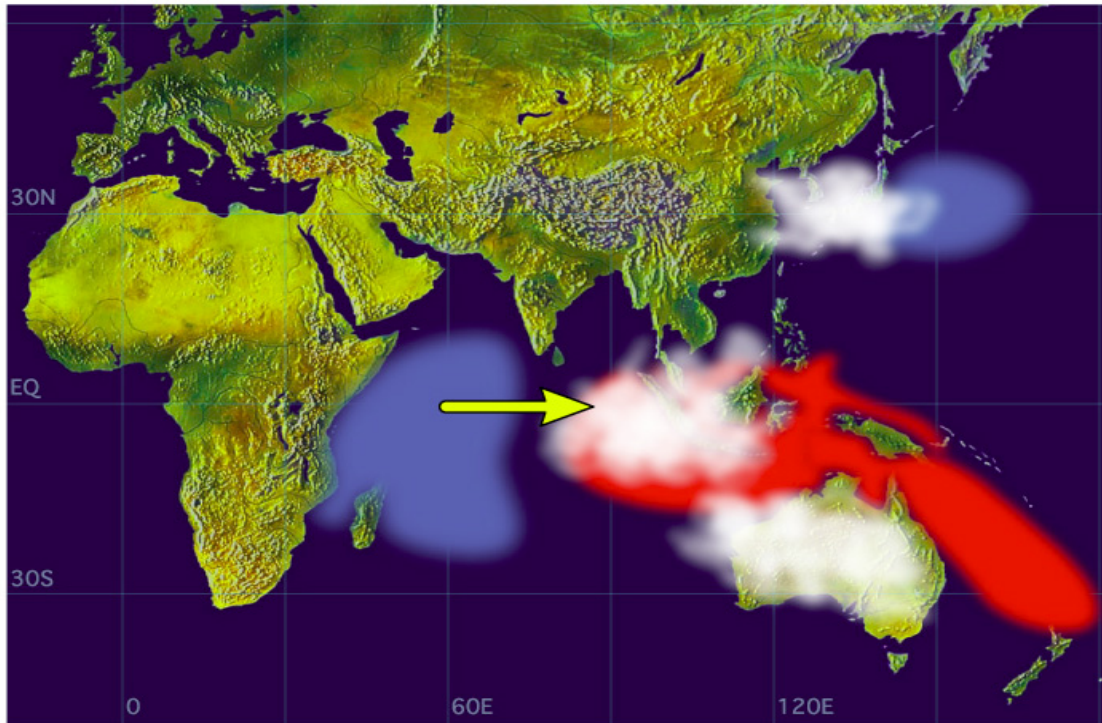


Figure 5-2. Schematic diagram of SST anomalies (red shading, warming; blue, cooling) during a negative IOD event. White patches indicate increased convective activity. Arrows indicate wind direction. (From: A.Suryachandra Rao., Frontier Research Center for Global Change).

Prof. Yamagata, Dr. Saji, and other researchers of the climate variations research program of Frontier Research Center for Global Change (FRCGC) created the name of IOD to represent the zonal dipole structure of the various coupled ocean-atmosphere

parameters, such as SST, OLR, and Sea Surface Height anomalies. Furthermore, convective patterns increase in the northern half of Africa, India, and off the eastern coast of Africa. Inverse conditions exist during a negative IOD event (Figure 5-2).

## B. DIPOLE MODE INDEX

The IOD events are represented by the Dipole Mode Index (DMI), which is defined as the zonal difference of sea surface temperature anomaly between the tropical western Indian Ocean ( $50^{\circ}\text{E}$ - $70^{\circ}\text{E}$ ,  $10^{\circ}\text{S}$ - $10^{\circ}\text{N}$ ) and the southeastern Indian Ocean ( $90^{\circ}\text{E}$ - $110^{\circ}\text{E}$ ,  $10^{\circ}\text{S}$ -equator) ([http://ioc3.unesco.org/oopc/state\\_of\\_the\\_ocean/sur/ind/dmi.php](http://ioc3.unesco.org/oopc/state_of_the_ocean/sur/ind/dmi.php)). The time series of the monthly mean DMI (Figure 5-3) clearly reveals the evidence of a large positive anomaly during 1994, 1997, and 2006. The most prominent amongst them is during 1997-1998. Although negative anomalies are not as strong as positive ones, they can be observed during years 1996, 1998, 2001, and 2005. The most prominent amongst them is 1998. For the subsequent analysis, the positive IOD events of 1997-1998 and the recent one during 2006 are considered. To see our results in context to the negative IOD events, the concentration will be on the events during 1998-1999 and 2001.

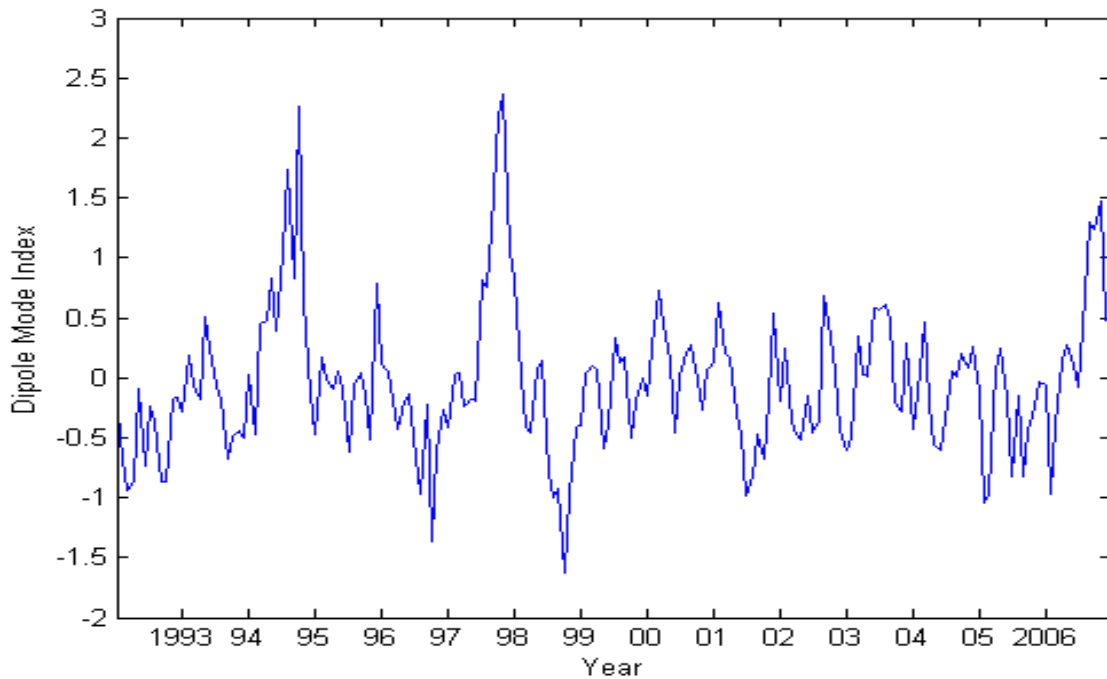


Figure 5-3. Dipole Mode Index for the period 1992 – 2006.



### **C. THE EASTWARD EQUATORIAL JET (OR WYRTKI JET)**

One of the most prominent features in the Indian Ocean Equatorial region is the eastward flowing Equatorial jets that usually can be observed during the transition period between monsoons (Wyrtki, 1973). Several modeling studies were carried out to study the connection between the eastward equatorial jet and the IOD events. The results showed that the eastward equatorial jet weakens in a positive Dipole Mode event and strengthens in a negative Dipole Mode event (Vinayachandran et al., 2001). This feature has also been observed by Reppin et al. (1999) while making observations in the Indian Equatorial region during 1994's Positive Dipole event. This shows that, in context to the surface circulation in the Indian Ocean, the behavior of these jets tend to vary more than any other large-scale feature during any Dipole Mode event.

Satellite-based observational surface currents data was used to investigate the long-term connection between the eastward equatorial jet and the IOD events. Therefore, for the subsequent analysis only the behavior of these jets in response to different Dipole Mode events will be viewed. These eastward flowing jets can be seen along the equator in Figures 4-7a and b.

### **D. COMPLEX EFO ANALYSIS OF THE CURRENT DATA ALONG THE EQUATOR AND COMPARISON WITH DMI**

To see the variance in the spatial patterns along the equator from 45° E to 95° E, data was extracted for the area of interest. Then, a calculation of the 13-year arithmetic mean of the data set by using the basic statistical relation was performed,

$$\bar{x} = \frac{(x_1 + x_2 + x_3 + \dots + x_n)}{n} = \frac{\sum_{i=1}^n x_i}{n} \quad (5.1)$$

Complex Empirical Orthogonal functions were used to calculate the amplitude of the first four modes. The variance was calculated by computer-based program. Therefore, there were a finite number of modes that could be derived. In our case it was 50. After calculating, it was found that the first four modes cover the 91% of the variance as

illustrated in Table 5-1. In this case, to see the variance in surface circulation pattern, 91% variance could have revealed the bigger anomalies in the spatial patterns. Therefore, only the first four modes were taken into account for the subsequent analysis.

EOF Mode	Relative Variance	Cumulative Relative Variance
1 <sup>st</sup> Mode	66.95	66.95
2 <sup>nd</sup> Mode	13.27	80.22
3 <sup>rd</sup> Mode	6.98	87.19
4 <sup>th</sup> Mode	4.23	91.42

Table 5-1. Percentage of Variance of first four EOF Modes.

The Amplitude of the Variance for all four modes was analyzed to see if any relation exists with the general trend in DMI.

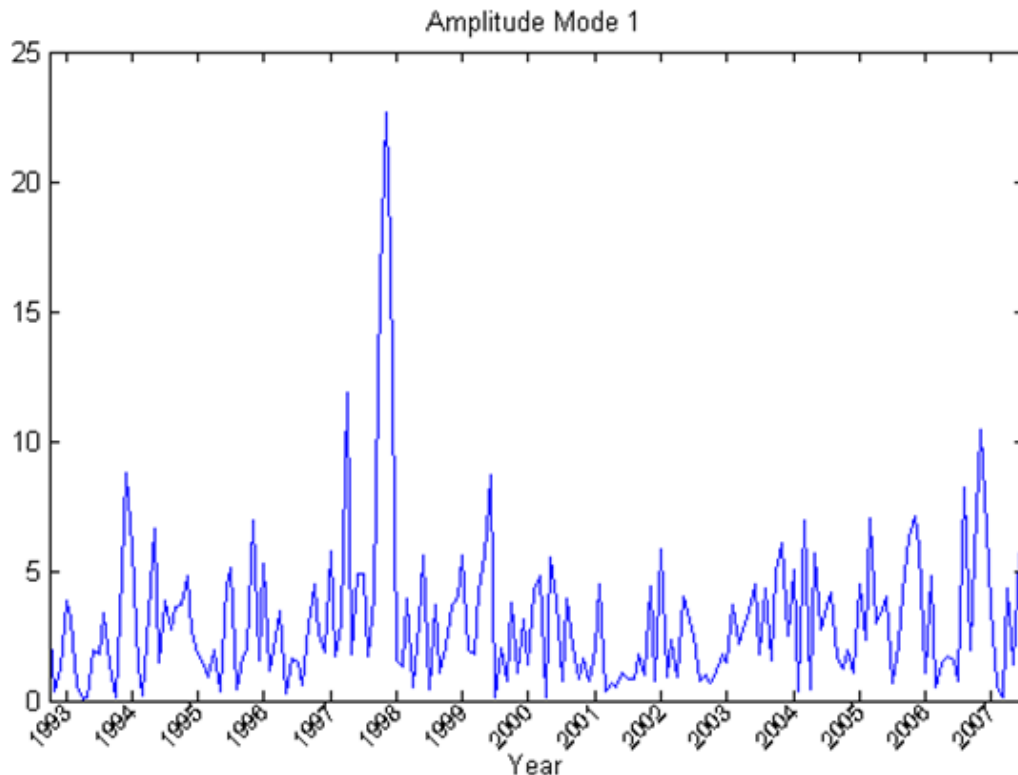


Figure 5-4. Amplitude of EOF Mode-1.

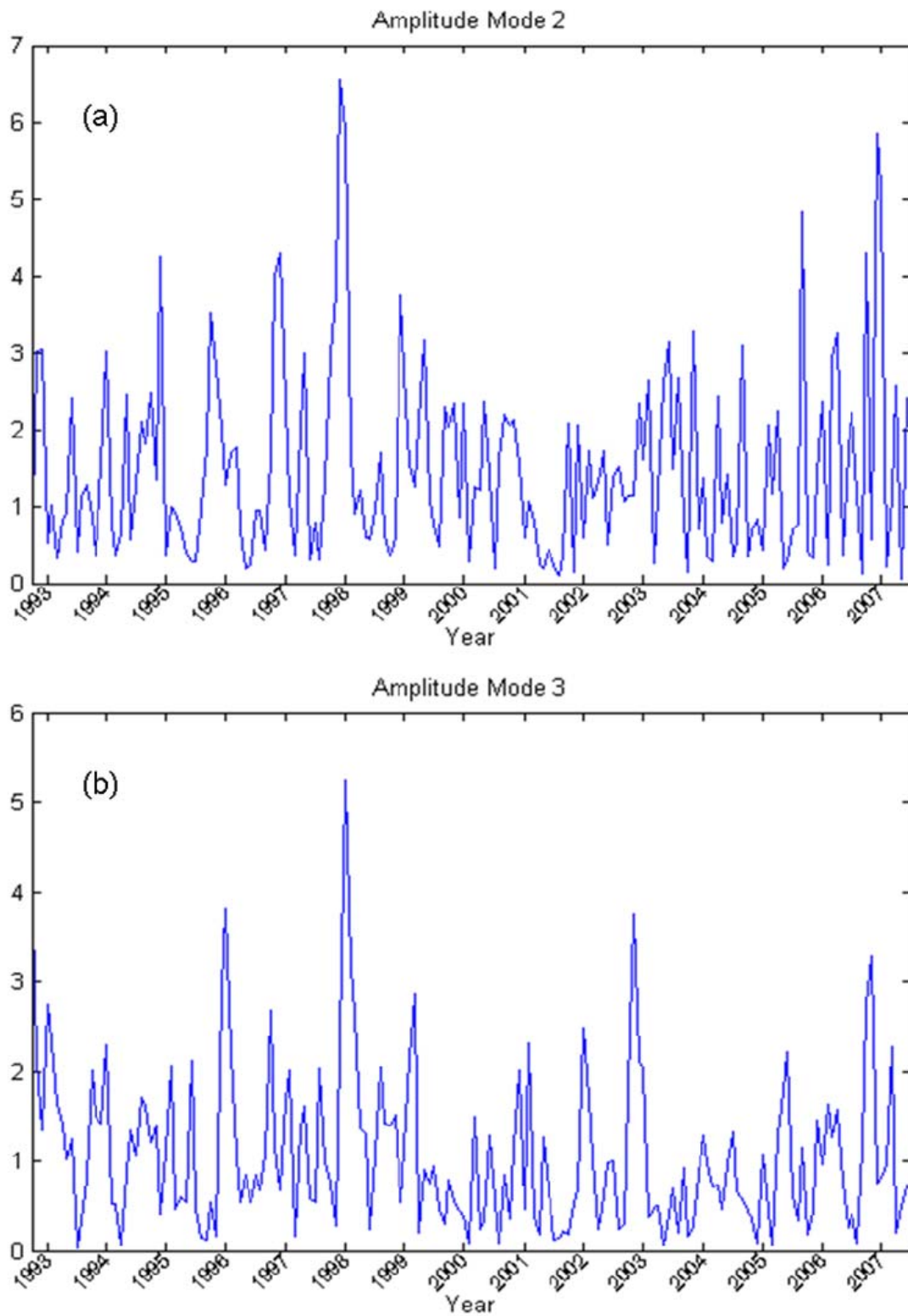


Figure 5-5. Amplitude of EOF a) Mode-2, b) Mode-3.

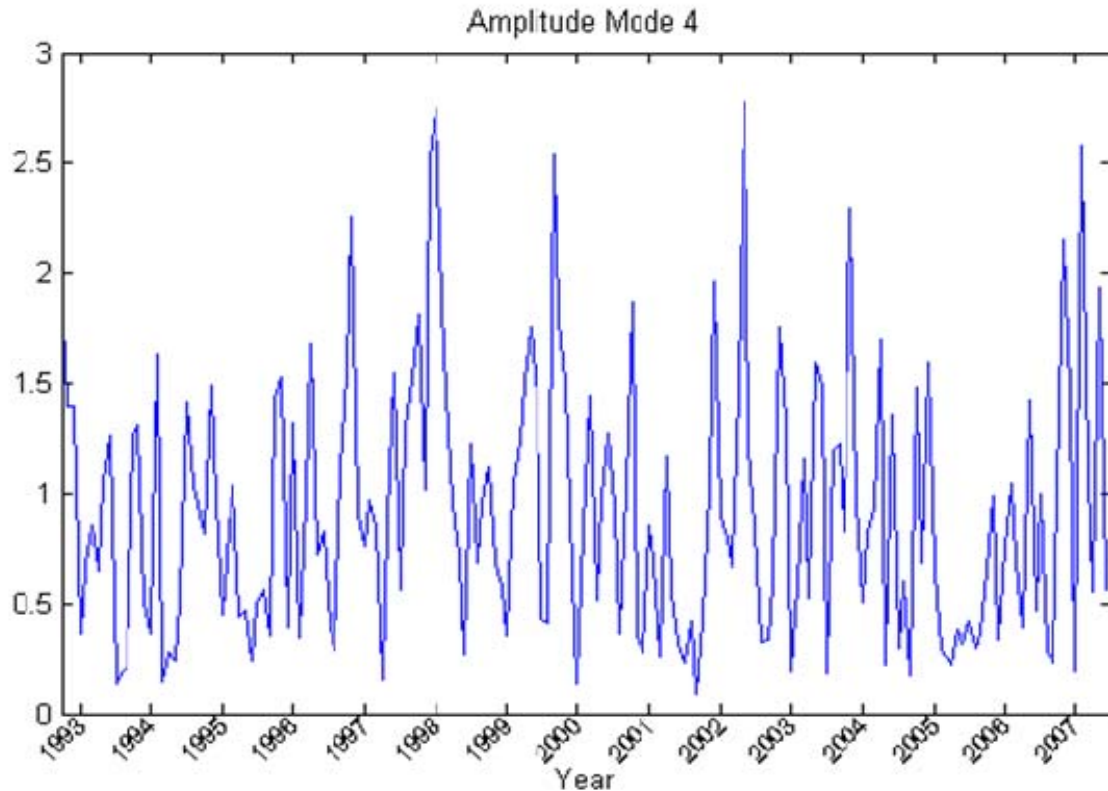


Figure 5-6. Amplitude of EOF Mode-4.

Figure 5-4 represents the amplitude of the first EOF mode. While comparing the amplitude of Mode-1 with the general trend in DMI, it was seen that the biggest variance is analogous to the trend in DMI during the year 1997-1998, the year of strongest positive Dipole Mode event in the recent history. Although not very conspicuous, small peaks of variance can be seen in the spatial patterns of currents along the equator during the years 1994 and 2006. These are again comparable with DMI and are the years of positive Dipole Mode event.

When amplitudes of variance from mode-2 to mode-4 were compared, it was clearly seen that the biggest anomaly during 1997-1998 was evident in all three modes. In mode-2, the evidence of a negative mode event that occurred during year 2005-2006 was also viewed. Therefore, generally speaking, the spatial anomaly of the currents along the equator to the occurrence of a Dipole Mode event can be directly related.

## E. EQUATORIAL JET DURING POSITIVE DIPOLE MODE EVENTS

To analyze the behavior of the equatorial jets during known positive Dipole Mode events, zonal current anomalies were calculated for the years of interest. Figure 5-7a depicts the 13-years' mean climatology of the zonal currents along the equator. Figures 5.7b-d depict the anomaly of the zonal currents for the years with known positive Dipole Mode events.

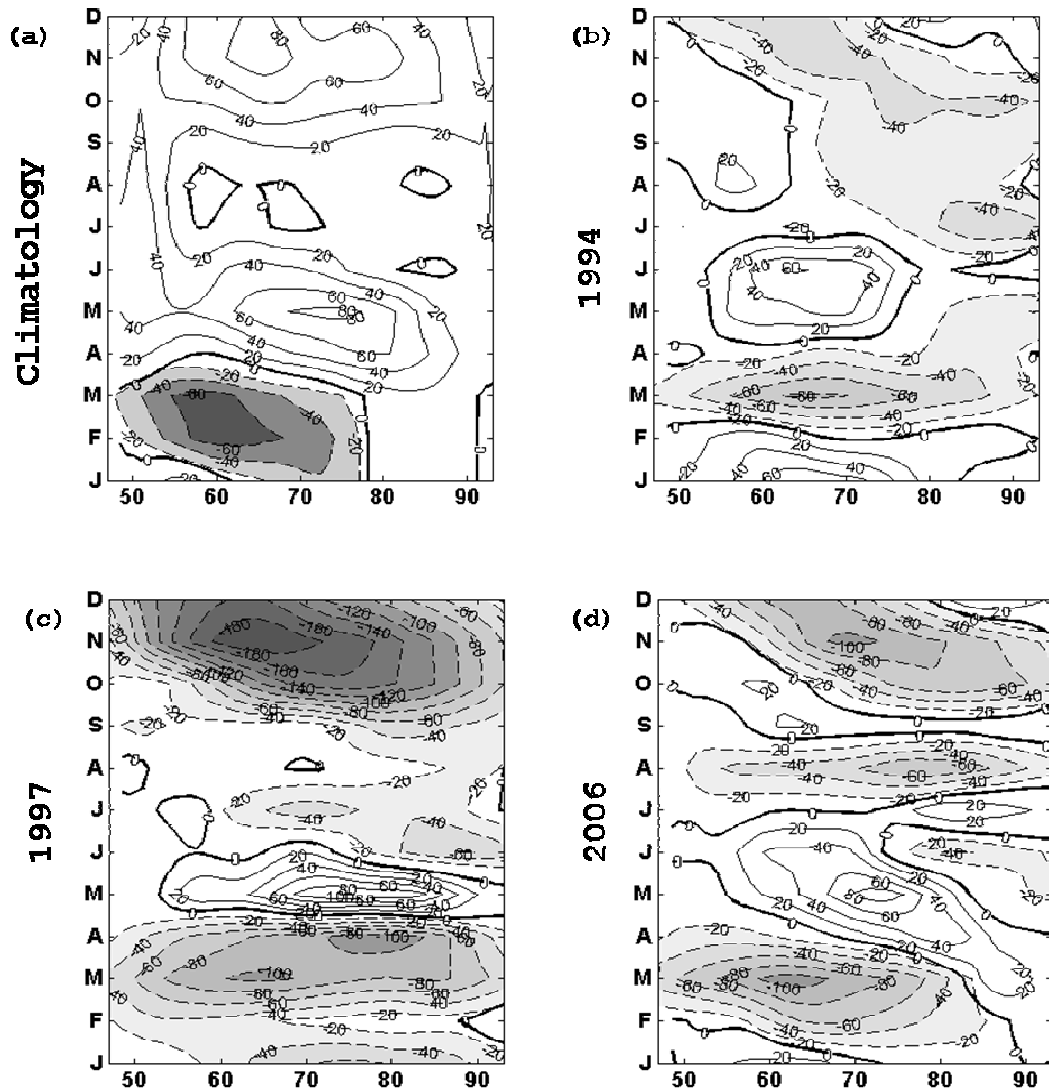


Figure 5-7. (a) Climatology of zonal currents ( $\text{cm s}^{-1}$ ) along the equator derived for satellite based observational data; (b) Anomaly of zonal currents during a positive Dipole Mode event year 1994, (c) Year 1997, and (d) Year 2006.

It can be clearly seen that all these years show consistent negative anomalies. This validates the previous studies with the observation that these jets slow down during a positive Dipole Mode event. This slowing event of the jets is analogous to the strong westward winds during a Positive Dipole Mode event. From the results, it was also seen that the intensity of negative anomaly is analogous to the strength of a particular Dipole Mode event. The biggest negative anomalies occurred during the latter part of 1997 (Figure 5-7c) which is the strongest known positive Dipole Mode event in recent history. Negative anomalies can also be seen in the most recent positive Dipole Mode event (Figure 5-7d) which was in the latter part of 2006. The same can also be verified from the Dipole Mode Index (DMI).

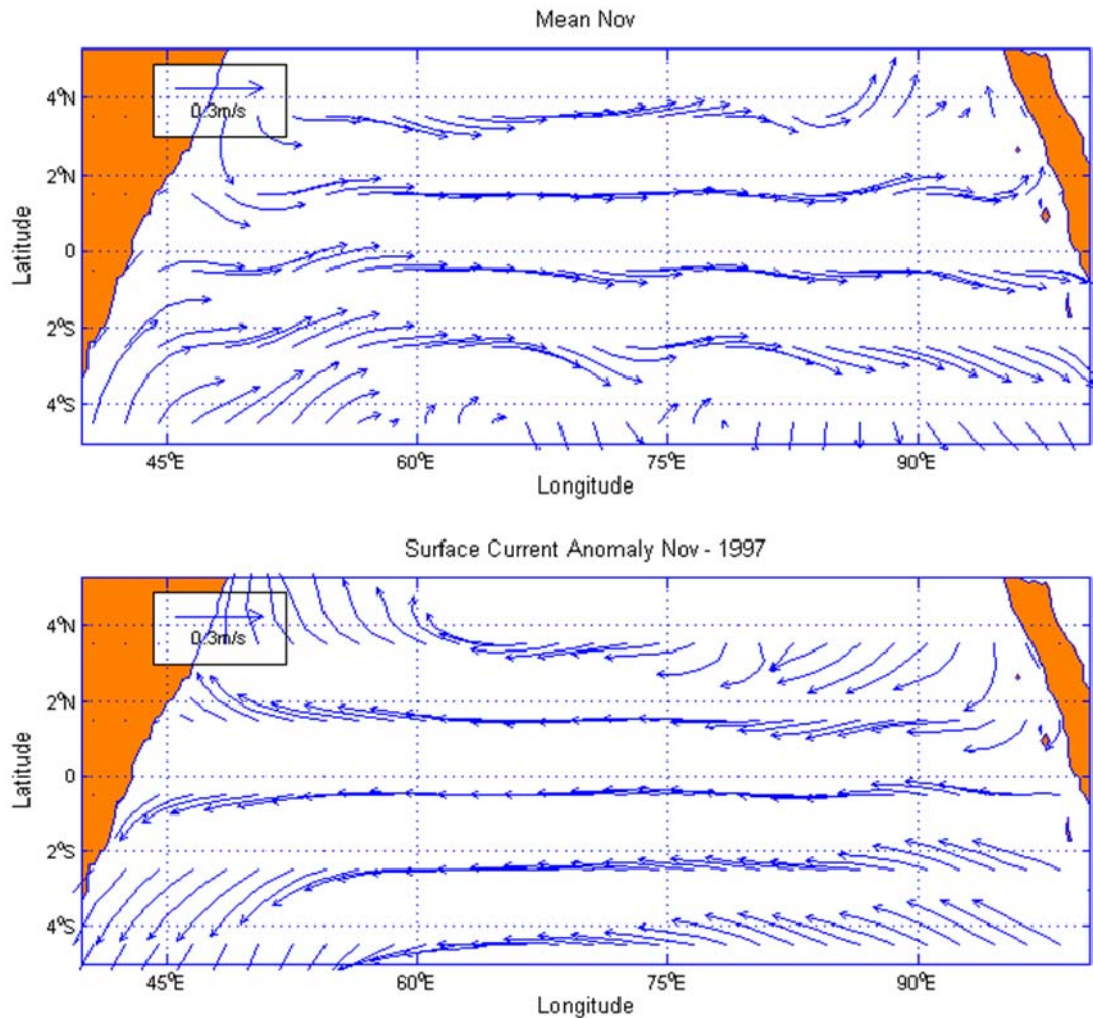


Figure 5-8. (a) 13-year mean climatology of surface currents along the equator during November, (b) Surface currents anomaly during November 1997.

To see more closely how equatorial jets altogether reverse their direction of flow during a positive Dipole Mode event, vector plots for the equator region were generated showing the anomaly for the months with strongest DMI. Then, it was compared with the mean climatology of that particular month. For the Dipole event of 1997, the maximum DMI was recorded for November. Figure 5-8 illustrates the 13-year mean climatology of surface currents along the equator during November (Figure 5-8a) and, also, shows the anomaly during November 1997 (Figure 5-8b). It is dramatic to see how strongly the wind patterns during a positive Dipole Mode event affect the general surface circulation at the equator.

#### **F. EQUATORIAL JETS DURING NEGATIVE DIPOLE MODE EVENTS**

To analyze the behavior of the equatorial jets during known negative Dipole Mode events, zonal current anomalies were calculated for the years with known negative Dipole Mode events. Figure 5-9 illustrates the anomaly of the zonal currents for the years with known negative Dipole Mode events. From the figure, positive anomalies were evident in all three years. It reached a maximum in 1998 where the positive anomaly reaches up to  $80 \text{ cm s}^{-1}$ . The results from satellite-based observational data confirmed the results of previous studies: it was observed that equatorial jets get stronger during a negative Dipole Mode event. The strong eastward jets may be caused by the strong eastward winds during a negative Dipole Mode event. Positive anomalies of the zonal currents can also be seen during the most recent year of negative Dipole Mode event during 2001 (Figure 5-9d). From the figure, it can also be observed that the intensity of positive anomaly is associated with the strength of a negative dipole event, which is represented by DMI.

To further see the behavior of equatorial jets during a negative Dipole Mode event, vector plots were generated. During the negative Dipole Mode event of 1996, the strongest DMI was recorded during the month of October. Again, Figure 5-10 serves as a sample vector plot of what the equatorial jets look like during a negative Dipole Mode event. The figure contains the 13-year mean climatology of surface currents along the equator during the month of October (Figure 5-10a) and, also, illustrates the anomaly

during October 1996 (Figure 5-10b). From the figure, we can clearly observe positive anomaly during the month of October as still in the anomaly plot we can see that the currents are moving in eastward direction.

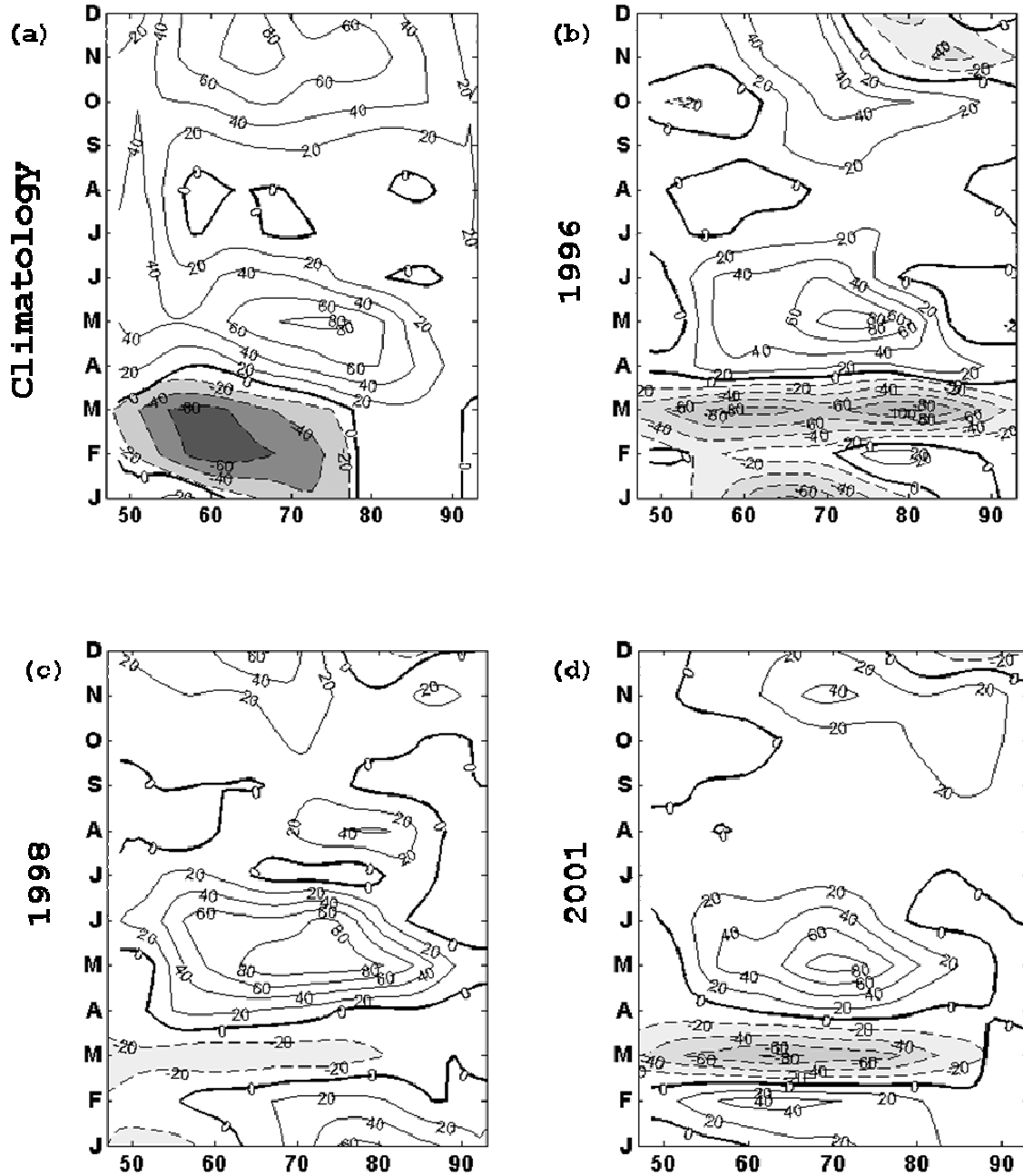


Figure 5-9. (a) Climatology of zonal currents ( $\text{cm s}^{-1}$ ) along the equator derived for satellite based observational data; (b) Anomaly of zonal currents during Negative Dipole mode event year 1996, (c) year 1998, and (d) year 2001.



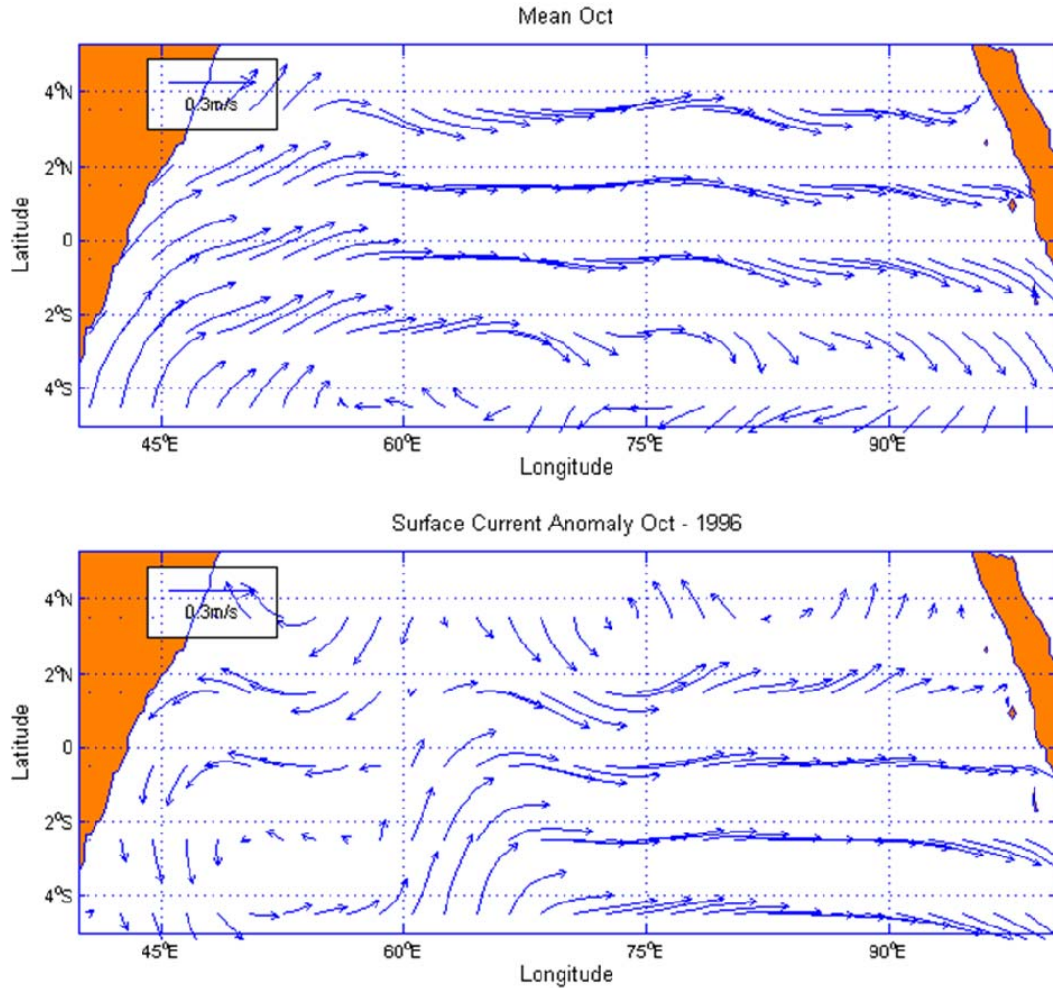


Figure 5-10. (a) 13-year mean climatology of surface currents along the equator during October, (b) Surface currents anomaly during October 1996.

From the above results and discussion, it is concluded that the satellite-based observational data can be used as an important tool to diagnose and even forecast the occurrence of an upcoming Dipole Mode event. The most useful thing about the OSCAR data set is that it is being updated on a regular basis (after every five days). Further, its availability is speedy compared to spot measurements. Although the data set may have certain inherent issues with the quality and accuracy, reasonably accurate results can still be obtained by applying certain mathematical techniques (such as OSD). Similar methodology, as we have utilized to analyze the Indian Ocean Dipole Mode events, can be used to investigate other large-scale ocean phenomena as well.

## **VI. PRACTICAL APPLICATIONS**

One of the most practical features of the OSCAR data is its near real-time and consistency (data available every five days). Because of this attribute of the data, its use for operational and tactical purpose becomes extremely useful: the results produced from this data set provide more realistic depiction of the synoptic surface currents in any area of interest. The data is equally useful for scientific purposes as well. In this subsection, we will briefly see how the knowledge of ocean surface currents can be practically used.

### **A. OPERATIONAL USES**

In this subsection, there will be a brief discussion about the possible operational uses of studying ocean surface currents.

#### **1. Ocean Currents and Mine Warfare**

Mine warfare is an integral part of naval warfare. Naval mine is one of the most cost effective weapons as it is inexpensive, easy to conceal, easy to deploy, and requires almost no maintenance. These attributes of the naval mine make it the favorite for nations with small naval power. Mines can be used strategically and tactically for denying access and defense of vital facilities, such as ports, anchorages, and offshore structures. Mines can change the shape of a battle space and can effectively damage the operations of naval forces. One of the important types of mine is the drifting mine. Drifting mines are usually used to completely refute access of friend and foe to a battle space. The mines are easier to deploy but are very difficult to sweep and hunt. The synoptic ocean surface currents affect the surface mine drifting. Deploying locations of the mines could be decided by knowing the most recent surface circulation pattern in a particular region. Thus, better understanding of ocean surface currents will lead us to better and more effective mine warfare.

#### **2. Search and Rescue at Sea**

In both peacetime and battle space environments, search and rescue operations require meticulous planning and careful execution. Amongst other environmental factors,

ocean surface circulation is the most important factor in planning a search and rescue operation. Ocean circulation pattern could be used to estimate the likely position of men and material to be rescued. By doing this, rescue effort can concentrate in a smaller and more probable area of interception. The good knowledge of ocean surface circulations can tremendously reduce the search and rescue effort by channeling it to a smaller area of interest.

### **3. Planning for an Economical Passage**

Surface ocean circulation patterns could be used to plan for a more economical passage. For longer voyages, without jeopardizing the shortest route, routes that are along the general flow of the ocean can be planned. By doing this, fuel consumption can be reduced and moves will be faster.

### **4. Monitoring Chemical Pollutants and Oil Spills**

In an event of intentional or unintentional spills of chemical pollutants and oil, ocean surface currents could be used to determine the spill. This is especially true in the coastal regions with very fast surface currents, such as the Gulf Stream, Kuroshio, and Somali Current. It tells us how fast to act in terms of remedial measures. Better understanding of ocean currents can also help in planning and executing such remedial measures. Thus, a good knowledge of ocean surface currents can not be undermined in context to monitoring unwanted liquid spillage in the ocean's upper surface.

## **B. SCIENTIFIC USES**

In this subsection, there will be a brief discussion about the possible scientific and technical uses of studying ocean surface currents.

### **1. Ocean Currents as a Source of Energy**

In today's industrialized world, the importance of sustainable energy sources cannot be undermined. The bigger economies of the world are always looking for newer ways to produce good amounts of energy. Ocean currents have the maximum strength near the surface and most of these are wind-driven. Power extraction from a flowing

source, such as ocean currents, depends on speed and density. Water is about 835 times denser than wind so, for equal area of intercepted flow, the energy contained in 12 mph would be the same as for a wind mass flowing at 110 mph (Technology white paper, May 2006). Also explained in the Technology white paper is that the estimated world wide power in world's ocean is about 5,000 GW with the power densities of about 15 KW/m<sup>2</sup>. The Technology white paper, May 2006, also comments that if only 1/1000 of the energy in Gulf Stream is utilized, it will be about 21,000 times more energy than in the Niagara Falls. With this little comparison, it is clear that worldwide ocean currents house a tremendous amount of energy in them. Most of it is unused.

## **2. Large-Scale Climate and Synoptic Diagnostics**

In terms of the OSCAR data set as the near real-time data of ocean surface currents as regularly available, with 1° x 1° resolution, it can, therefore, be used for large-scale synoptic diagnostics. Different large-scale features in the ocean surface currents could be analyzed regularly to see the variability. One of the examples in this context is the Indian Ocean Dipole phenomena. As seen in Chapter V, the occurrence of IOD can also be diagnostic via analysis of ocean surface currents. Besides this, variability in the large-scale eddies can also be monitored through ocean currents. Further, change in their general circulation behavior can be analyzed or used for large-scale climate diagnostics. In short, it can be said that overall ocean surface circulation constitutes an important factor in the overall climatology of a certain area.

THIS PAGE INTENTIONALLY LEFT BLANK

## VII. SUMMARY

The OSCAR, from 1993 to 2006, satellite altimetry data, was used to analyze the seasonal behavior of the surface circulations in the Indian Ocean region. More focus was given to the three most dynamic regions of the Indian Ocean: Somali Current, North Arabian Sea, and Bay of Bengal. The same data set was also used to determine the link between the eastward flowing equatorial jets and the Indian Ocean Dipole Mode events. Zonal current anomalies along the equator during a Dipole Mode event showed that occurrence of such an event directly affects the flow pattern of these equatorial jets (Wyrki jets).

The raw altimetry (OSCAR) data was refined by using the Optimal Spectral Decomposition method. This study shows the tremendous ability of this method to improve the noisy OSCAR data with realistic depiction of the coastal boundary currents. The strength of this method can be judged from the fact that after reconstruction, the non-evident boundary currents, such as Gulf Stream, Kuroshio, and Somali current, were now evident and the flow patterns could be clearly seen.

Using the reconstructed altimetry data, the mean seasonal variability of ocean surface circulations in the Indian Ocean region was studied. This study confirms, with the exception of a few small-scale features, the seasonal pattern of Indian Ocean surface circulations that was seen in previous studies. The reason why OSCAR data has a difficult time identifying small-scale features may be its resolution: it reduces down to  $1^\circ \times 1^\circ$ . The visuals produced from the data set show that, during summer monsoon, SEC and EACC supply the northward flowing Somali current. Part of the Somali current recirculates a little south of the equator to form the “Southern Gyre;” the other part moves in the northward direction. Further north during this time, another gyre forms which is known as the “Great Whirl.” The Southwest Monsoon Current (SMC) south of Sri Lanka flows eastward. During this season, the East Indian Coastal Current (EICC), with a weaker strength, flows northward along the eastern coast of India, whereas the general flow inside the bay is eastward. Along the eastern coast of Madagascar, the South

Equatorial Current (SEC) splits up into two branches: one move northward as the Northeast Madagascar Current (NEMC); the other moves southward as the Southeast Madagascar Current (SEMC).

During the winter monsoon, the East African Coast Current (EACC) meets the then southward flowing surface Somali current in a confluence zone. The two flows then supply the eastward flowing South Equatorial Countercurrent (SECC). At the eastern end of the SECC, the South Java Current flows southeastward. At this time of year, the southerly flowing Somali current gets input from the westward flow in the Arabian Sea. This westward flow is mostly contributed by the westward flowing Northeast Monsoon Current (NMC) south of Sri Lanka. After circulating around the Laccadive High, the NMC also supplies the WICC. During the winter season, there seems to be a clockwise moving gyre in the Bay of Bengal. The EICC attached to it seems to have a southward flow. In Southern Hemisphere Region, there is a broad zonal eastward flow of the South Equatorial Current (SEC). This is driven by the Southeast Trades. The visuals produced from altimetry data show that ocean currents south of about 15° S do not show much seasonal variability; therefore, SEC shows almost the same flow pattern in both seasons.

The behavior of the eastward-flowing equatorial jets (Wyrcki jets), in conjunction with the Indian Ocean Dipole events, was studied. The results showed that Dipole events directly affect the flow of the eastward equatorial jets. The unusual change in the flow of these jets is attributable to the changed flow pattern of the wind forcing as compared to their usual seasonal flow. This study confirms all previous studies: the eastward flowing equatorial jet weakens in a positive Dipole Mode event and strengthens in a negative Dipole Mode event. Both zonal current anomalies and vector anomaly plots depicted the same results. In short, it was concluded that satellite-based observational data is an important tool to diagnose and forecast the occurrence of an upcoming Dipole Mode event.

The most practical feature of OSCAR data is its currency and consistent flow (data available after every five days). As a result, its use for operational and tactical purposes becomes extremely useful. This is because the results produced from this data set provide more current and realistic depiction of the overall surface currents'



climatology in a particular area of interest. The data is equally useful for scientific purposes. For operational use, this ocean surface currents' data can be used for mine warfare, search and rescue operations, planning economical passages, and monitoring chemical pollutants and oil spills. In scientific context, the data can be used for developing energy sources using ocean currents and for large scale climate diagnostics.

For future research, this study recommends that OSCAR data can be used to analyze ocean surface circulations in other parts of the world as well. Although the satellite based data has inherent concerns pertaining to resolution and accuracy, it still can be useful in identifying mesoscale features in the ocean. With considerable refinement (OSD) and correct methodology this data can also be utilized to examine large scale climate phenomena, such as Indian Ocean Dipole events, El Nino, and La Nino. Comprehensive knowledge of the world ocean surface circulations will also serve vital to the Naval Forces in planning and executing of their missions over the sea.

THIS PAGE INTENTIONALLY LEFT BLANK

## LIST OF REFERENCES

- Boëhm, E., Morrison, J. M., Manghnani, V., Kim, H.-S. and Flagg, C. N. (1999). The Ras al Hadd Jet: remotely sensed and acoustic Doppler current profiler observations in 1994–1995. *Deep-Sea Research II*, 46, 1531–1549.
- Bonjean, F., Gunn, J.T. and Lagerloef, G.S.E. (2004). *OSCAR User's Manual*, NOAA/NESDIS Internal Report, 48pp, ESR, 2004.
- Bruce, J. G., Fieux, M. and Gonella, J. (1981). A note on the continuance of the Somali eddy after the cessation of the Southwest monsoon. *Oceanologica Acta*, 4, 7–9.
- Bruce, J. G., Johnson, D. R., & Kindle, J. C. (1994). Evidence for eddy formation in the eastern Arabian Sea during the northeast monsoon. *Journal of Geophysical Research*, 99, 7651–7664.
- Cane, M. (1980). On the dynamics of equatorial currents, with application to the Indian Ocean. *Deep-Sea Research*, 27A, 525–544.
- Central Intelligence Agency. (2008). *World Fact Book*, Retrieved 26 April 2008 from <https://www.cia.gov/library/publications/the-world-factbook/geos/xo.html>.
- Chu, P. C., Ivanov, L. M. and Melnichenko, O. M. (2005). Fall-winter current reversals on the Texas-Louisiana continental shelf. *Journal of Physical Oceanography*, 35, 902-910.
- Chu, P. C., Ivanov, L. M. and Margolina, T. M. (2004). Rotation method for reconstructing process and field from imperfect data. *International Journal of Bifurcation and Chaos*, 14 (8), 2991-2997.
- Chu, P. C., Ivanov, L. M. and Margolina, T. M. (2005). Seasonal variability of the Black Sea Chlorophyll-a concentration. *Journal of Marine Systems*, 56, 243-261.
- Chu, P. C., Ivanov, L. M., Melnichenko, O. V. and Wells, N. C. (2007). On long baroclinic Rossby waves in the tropical North Atlantic observed from profiling floats. *Journal of Geophysical Research*, 112, C05032, doi:10.1029/2006JC003698.
- Chu, P. C., Ivanov, L. M., Korzhova, T. P., Margolina, T. M. and Melnichenko, O. M. (2003a). Analysis of sparse and noisy ocean current data using flow decomposition. Part 1: Theory. *Journal of Atmospheric and Oceanic Technology*, 20 (4), 478-491.

- Chu, P. C., Ivanov, L. M., Korzhova, T. P., Margolina, T. M. and Melnichenko, O. M. (2003b). Analysis of sparse and noisy ocean current data using flow decomposition. Part 2: Application to Eulerian and Lagrangian data. *Journal of Atmospheric and Oceanic Technology*, 20 (4), 492-512.
- Cutler, A. N. and Swallow, J. C. (1984). Surface currents of the Indian Ocean. (To 25°S, 100°E). I. O. S. Technical Rept. 187.
- Dueing, W. and Schott, F. (1978). Measurements in the source region of the Somali Current during the monsoon reversal. *Journal of Physical Oceanography*, 8, 278–289.
- Eigenheer, A. and Quadfasel, D. (2000). Seasonal variability of the Bay of Bengal circulation inferred from TOPEX/POSEIDON altimetry. *Journal of Geophysical Research*, 105, 3243–3252.
- Energy Information Administration. (2004). Report on “World Oil Transit Chokepoints.”
- Fischer, J., Schott, F. and Stramma, L. (1996). Currents and Transports of the Great Whirl-Socotra Gyre System during the Summer Monsoon August 1993. *Journal of Geophysical Research*, 101, 3573–3587.
- Flagg, C. A., & Kim, H.-S. (1998). Upper ocean currents in the northern Arabian Sea from shipboard ADCP measurements collected during the 1994–1996 U.S. JGOFS and ONR Programs. *Deep-Sea Research II*, 45, 1917–1959.
- Godfrey, J. S. (1996). The effect of the Indonesian Throughflow on ocean circulation and heat exchange with the atmosphere: a review. *Journal of Geophysical Research*, 101, 12217–12237.
- Hacker, P., Firing, E., Hummon, J., Gordon, A. and Kindl, J. C. (1998). Bay of Bengal currents along the northeast monsoon. *Geophysical Research Letters*, 25, 2769–2772.
- Han, W., McCreary, J. P. Jr., Anderson, D. L. T. and Mariano, A. J. (1999). On the dynamics of the eastward surface jets in the equatorial Indian Ocean. *Journal of Physical Oceanography*, 29, 2191–2209.
- Iizuka, S., Matsuura, T. and Yamagata, T. (2000). The Indian Ocean SST Dipole Simulated in a Coupled General Circulation Model. *Geophysical Research Letters*, 27, 3369-3372.
- Ivanov, L.M., A. D. Kirwan Jr., and T. M. Margolina, 2001a: Filtering noise from oceanographic data with some applications for the Kara and Black Seas. *J. Mar. Syst.*, **28**, 113–139.

- Jagdish, S. (2002). A Generic Concept of Customer Behavior. *Journal of Customer Behavior*, Vol. 1 (2002), 1-5.
- Jagdish, S. (2002). Future of Relationship Marketing. *Journal of Services Marketing*, Vol. 16, No. 7, (2002), 590-592.
- Nazery, K. (2005). The Role of the Indian Ocean in Facilitating Global Maritime Trade. Retrieved 29 April 2008 from <http://www.mima.gov.my/mima/htmls/papers/pdf/nazery/indian.pdf>.
- O'Brien, J. J., and Hurlburt, H. E. (1974). An equatorial jet in the Indian Ocean theory. *Science*, 184, 1075–1077.
- Ocean Surface Current Analysis – Real Time (OSCAR) Data Base. (2008). Retrieved 2 May 2008 from <http://www.oscar.noaa.gov/index.html>.
- Quadfasel, D. and Cresswell, G. R. (1992). A note on the seasonal variability of the south Java Current. *Journal of Geophysical Research*, 97, 3685–3688.
- Quadfasel, D. and Schott, F. (1982). Water Mass Distribution at Intermediate Layers Off the Somali Coast during the Onset of the Southwest Monsoon, 1979. *Journal of Physical Oceanography*, 12, 1358–1372.
- Rao, R. R. and Sivakumar, R. (2000). Seasonal variability of near-surface thermal structure and heat budget of the mixed layer of the tropical Indian Ocean from a new global ocean temperature climatology. *Journal of Geophysical Research*, 105, 985–1015.
- Rao, R. R., Molinari, R. L. and Festa, J. F. (1989). Evolution of the climatological near-surface thermal structure of the tropical Indian Ocean: 1. Description of mean monthly mixed layer depth, and sea surface temperature, surface current, and surface meteorological fields. *Journal of Geophysical Research*, 94, 10801–10815.
- Reppin, J., Schott, F. A., Fischer, J. and Quadfasel, D. (1999). Equatorial currents and transports in the upper central Indian Ocean: Annual cycle and interannual variability. *Journal of Geophysical Research*, 104:15495–15514.
- Saji, N. H., Goswami, B. N., Vinayachandran, P. N. and Yamagata, T. (1999). A dipole in the tropical Indian Ocean. *Nature, London*, 401, 360–363.
- Schott, F., & Quadfasel, D. (1982). Variability of the Somali Current and associated upwelling. *Progress in Oceanography*, 12, 357–381.
- Schott, F., Swallow, J. C., & Fieux, M. (1990). The Somali Current at the equator: annual cycle of currents and transports in the upper 1000 m and connection to neighboring latitudes. *Deep-Sea Research*, 37, 1825–1848.

- Schott, F., Fischer, J., Garternicht, U., & Quadfasel, D. (1997). Summer monsoon response of the Northern Somali Current, 1995. *Geophysical Research Letters*, 24, 2565–2568.
- Schott, F. and Fischer, J. (2000). Winter monsoon circulation of the northern Arabian Sea and Somali Current. *Journal of Geophysical Research*, 105, 6359–6376.
- Schott, F., Reppin, J., Fischer, J. and Quadfasel, D. (1994). Currents and transports of the Monsoon Current south of Sri Lanka. *Journal of Geophysical Research*, 99, 25127–25141.
- Schott, F. A. and McCreary, J. P. Jr. (2001). The Monsoon Circulation of Indian Ocean. *Progress in Oceanography*, 51 (2001) 1-123.
- Shetye, S. R. and Shenoi, S. S. C. (1988). The seasonal cycle of surface circulation in the coastal North Indian Ocean. *Proceedings of the Indian Academy of Science (Earth and Planetary Science)*, 97, 53–62.
- Shetye, S. R., Gouveia, A. D., Shenoi, S. S. C., Sundar, D., Michael, G. S. and Nampoothiri, G. (1993). The western boundary current of the seasonal subtropical gyre in the Bay of Bengal. *Journal of Geophysical Research*, 98, 945–954.
- Shetye, S. R., Gouveia, A. D., Shenoi, S. S. C., Vinayachandran, P. N., Sundar, D., Michael, G. S. and Nampoothiri, G. (1996). Hydrography and circulation in the western Bay of Bengal during the northeast monsoon. *Journal of Geophysical Research*, 101, 14011–14025.
- Shi, W., Morrison, J. M., Böhm, E., & Manghnani, V. (2000). The Oman upwelling zone during 1993, 1994 and 1995. *Deep-Sea Research II*, 47, 1227–1247.
- Sirott, J., Denbo, D.W. and Zhu, W.H. (2004). Dapper: An OPeNDAP Server for In-Situ Data. In *Proceedings of the 20th International Conference on Interactive Information and Processing Systems (IIPS) for Meteorology, Oceanography, and Hydrology*, 2004 AMS Annual Meeting, Seattle, WA, 12–15 January 2004, Paper 9.12.
- Stramma, L., Fischer, J. and Schott, F. (1996). The flow field off southwest India at 8°N during the southwest monsoon of August 1993. *Journal of Marine Research*, 54, 55–72.
- Swallow, J. C., Fieux, M. and Schott, F. (1988). The boundary currents east and north of Madagascar, Part I: Geostrophic currents and transports. *Journal of Geophysical Research*, 93, 4951–4962.
- Swallow, J. C., Schott, F. and Fieux, M. (1991). Structure and transport of the East African Coastal Current. *Journal of Geophysical Research*, 96, 22254–22267.

- Technology White Paper (2006) on “*Ocean Currents Energy Potential on the U.S. Outer Continental Shelf*.” Retrieved 10 May 2008 from [http://ocsenergy.anl.gov/documents/docs/ocs\\_eis\\_whitepaper\\_current.pdf](http://ocsenergy.anl.gov/documents/docs/ocs_eis_whitepaper_current.pdf).
- The State of Indian Ocean Climate, Time Series of Dipole Mode Index. (2008). Retrieved 24 April 2008 from [http://ioc3.unesco.org/oopc/state\\_of\\_the\\_ocean/sur/ind/dmi.php](http://ioc3.unesco.org/oopc/state_of_the_ocean/sur/ind/dmi.php).
- Tomczak M. and Godfrey, J. S. (1994). *Regional Oceanography AN Introduction*, Pergamon Publishers, New York, 175-179.
- Vinayachandran, P. N., Iizuka, S. and Yamagata, T. (2001). Indian Ocean Dipole Mode events in an ocean general Circulation Model. To appear in *Deep Sea Research II Special Topic Volume “Physical Oceanography of the Indian Ocean during the WOCE period.”*
- Vinayachandran, P. N., Saji, N. H. and Yamagata, T. (1999b). Response of the equatorial Indian Ocean to an unusual wind event during 1994. *Geophysical Research Letters*, 26, 1613–1616.
- Wyrski, K. (1973). An Equatorial Jet in the Indian Ocean. *Science*, 181, 262–264.



THIS PAGE INTENTIONALLY LEFT BLANK

## **INITIAL DISTRIBUTION LIST**

1. Defense Technical Information Center  
Ft. Belvoir, Virginia
2. Dudley Knox Library  
Naval Postgraduate School  
Monterey, California
3. Professor Mary L. Batteen  
Naval Postgraduate School  
Monterey, California
4. Professor Peter C. Chu  
Naval Postgraduate School  
Monterey, California
5. Lt. Haris Sarwar Rana  
Naval Postgraduate School  
Monterey, California
6. Dr. Charles Sun  
National Oceanic and Atmospheric Administration  
Suitland, Maryland